British Geological Survey
NATURAL ENVIRONMENT RESEARCH COUNCIL

Three-dimensional gravity modelling of the Labrador Sea - Baffin Bay region

Energy and Marine Programme

Commissioned Report CR/13/089

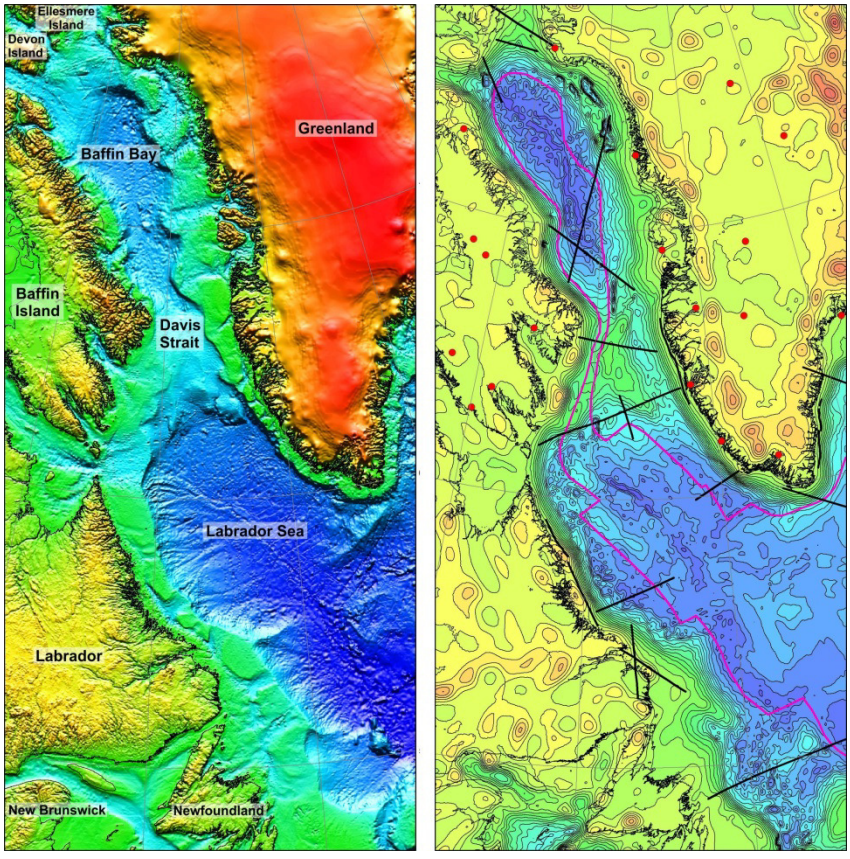

BRITISH GEOLOGICAL SURVEY

ENERGY AND Marine PROGRAMME

COMMISSIONED REPORT CR/13/089

Three-dimensional gravity modelling of the Labrador Sea - Baffin Bay region

G S Kimbell

.

Keywords

Labrador Sea; Davis Strait; Baffin Bay; Greenland; gravity modelling.

Front cover

Images of topography and modelled crustal thickness across the study area. The latter includes the continent-ocean boundary and locations of seismic experiments used in the assessment of the model.

Bibliographical reference

KIMBELL, G S. 2013. Three-dimensional gravity modelling of the Labrador Sea - Baffin Bay region. *British Geological Survey Commissioned Report*, CR/13/089. 84pp.

Keyworth, Nottingham British Geological Survey 2013

BRITISH GEOLOGICAL SURVEY

The full range of our publications is available from BGS shops at Nottingham, Edinburgh, London and Cardiff (Welsh publications only) see contact details below or shop online at www.geologyshop.com

The London Information Office also maintains a reference collection of BGS publications, including maps, for consultation.

We publish an annual catalogue of our maps and other publications; this catalogue is available online or from any of the BGS shops.

The British Geological Survey carries out the geological survey of Great Britain and Northern Ireland (the latter as an agency service for the government of Northern Ireland), and of the surrounding continental shelf, as well as basic research projects. It also undertakes programmes of technical aid in geology in developing countries.

The British Geological Survey is a component body of the Natural Environment Research Council.

British Geological Survey offices

BGS Central Enquiries Desk
Tel 0115 936 3143 Fax 0115 936 3276
email enquiries@bgs.ac.uk

Kingsley Dunham Centre, Keyworth, Nottingham NG12 5GG
Tel 0115 936 3241 Fax 0115 936 3488
email sales@bgs.ac.uk

Murchison House, West Mains Road, Edinburgh EH9 3LA
Tel 0131 667 1000 Fax 0131 668 2683
email scotsales@bgs.ac.uk

Natural History Museum, Cromwell Road, London SW7 5BD
Tel 020 7589 4090 Fax 020 7584 8270
Tel 020 7942 5344/45 email bgslondon@bgs.ac.uk

Columbus House, Greenmeadow Springs, Tongwynlais, Cardiff CF15 7NE
Tel 029 2052 1962 Fax 029 2052 1963

Maclean Building, Crowmarsh Gifford, Wallingford OX10 8BB
Tel 01491 838800 Fax 01491 692345

Geological Survey of Northern Ireland, Colby House, Stranmillis Court, Belfast BT9 5BF
Tel 028 9038 8462 Fax 028 9038 8461
www.bgs.ac.uk/gsni/

Parent Body

Natural Environment Research Council, Polaris House, North Star Avenue, Swindon SN2 1EU
Tel 01793 411500 Fax 01793 411501
www.nerc.ac.uk

Website www.bgs.ac.uk
Shop online at www.geologyshop.com

Foreword

The original Passive Margins Modelling Project (PmmP) undertook a programme of research on the north-east Atlantic continental margin during 1999-2002, and was financed by a consortium comprising the British Geological Survey and a group of industry sponsors. Since then, further PmmP projects have been undertaken when additional funds have become available as a result of new companies joining the sponsoring group. The first such project resulted in an update to the project GIS (Kimbell, 2008). The second project is described in this report and involved an update to the modelling methodology and its application to a new investigation of the Labrador Sea – Davis Strait – Baffin Bay region.

Acknowledgements

The following companies have sponsored the Passive Margins Modelling Project and their support is gratefully acknowledged:

Anadarko North Sea Company Ltd.
AS Norsk Shell
Chevron Upstream Europe
ConocoPhillips (U.K.) Ltd.
ENI UK Limited
E.ON E&P UK Limited
Statoil (U.K.) Ltd.

Contents

FIGURES

TABLES

Summary

A lithospheric model has been constructed for a 3500 x 1700 km region covering the Labrador Sea, Davis Strait, Baffin Bay and adjacent onshore parts of Greenland and Canada. The project employed data compiled from publicly available sources and a modelling methodology adapted from that of Kimbell et al. (2002, 2004). Thermal modelling routines were developed which simulated temperatures beneath cratonic areas and the influence on the temperature regime of both Cretaceous rifting and Palaeogene ocean spreading. The simulated temperatures were used to estimate upper-mantle densities incorporated in a 3D gravity model in which Moho and top basement interfaces were optimised on the basis of comparison with observed long and short wavelength gravity anomalies respectively. The model was calibrated and assessed by comparison with the results of seismic experiments (receiver function studies and deep seismic refraction profiles).

The Moho depths predicted by the 3D model are similar to those estimated from receiver function studies in Greenland, but generally several kilometres shallower than the those on Baffin Island. The data available for comparison in the latter case are very limited, but if the difference is real it might be explicable in terms of lower heat flow (and colder upper mantle) than was assumed in the modelling of the latter area. Farther south on the Canadian margin, beneath Labrador and Newfoundland, modelled Moho depth estimates are broadly compatible with the seismic observations, provided allowance is made for departures from the assumed density model (low density crust associated with the Nain Plutonic Suite beneath the central part of the Labrador coast and high-density underplating beneath its southern part). In the offshore area the general agreement between modelled Moho and the seismic Moho suggests that the modelling assumptions and methodology are appropriate, but there are local departures. For example the modelled Moho is deeper than the seismic Moho beneath the Davis Strait and this is interpreted to be due to relatively low density upper-mantle in that area, either because of a thermal anomaly in excess of that assumed in the modelling or because of depletion associated with melt extraction.

Comparison with independent data sources indicates that the optimised top basement model identifies genuine features that were not well-represented in the starting model, but that the calibration of depth to basement can be poor, particularly where there is evidence of incipient instability in the inversion. The cover sequence model did not include a discrete representation of volcanic sequences, so contains additional inaccuracies where these are present. A series of basins of probable Cretaceous age are identified on the margins of Baffin Bay and a complex internal structure suggested for the major Saglek and Hopedale basins on the Labrador margin. A complex structure is also suggested for the basins of the Northeast Newfoundland Shelf, which agrees with structural mapping from other sources.

Overall, the project has demonstrated the feasibility of constructing a reconnaissance-level 3D model covering a large area from relatively limited resources. In this case the model includes continental margins extending for a strike length in excess of 6000 km. There is potential for more detailed follow-up within the present study area, of which a key component would be the refinement of the initial cover sequence model. The East Greenland margin is an attractive target for a future reconnaissance study.

1 Introduction

The initial Passive Margins Modelling Project (PmmP) involved the investigation of the North-east Atlantic margin, and included the development of regional 3D lithospheric modelling methods (Kimbell et al., 2002; Kimbell, 2002). A second phase updated the project GIS, and highlighted the increasing availability of global datasets relevant to such investigations (Kimbell, 2008). The third phase of the project, which is described in this report, has moved to a new region and addressed new challenges. The area selected embraces the north-east Canadian and West Greenland margins and includes geological elements ranging from Archaean cratons to Palaeogene oceanic crust. It includes both magma-poor and magma-rich conjugate continental margins. The objectives of the project were to adapt the modelling methodology to these new challenges, and changes in the computational platform, and to test its effectiveness by generating a 3D lithospheric model of the selected area using publicly available data sources.

The study area (Figure 1) is a rectangle defined by the following coordinates:
-300000 - 1400000 mE, 5200000 - 8700000 mN (UTM Zone 21)

The north-west to south-east axis of the study area is occupied by a small ocean basin which is flanked by the extended NE Canadian and SW Greenland margins, and these are in turn flanked by Precambrian basement massifs. In outline, its evolution involved the following key stages:

(i) Much of the continental basement beneath the region was formed by the amalgamation of Archaean cratonic blocks along Palaeoproterozoic orogenic belts (Figure 2; e.g. St-Onge et al., 2009). These elements can be correlated between north-east Canada and south-west Greenland as indicated in Figure 2. Subsequent (Mesoproterozoic) accretionary orogenesis led to the formation of the Grenville Orogen in the south and this was followed by the Palaeozoic development of the Appalachian orogenic belt.

(ii) Incipient stretching is indicated by minor intrusions formed in West Greenland during the period 220-150 Ma, with increased extension indicated by a 30 km long dyke swarm formed around 150 Ma (Larsen et al., 2009). Major rifting along the axis of the future Labrador Sea commenced in the Early Cretaceous (140-133 Ma; Berriasian-Hauterivian; Larsen et al., 2009), and there are igneous manifestations of this event in the form of a coast-parallel dyke swarm in SW Greenland (Larsen et al., 2009) and volcanic rocks of the Alexis Formation on the Labrador margin (Balkwill, 1987). Rifting continued into the Aptian-Albian, with deposition of the Early Cretaceous Bjarni Formation on the Labrador Shelf and Kitsissut and Appat sequences on the SW Greenland Shelf. This Early Cretaceous phase of rifting is also inferred to be responsible for the initiation of deep sedimentary basins on the margins of Baffin Bay (Jackson et al., 1992; Whittaker et al., 1997).

(iii) Further rifting occurred in the Late Cretaceous, during which the Markland Formation was deposited on the Labrador Shelf and Kangeq sequence on the SW Greenland Shelf (Dickie et al., 2011). This culminated in continental separation in latest Cretaceous – earliest Paleocene times. The initial separation appears to have been magma poor and resulted in the development of 'transition zones' on both margins (Chian et al. 1995a,b). These zones have been variously identified as highly stretched continental crust (Chalmers and Lauresen, 1995), slow-spreading oceanic crust (Srivastava and Roest, 1999) or unroofed and serpentinised continental upper mantle (Chian et al. 1995a,b; Chalmers and Pulvertaft, 2001, Reston and Pérez-Gussinyé, 2007). Chian et al. (1995a, b) date the transition zone formation to the interval spanned by chrons C33 to C31, whereas Chalmers (1991) extends it to C27.

(iv) Igneous ocean crust started to form in the Labrador Sea during the Paleocene, with C27N as the earliest undisputed oceanic magnetic anomaly. Ocean spreading is also inferred to have commenced in Baffin Bay during the Paleocene (e.g. Oakey and Chalmers, 2012; Suckro et al., 2013), although there the associated magnetic anomalies are poorly resolved by current data. The transform between these ocean basins (the Ungava Fault Complex) lies beneath the Davis Strait and is characterised by high seismic velocities indicative of highly intruded continental crust or new igneous crust formed at this time (Funck et al., 2007; Suckro et al., 2013). The Paleocene was also characterised by the development of the Disko Volcanic Province, volcanism on the Northern Labrador and Southern Baffin margins (Skaarup et al., 2006), and deposition of volcanic rocks in the Saglek Basin on the Labrador Shelf (Jauer and Budkewitsch, 2010).

(v) There was a change in oceanic spreading direction (from NE-SW to broadly N-S) at around the Paleocene-Eocene boundary (chron C24) which was a consequence of the plate reorganisation associated with the initiation of spreading between East Greenland and North-west Europe (Srivastava, 1978; Suckro et al., 2012, 2013; Oakey and Chalmers, 2012). This coincided with a second, more minor, pulse of magmatism observed on the West Greenland margin (Storey et al., 1998; Larsen et al., 2009).

(vi) The ocean spreading rate slowed in the Middle Eocene (C20) and spreading had stopped by C13 (latest Eocene – earliest Oligocene) (Roest and Srivastava, 1989).

(vii) The West Greenland margin is inferred to have been subjected to three periods of uplift during the Neogene, starting at 36-30 Ma, 11-10 Ma and 7-2 Ma, and the present-day topography was established during these episodes rather than earlier rifting (Japsen et al., 2005, 2006).

2 Data sources

Topographic, gravity, magnetic and sediment thickness data have been assembled for this project, as described below. The compilations are in the form of grids, typically with a node spacing of 2 km and covering the study area rectangle specified in Section 1. The maps and images generated from these datasets (and from the modelling results presented in Section 5) were produced using the GIS tools developed during the previous PmmP project (Kimbell, 2008).

2.1 TOPOGRAPHIC GRID

Version 6 of the SRTM30_PLUS topographic model (Becker et al., 2009) was used for this study (© The Regents University of California. All rights reserved). The model was developed by the Scripps Institution of Oceanography (SIO) and incorporated data from the National Oceanic and Atmospheric Administration (NOAA), the US Navy, the National Geospatial-Intelligence Agency (NGA) and the General Bathymetric Chart of the Oceans (GEBCO). The onshore component of the model is based on data from the Shuttle Radar Topography Mission (SRTM) and ICESat. The bathymetric component of the model is constrained by marine soundings, which were compiled and edited from a variety of sources; between these control points the model detail was constructed using satellite-derived gravity data (Smith and Sandwell, 1997).

Figure 1 is an image of the topographic model, while Figure 3 illustrates a version in which the Greenland icecap thickness model of Bamber et al. (2001) has been removed in order to estimate the bedrock topography.

There is a potential problem with using a topographic model derived from gravity data as it is possible that it has been distorted by effects due to bedrock density variation. It is the calibration from marine sounding data that prevents this occurring, so the better the coverage of such soundings the better the quality of the model. The coverage is best in the Labrador Sea, particularly on the Canadian side and sparser in the deep water parts of Baffin Bay and the Davis Strait (Becker et al., 2009; their fig.2 is indicative, although further soundings have been incorporated in the version of the topographic model used).

2.2 GRAVITY GRID

The gravity compilation employs the following data sources:

(i) Free-air gravity anomalies in offshore areas derived from satellite altimetry by the Scripps Institution of Oceanography (Sandwell and Smith, 1997). Version 18.1 of their global gravity grid was employed (© The Regents University of California. All rights reserved).

(ii) Bouguer gravity anomalies over Greenland from the Arctic Gravity Project (Kenyon et al., 2008), which is distributed by the National Geospatial-Intelligence Agency (http://earth-info.nga.mil/GandG/wgs84/agp/). The project produced public domain gravity grids derived from airborne, surface and submarine data in the Arctic from a multitude of sources. The grids were prepared by a working group under the International Gravity and Geoid Commission, International Association of Geodesy. The ice-cap thickness was taken into account when calculating the Bouguer corrections.

(iii) Bouguer gravity anomalies over northern Canada available for download from Natural Resources Canada. The data used for this project were downloaded in 2011 and the appropriate citation is:

2011: Canadian Geodetic Information System
Geoscience Data Repository
Geodetic Survey Division
Earth Sciences Sector
Natural Resources Canada
Government of Canada

An image of the merged gravity compilation is shown in Figure 4. There is noise at the coastline in the merged gravity field which is a consequence of the rugged topography and poor sampling of the gravity field along the coastal strip.

The version of the gravity field used in the modelling was modified to account for the 'indirect effect' (Chapman and Bodine, 1979; Hinze et al., 2005), which is due to the difference between the geoid (the datum to which the original the gravity measurements were referred) and the spheroid (the datum for the gravitational reference field). The geoid elevation data used to make this correction were based on the Earth Gravitational Model 2008 (Pavlis et al., 2012).

2.3 MAGNETIC GRIDS

Two magnetic grids have been created for the study area:

(i) Magnetic anomalies from the GAMMAA5 compilation which was published through an open-file report of the Geological Survey of Canada (Verhoef et al., 1996;). This data source covers the entire study area.

(iv) Magnetic anomalies over the south-western part of the study area downloaded from the Natural Resources Canada website. This includes higher resolution mapping of magnetic variations over the onshore regions of Canada. The citation for this dataset is:

2011: Canadian Aeromagnetic Data Base
Geoscience Data Repository
Geodetic Survey Division
Earth Sciences Sector
Natural Resources Canada
Government of Canada

Images of these two datasets are shown in Figures 5 and 6 respectively.

2.4 INITIAL SEDIMENT THICKNESS GRID

The initial sediment thickness grid was constructed primarily from the following data sources:

(i) The model of Louden et al. (2004), which covers the area south of 70ºN

(ii) A map of depth to basement published by the Geological Survey of Canada (Grant, 1988) which was employed in the area north of 70ºN.

Figure 7 is a contour map of the initial sediment thickness model and Figure 8 shows the initial top basement contours in the mainly offshore area over which this interface was subsequently optimised by gravity inversion.

3 Thermal modelling

3.1 INTRODUCTION

Previous studies have demonstrated the need to take into account the effect of temperature variations in the upper mantle when modelling regional gravity variations in continental margin settings (e.g. Kimbell, 2002; Kimbell et al., 2004, 2010). In those examples, the primary focus was in the thermal impact of breakup and the formation of oceanic lithosphere. The influence of lateral heat transfer from the oceanic regime into the adjacent continental crust was simulated but beyond this a simple average continental geotherm was adopted. For the present study, a more sophisticated approach has been attempted. The aim was to simulate the geotherms that characterise the shield regions on either side of the zone of rifting and the thermal impact of both the pre-breakup and breakup rifting phases.

3.2 CONTINENTAL HEAT FLOW MEASUREMENTS

Relevant heat flow information is summarised in Table 1. The limited observational evidence from bedrock temperature gradients in south-west Greenland suggests a mean heat flow of about 40 mW/m^2 (data primarily from Sass et al., 1972). This is corroborated by a heat flow map based on observed basal temperatures from boreholes through the ice sheet (Tarasov and Peltier, 2003), which indicates a typical heat flow of 40-45 mW/m^2 in this area. Onshore heat flow measurements on the Precambrian basement on the Canadian side of the study area are also very sparse (Grasby et al., 2009; Global Heat Flow Database at http://www.heatflow.und.edu/). Mareschal et al. (2000) report a very low measured heat flow of 22 mW/m^2 near Voisey Bay on the coast of Labrador (c. 62ºW, 56ºN), where an extension of the North Atlantic Craton of southern Greenland is exposed (Figure 2). Three measurements on the Grenville Orogen near Quebec (c. 66.7ºW, 50.5ºN) average 28.7 mW/m^3 (Guillou-Frottier et al. 1995; Pinet et al., 1991). Further south, 34 measurements on the Appalachian Orogen in Newfoundland and New Brunswick have an average value of 46.6 mW/m^2. High heat flows have been reported from oil exploration wells over the extended continental crust of the North-east Canadian rifted margin (Reiter and Jessop, 1985; Wielens et al., 2006), but these have questioned by Goutorbe et al. (2007) who suggested that they could be distorted by overestimates of rock thermal conductivity. The latter authors provided new heat flow estimates employing thermal conductivity values estimated from geophysical logs using a neural network process, and these provided lower and more uniform values, averaging between 40 and 50 mW/m^2.

Table 1 Summary of continental heat flow data. N is the number of sites and the heat flow is quoted as the mean ± standard deviation. The sources are: (a) Perry et al. (2010); (b) the Global Heat Flow Database of the International Heat Flow Commission at http://www.heatflow.und.edu/ (2010 revision); (c) Mareschal et al. (2000); (d) Goutorbe et al. (2007), as reported in the Global Heat Flow Database.

	Whole province			Within study area		
Area	**N**	**Heat flow (mW/m^2)**	**Source**	**N**	**Heat flow (mW/m^2)**	**Source**
Greenland				8	39.5 ± 8.7	b
Labrador (North Atlantic Craton)				4	21.5 ± 0.4	c
Superior Province	70	40.9 ± 7.3	a			
Grenville Province	30	41 ± 11	a	3	28.7 ± 8.6	b
Canadian Appalachians	43	56 ± 12	a	34	46.6 ± 8.6	b
Labrador Shelf				23	49.0 ± 6.2	d
Davis Strait				2	42 ± 6	d
Newfoundland Shelf				45	45.6 ± 13.5	d

3.3 CONTINENTAL GEOTHERMS

Continental geotherms in areas that have not undergone substantial lithospheric extension were estimated by assuming a constant mantle heat flow, which was set at 15 mW/m^2 following Perry et al. (2006, 2010). Homogenous crustal heat production was assumed and its value was adjusted on the basis of the local crustal thickness and the difference between the heat flow at the Moho and at the surface. As noted, for example, by Denlinger (1992) and McKenzie et al. (2005), it is advisable to include allowance for the temperature-dependence of thermal conductivity in the calculation of geotherms. This has been done using the formulation of Xu et al. (2004) to define the lattice component of mantle thermal conductivity and that of Hofmeister (1999) to define its radiative component. It is this temperature-dependence that gives the slight upward concavity in the deeper part of the geotherms (Figure 9), before they inflect sharply at the isentrope for the potential temperature at the base of the lithosphere (see further discussion below).

Figure 9 illustrates the sensitivity of the geotherms to surface heat flow (upper panel) and crustal thickness (lower panel). The calculated geotherm is relatively insensitive to crustal thickness, and this is conducive to the incorporation of the scheme into the gravity modelling methodology. Comparison with results from south-west Greenland (Sand et al., 2009) and north-east Canada (Kirkland Lake, c. 750 km west of the study area; Perry et al., 2010) suggests that the geotherms are compatible with trends identified by geothermobarometry using mantle xenoliths (Figure 9). The comparison indicates heat flows of between 20 mW/m^2 and 50 mW/m^2, which is in agreement with the limited observational data. In principle, it would be possible to use the pattern of surface heat flow as an input to the thermal and gravity modelling, and the software has been developed with this in mind (heat flow is input in the form of a grid). In practise, however, heat flow variation across the shield areas is so poorly resolved that it was decided to assume a uniform value of 40 mW/m^2 in these areas in the initial model described in this report. The sensitivity of the depth of the isostatic Moho to assumed heat flow has been examined using the software described in Section 5.1 and this indicates a rule of thumb that a change in heat flow of 10 mW/m^2 translates to a shift in the isostatic Moho of about 2 km (reducing the assumed heat flow deepens the isostatic Moho and vice versa).

3.4 OCEANIC GEOTHERMS

Oceanic geotherms were calculated using cooling half space (ocean age < 70 Ma) or plate (ocean age ≥ 70 Ma) models. An empirical correction for the effect of temperature on thermal conductivity was incorporated which provides a satisfactory fit to the calculations of Denlinger (1992) and McKenzie et al. (2005) over the required age range. Figure 10 uses this formulation and a contoured display to illustrate how temperature within the oceanic lithosphere varies with age and depth.

Estimates of the age of the ocean crust within the study area were based on the global grid of Müller et al. (2008), but with the continent-ocean boundary modified as a result of data analysis and literature review conducted for this study (Figure 11). In the Labrador Sea the continent-ocean boundary has been placed on the seaward side of the zone of transitional crust identified on both margins by Chian et al. (1995,b).

3.5 EFFECT OF CRETACEOUS RIFTING

As described above, the region was subjected to a period of rifting extending from the Early Cretaceous (c. 140 Ma) through to the onset of seafloor spreading in the earliest Palaeogene (62-65 Ma). Dickie et al. (2011) distinguish Early Cretaceous and Late Cretaceous phases of rifting, with the latter associated with mantle unroofing in the transition zone. Allowance has been made for the thermal effect of this continental rifting in the modelling, although it was not considered justifiable to attempt to incorporate multiple rift phases in the current simulation. Instead a rifting thermal anomaly was calculated using the method of McKenzie (1978), assuming instantaneous rifting in the mid-Cretaceous (110 Ma) with the extension factor based on the difference between modelled crustal thickness and reference thickness of 35 km.

3.6 THE LITHOSPHERE-ASTHENOSPHERE BOUNDARY

The lithosphere-asthenosphere boundary marks the transition from a regime in which conduction is the primary means of heat transfer to one in which convection dominates. From the point of view of the modelling discussed in this report, the key characteristic of this transition will be a marked reduction in geothermal gradient, due to the greater efficiency of convective heat transfer.

One way of estimating the thickness of the lithosphere is to extrapolate the geotherm until it intersects the isentrope (adiabat) of the convecting mantle (i.e. the temperature it would have if it was decompressed to atmospheric pressure, without any change in entropy). For example, McKenzie et al. (2005) assume an isentrope which has a potential temperature of 1315°C and a gradient of 0.5°C/km (see Figure 9). This provides guidance where the mantle solidus lies at temperatures well above those of the isentrope. However, if the geotherm approaches the solidus before reaching the isentrope, changes in rheology are likely to lead to a reduction in temperature gradient at shallower depth. One rule of thumb is that the base of the layer in which conductive heat transfer dominates lies at about 0.85 times the solidus temperature (Pollack and Chapman, 1977). A key factor controlling the mantle solidus is its volatile content, with the 'wet' mantle having lower solidus temperatures than 'dry' mantle, so there may be lateral variations associated with mantle heterogeneity.

The rheological change at the base of the lithosphere is detectable as the top of the low velocity zone, and this can provide important direct evidence. Kumar et al. (2005) investigated the depth to this boundary beneath the NW Atlantic region using the S-receiver function method. They estimated that it lay at a depth of 100-120 km beneath West Greenland (and shallower beneath central and east Greenland; cf. Petrunin et al., 2013). Comparison with the geotherms presented above (Figure 9) indicates that this is significantly shallower than the standard isentrope.

In the previous modelling conducted for the PmmP project, the 1100°C isotherm was used as a proxy for the base of the lithosphere, on the basis of an empirical comparison with the depth of

the low-velocity layer in the oceanic upper mantle (Kimbell, 2002; Kimbell et al., 2004). The same temperature had been suggested by Pollack and Chapman (1977), who noted a systematic relationship between a family of geotherms developed from a global heat flow compilation and the depth to the low velocity zone. Kukkonen (1998) used thermal simulations to infer that the lithosphere-asthenosphere boundary was approximated by the 1100°C isotherm beneath the Fennoscandian Shield. Kawakatsu et al. (2009) identified the boundary beneath the Pacific oceanic plate using receiver functions from ocean-bottom seismometers, and their results agree well with the 1100°C isotherm. Tesauro et al. (2009) also advocated using a temperatures below that of the mantle isentrope to define the base of the European lithosphere, and in that case used the 1200°C isotherm.

On the basis of the above considerations and also as a result of modelling trials using inputs from the present study area, the 1100°C isotherm has been retained as a proxy for the base of the lithosphere in the modelling discussed in this report. This may underestimate lithospheric thickness in dry upper mantle beneath the shield regions (see, for example, the geothermobarometric results in Figure 9) but, on current evidence, is regarded as the best working assumption for the intervening area.

3.7 SIMULATION OF LATERAL HEAT TRANSFER IN THE VICINITY OF THE CONTINENT OCEAN BOUNDARY

The above sections outline factors (temperature profiles in the shield areas, influence of Cretaceous rifting, development of the oceanic lithosphere) that contribute to the current thermal regime across the study area. The simulation methods discussed so far adopt a simple 1D assumption, but it is also necessary to consider 2D effects, particularly near the continent-ocean boundary where there will have been strong lateral thermal contrasts during the initiation of sea-floor spreading. This aspect was investigated using the THERMIC finite-element thermal modelling program (Bonneville and Capolsini, 1999). A model was constructed in which new oceanic lithosphere was constructed at a half spreading rate of 10 km/Ma and the evolution of the temperature ramp across the continent-ocean boundary monitored at different times after breakup. This analysis suggested the present-day thermal transition could be represented with reasonable accuracy by a ramp which varies in width linearly with the age of the ocean crust adjacent to the boundary: from 140 km wide where the age is 40 Ma to 200 km wide where the age is 100 Ma. This scheme is appropriate for the margins of the broader ocean basins, but not for the postulated narrow zone of oceanic lithosphere associated with the Ungava Fault Zone in the Davis Strait (Figure 11). In that case a model was developed which monitored the thermal evolution in the vicinity of a 50 km wide ‘dyke’ injected at 60 Ma. This was used to estimate present-day temperatures along the axis of the dyke and the widths of the thermal ramps on either side.

4 Three-dimensional gravity modelling method

4.1 SOFTWARE DEVELOPMENT

Previous regional gravity modelling for the PmmP project was conducted using software developed on Silicon Graphics Unix workstations. This included the isostatic, thermal and flexural routines developed within the project and the gravity computations using the Gmod program (Dabek and Williamson, 1999). More recently, the Geosoft Oasis montaj software package has been adopted for much of the BGS potential field processing and modelling, including 3D gravity and magnetic modelling using the GM-SYS program. This software is implemented in the PC environment and there would be inefficiencies in attempting to integrate it with legacy Unix-based routines. For this reason, the software development conducted for the present project included the implementation of the new PmmP routines as a Geosoft executable (GX) that can be run directly from Oasis montaj. It was more efficient to adapt the existing Fortran routines rather than re-write in the code (based on the C language) normally used for GX development. The method used has been described by Phillips (2007); it involves using ancillary C code to communicate between the Oasis montaj environment and the Fortran routines.

Figure 12 illustrates the new interface that can be invoked from within Oasis montaj. The program calculates continental and oceanic geotherms, including allowance for Cretaceous (pre-breakup) rifting on the latter, and applies the thermal 'ramp' corrections across the continent-ocean boundary. A geotherm is calculated at each grid node at 1 km depth intervals and mantle densities are calculated from the temperatures using the corrections for thermal expansion and overburden stress described by Kimbell (2002) and Kimbell et al. (2004). The densities are then averaged within five mantle 'layers' which fill the model between the Moho and its base at 200 km depth. The program can be used to modify the Moho such that the load at the 200 km horizon is equalised, i.e. local isostatic equilibrium is established. In this case several iterations are used to accommodate any changes in mantle density resulting from the Moho adjustment.

4.2 ROCK DENSITIES

Following the reasoning of Kimbell (2002; 2004), the average density of the crystalline crust in the model was set at 2.85 Mg/m^3 and the crust was divided into upper and lower layers of equal thickness and densities of 2.75 and 2.95 Mg/m^3 respectively. The shale compaction curve of Sclater and Christie (1980) was used to define the density variation within the sedimentary layer. Inspection of stratigraphic logs from around the region indicates that shale is the most common lithology, and comparison with the density log from the Qulleq-1 well on the West Greenland margin (Figure 13) suggests that the shale compaction curve is a reasonable compromise in that area.

The standard compaction curve was not considered appropriate in the Gulf of St Lawrence area in the south-western corner of the model, where the Maritimes Basin contains a thick sequence of Late Palaeozoic age (Dietrich et al., 2011) with velocities of 3.6 – 4.0 km/s (Jackson, 2002). In this case a uniform density of 2.50 Mg/m^3 was assumed for the sedimentary layer.

4.3 MODELLING PROCEDURE

The construction of a 3D model for the study area involved the following steps:

1. The program described in Section 5.1 was used to calculate the isostatic Moho across the whole region. In order to do this, the topographic input was adjusted to make allowance for the Greenland Ice Sheet using the ice thickness model of Bamber et al. (2001). The isostatic Moho was defined relative to a 'reference lithosphere' which had an average density (between datum and 200 km depth) of 3.2525 Mg/m^3, established by comparsion

with a range of deep seismic control (see below). This equates to a sea-level crustal thickness of 36.3 km when the heat flow is 40 mW/m^2.

2. The isostatic Moho was smoothed using a low-pass Butterworth filter with a central wavelength of 200 km and a degree of 8. The gravity field predicted by this model was calculated for comparison with the observations. In the onshore areas it was assumed that the Bouguer correction had removed the gravity effect of all material above the datum, which was used as the calculation surface for the subsequent modelling. This is an obvious simplification, but was considered adequate because intra-crustal density variations within the onshore area were not a primary target for the present project.

3. The Moho was optimised over the entire study area to reduce long-wavelength differences between observed and calculated fields. A low-pass filter with a ramp between 90 and 120 km was applied and, at this stage, a simple crystalline crust with a uniform density of 2.85 Mg/m^3 was assumed.

4. Seismic evidence suggests that relatively short wavelength Moho features can occur in the offshore area where it has been modified by high degrees of extension. For this reason a further inversion step was undertaken which was confined to the offshore (Labrador Sea through to Baffin Bay) area and employed a low-pass filter with a ramp between 50 and 70 km.

5. The top basement surface was optimised in order to provide a better fit with remaining shorter wavelength residual anomalies. In this case the low-pass filter had a ramp between 23 km and 33 km. This inversion step was excluded in areas where the basement is present at outcrop.

6. The single layer crust was replaced by one which was divided into upper and lower parts of equal thickness and densities of 2.75 Mg/m^3 and 2.95 Mg/m^3 respectively. Further optimisation steps were then undertaken on the Moho and top basement interfaces, with the shifts these introduced modified to reflect the influence of the resulting movement of the mid-crustal interface.

The modelling was initially conducted using a grid with 8 km node spacing, but this was refined to 4 km for the final stages of basement optimisation.

4.4 MODELLING RESULTS

The final optimised model is illustrated in the following figures and presented in digital form in the project GIS (see Appendix 2):

Figure 14 Depth to Moho (relative to datum)
Figure 15 Sediment thickness
Figure 16 Depth to top basement (relative to datum) in the offshore area
Figure 17 Thickness of crystalline crust
Figure 18 Calculated gravity field over the optimised model
Figure 19 Residual (observed – calculated) gravity field

The calculated field values are not directly comparable with the observed field shown in Figure 4 because the long-wavelength indirect effect (Chapman and Bodine, 1979) was added to the latter prior to inversion. This effect varies between -7 and + 14 mGal, increasing from west to east, and is allowed for in the residual anomalies shown in Figure 19.

It is difficult to convey the details of the contour values in A4 figures such as these, and the reader is referred to the GIS versions of the various model components (see Appendix 2) to interrogate these in more detail.

The overall root mean squared (rms) difference between observed and calculated fields is 8.93 mGal. As no attempt was made to model intra-crustal density variations in areas of basement

outcrop, these areas are generally characterised by more conspicuous short-wavelength residual gravity variations than the basinal (offshore) areas (Figure 19). If the calculation of the rms error is confined to the latter areas (as shown, for example, in Figure 16) it reduces to 5.21 mGal.

5 Analysis of the modelling results

The modelling results have been assessed by comparing the predicted crustal structure with the results of deep seismic experiments. Key interfaces have been digitised from the published models for 19 wide-angle/refraction seismic profiles across the region (Figure 20) and the equivalent interfaces extracted from the 3D model for comparison. In addition, the model has been compared with the results of receiver function analyses in both Greenland and Baffin Island (Kumar et al., 2007; Thompson et al., 2010). In Figure 21 the locations of the deep seismic experiments are superimposed on the modelled thickness of crystalline crust, together with the assumed location of the continent-ocean boundary. Further comparisons have been made with structural mapping from seismic reflection data, which did not form an input to the 3D model. The key consideration in that case was whether the gravity inversion has extracted information about basin configuration that is corroborated by other sources.

The model displays the expected contrast between thick (c. 40 km) crystalline crust beneath the areas of exposed basement to the north-east and west and much thinner crust in the intervening, extended region. The crust beneath the Davis Strait is distinctly thicker than that beneath Baffin Bay and the Labrador Sea. Minimum thicknesses of less than 6 km are encountered in parts of the oceanic area and the hyperextended segments of the continental margins.

The following discussion will first consider how well the model reproduces seismic estimates of crustal thickness in the areas of exposed basement and then analyse the results from the basinal area. For ease of illustration, northern (Baffin Bay – northern Davis Strait), central (Labrador Sea – southern Davis Strait) and southern (Newfoundland Shelf – Gulf of St Lawrence) sub-areas have been identified for display in greater detail (Figures 26, 33 and 41 respectively). Key named features have been given abbreviations to allow identification on the diagrams and these are listed in Appendix 1.

5.1 CRUSTAL THICKNESS IN AREAS OF EXPOSED BASEMENT

In Greenland, the mean difference between the receiver function Moho depth estimates and those derived from the 3D model is small (0.1 km), although the individual comparisons have a relatively large range of -8.8 to +6.4 km (Figure 20). The biggest discrepancies occur in the coastal strip, where there is rapid lateral variation in crustal thickness (Figure 21). The predicted crustal thickness pattern beneath Greenland reflects the bedrock topography, with the thickest crust beneath the elevated areas around the edges of the land mass, suggesting a strong isostatic influence (Figures 3 and 21). The modelling results are similar to those reported by Braun et al. (2007), although they do not suffer from the mismatches with seismic evidence in central Greenland noted by the latter authors, which were due in large part because they used earlier receiver function estimates (Dahl Jensen et al., 2003) rather than the recalculations by Kumar et al. (2007). The crustal thickening beneath the topographic highs in the present model is developed in a series of 'lozenges' beneath the higher ground. These generally coincide with local Bouguer gravity anomaly minima so may reflect density variations at shallower depth which are not properly simulated by the part of the model, leading to some distortion of optimised Moho topography.

The Moho depths calculated from receiver functions on Baffin Island are, on average, 2.8 km shallower than the interpolated values from the 3D model at the same site. Again the range is large (-7.6 to +5.5 km) and there are only 7 samples, so it was not considered justifiable to attempt to modify the modelling assumptions on the basis of this comparison. If further results suggest a significant bias it would be worth considering whether this is due to the heat flow assumption in the model (40 mW/m^2). As described above, an assumption of lower heat flow would result in greater crustal thickness estimates in the ratio of approximately 2 km for each 10 mW/m^2. Other factors that could influence the accuracy of the model are intra-crustal density variations and variations in the density of the mantle relating to chemical (depletion) rather than

thermal effects. Seismic experiments along the northern part of the Labrador coast (Line 4 of Funck and Louden, 1998 and Line 7 of Funck et al. 2006; Figures 22 and 23 respectively) detected the Moho at shallower depths than predicted by the 3D model, with the difference becoming more marked towards the south. The sense of this difference is opposite to what would be expected from the low heat flows measured in this area (Mareschal et al., 2000). Although the location of these lines along the edge of a zone of rapid crustal thickness change makes them less than ideal for such comparisons, reference to the results from a perpendicular line by Funck et al. (2000) suggest a geological explanation. That indicates a c. 5 km deepening of the Moho across the boundary between the North Atlantic (Nain) Craton and the Palaeoproterozoic orogenic belt to the west, with Moho depths in the latter area closer to those of the 3D model. The cratonic block contains the Nain Plutonic Suite, within which anorthositic and granitic rocks predominate. It is thus possible that the thinness of the cratonic crust in this area relates to its relatively low density.

In the southern part of Labrador, the model Moho lies within a zone of high-velocity lower crust detected beneath lines 2 and 3 of Funck et al. (2001) (Figures 24 and 25), indicating approximate compatibility (i.e. if high velocity lower crust were introduced into the 3D gravity model it would bracket the current, simple Moho). An axis of thicker crystalline crust in the 3D model extends east-west just south of the Grenville Front. This is a response to a conspicuous gravity anomaly low that can be correlated with crustal thickening in a 'keel' detected by seismic refraction surveys (Berry and Fuchs, 1973).

The Moho has been detected at a depth of about 35 km beneath Newfoundland by seismic methods (Hughes et al., 1994; Marillier et al., 1994), and this agrees well with the 3D model in this area. The local apparent Moho depression on the southern side of the island appears to be a distortion associated with the gravity effect of an upper-crustal granite pluton.

5.2 THE BAFFIN BAY AREA

Optimised sediment thickness variations and the observed magnetic field in the Baffin Bay area are shown in Figures 26 and 27 respectively. The most northerly seismic comparison in this area is provided by line 3 of Funck et al. (2006) (Figure 28) and line 2 of Reid and Jackson (1997) (Figure 29). The difference between these is large, with the interpretation of Funck et al. (2006) suggesting a broadly similar crustal thickness to the 3D model and the Reid and Jackson (1997) interpretation suggesting a substantially thinner crust than the gravity model. An underestimate of sediment thickness in the latter can only explain part of the mismatch. The implication of the seismic models is that there is a large step in the Moho (and this is shown explicitly on another of the refraction models of Reid and Jackson, 1997), but this is not necessary to explain the gravity observations, which are compatible with more gradual northward crustal thickening. In terms of the resolution of sedimentary basins, the model detects the Cretaceous and younger Northwater and Kiatak basins (**NKB** in Figure 26; Neben et al., 2004; Tessensohn et al., 2004). More detailed imaging shows that it resolves the northward trend of the former and north-westward trend of the latter, as inferred from seismic reflection data by Neben et al. (2004) and Tessensohn et al. (2004), and suggests that the Kiatak Basin extends further north-westwards that indicated by those authors. Farther south, the Carey Basin (**CB**) also has a northward trend, but there is no indication in the model of a linkage between it and the Northwater Basin.

Reid and Jackson (1997) detected a layer of anomalous character beneath the south-eastern part of their seismic refraction line 4 (Figure 30) and inferred that this was serpentinised upper mantle. The gravity model cannot distinguish serpentinised upper mantle from igneous oceanic crust, but does indicate thin crust in this area which is compatible with the former interpretation. In map view, it is clear that the line extends onto the north-western end of the extinct spreading axis in the northern part of Baffin Bay (**SA1** in Figure 26), which is characterised in the model by thicker sediments and thinning of the crystalline crust, so this seismic line may not provide

wholly representative sampling of the oceanic basement beneath Baffin Bay. There is evidence in the model of the offsets in this spreading axis noted by Oakey and Chalmers (2012).

The north-eastern part of Baffin Bay contains a series of north-west trending basins of probable Cretaceous age, of which the Melville Bay Graben (**MBG**; Whittaker et al, 1997) is the most prominent. The gravity model suggests that the basin is distinctly compartmentalised into northern and southern (**SMBG**) components, and supports the seismic reflection evidence for a thick basin fill (more than 6 s twt in the deepest, southern part of the basin shown in fig. 5b of Whittaker et al., 1997). A seismic refraction line across this part of the basin (the northern end of line AWI-200805 of Suckro et al., 2012; Figures 26 and 31) did not detect the full thickness of the sedimentary sequence as suggested by seismic reflection and gravity data, perhaps because the seismic energy was channelled along a relatively shallow intra-basin high. The gravity inversion produces a distinct basement high about 50 km west of the southern Melville Bay Graben, over which the sedimentary cover is modelled to be absent. Seismic data indicate that this area is, in fact, sediment covered (≥ 1s twt; Whittaker et al., 1997, fig. 5b) suggesting that the basement has a relatively high density here, perhaps because of an igneous intrusion, as suggested by Whittaker et al. (1997). There is, however, little indication of an intrusive body in the available magnetic data (Figure 27).

There are also Mesozoic basins on the Canadian margin of Baffin Bay (Jackson et al., 1992). In the north the Lady Ann Basin appears as a pronounced feature in the gravity inversion (**LAB** in Figure 26). Farther south, the Scott Graben (**SG**) is resolved as a linear, north-west-trending basin. Funck et al. (2012) detected a 4 km deep sedimentary basin close to the western end of line AWI-200806 (Figure 32), which the gravity model suggests might lie between deeper basins 50 km to the north and 80 km to the south.

The 3D model is broadly consistent with the results from AWI-200805 (Suckro et al., 2012) in showing thin (oceanic) crust along the central portion of this line (Figure 31). There is a mismatch in the location of the zone across which the crust thickens on the north side of the ocean basin, which is due to the response of the inversion to a gravity high at approximately 500 km along the profile. Suckro et al. (2012) noted the potential discrepancy in their gravity model and accommodated it by an increase in crustal density rather than decrease in crustal thickness. Such a density anomaly could be due to an extension of the feature on the west side of the Melville Bay Graben discussed above. A zone of sedimentary thickening at about 200 km on this profile (more pronounced in the gravity inversion than the seismic model) is associated with the extinct spreading axis in the southern part of Baffin Bay (**SA2**). As with the feature in the north (SA1), there is evidence of an offset in this axis. SA1 and SA2 are linked by the 64ºW Fracture Zone (**64W** in Figure 26; Chalmers and Pulvertaft, 2001), which is also characterised by an axis of thicker sediments. At the southern end of AWI-200805 Suckro et al. (2012) infer that the bathymetric shallowing and reduction in sediment thickness is compensated by a lateral reduction in crustal density rather than the increase in thickness predicted by the gravity inversion. The crust must thicken in the near vicinity though, as the coast (and probable crustal thickness of ≥ 35 km) lies only about 60 km from the end of the profile.

The 3D gravity inversion provides a reasonable simulation of the structure interpreted from seismic refraction line AWI-200806 (Funck et al., 2012) except for the zone between about 300 km and 400 km (Figure 32). There is an offset in the zone of crustal thickening on the eastern side of the oceanic basin that appears to be due to the incorrect partitioning of the gravity signature between the top basement and Moho interfaces in the inversion, which was in part driven by inaccuracies in the initial sediment thickness model. This is, however, the most poorly constrained part of the seismic model, because of deviation of the shot profile from the line (Funck et al., 2012). Both gravity and seismic models show an axis of sedimentary thickening at about 340 km associated with sedimentary thickening in the Ungava Fracture Zone. Funck et al. (2012) found it difficult to simulate the gravity effect of the basin using the seismically-defined structure and a density that was compatible with the inferred velocity of its fill (4.7 – 4.9 km/s)

and depth of burial. Gregersen and Bidstrup (2008; their figs. 2 and 5) illustrated the seismic reflection character of this basin to the south of the refraction line (where it is very pronounced in the gravity model) and called it the North Ungava Basin (**NUB** in Figure 26). It lies between the northern part of the Davis Strait High (**DSH**) in the east and the Kangerluk Structure (**KS**; Gregersen and Bidstrup, 2008) in the west. In the gravity model this basin appears to link through to the Aasiaat Basin (**AB**) of Gregerson and Bidstrup (2008) towards the north, through a depocentre at 58.3ºW, 69ºN which correlates well with a seismic feature (Gregersen and Bidstrup, 2008, their fig. 15). There are contrasting interpretations of the age of the Aasiaat Basin, with Gregerson and Bidstrup (2008) assigning Cretaceous ages to reflectors they trace across it, and Funck et al. (2012) and Oakey and Chalmers (2012) contending that the western side of the basin (which contains the depocentre mentioned above) is floored by Paleocene oceanic crust.

The Nuussuaq Basin (**NUB**) underlies the eastern part of Disko Island and Disko Bugt. Analysis of seismic and potential field data indicates that Mesozoic sediments locally reach thicknesses of 6 km or more in this basin, adjacent to faults that bound half-grabens (Chalmers et al., 1999). The 3D model provides some indication of the areas of thicker sediments, but does not resolve these local deepenings.

5.3 THE DAVIS STRAIT AREA

The Davis Strait area is characterised by extensive Paleocene volcanic rocks, including seaward-dipping reflectors in its north-western part (Skaarup et al., 2006). The Ungava Fault Zone formed a transform through this area, linking oceanic spreading in the Labrador Sea and Baffin Bay (Figure 11). The 3D model clearly indicates thicker crust beneath the Davis Strait than beneath the ocean basins to the north and south (Figure 21). Modelled sediment thickness and magnetic images for this area are shown in Figures 33 and 34 respectively.

Line AWI-200807 (coincident with seismic reflection profile BGR08-301) revealed a c. 45 km zone of high velocity crust beneath Ungava Fault Zone in the northern part of the strait which was interpreted as either highly stretched and heavily intruded continental crust or new igneous crust (Suckro et al., 2013; Figure 35). The 3D model simulates this by a reduction in the thickness of the crystalline crust above denser mantle (Figure 35). On either side of this anomalous zone the modelled crustal thickness is deeper than that interpreted from the seismic refraction data. In the west this can in part be explained by the seismic ray coverage (the seismic Moho is not constrained west of 30 km), but there is also the fact that the seismic survey detected a basaltic layer in this area which probably has a lower density than upper crystalline crust and which was not included in the gravity model.

Farther south the NUGGET-1 seismic refraction profile also detected a zone of high velocity crust in the vicinity of the Ungava Fault Zone, which was interpreted as oceanic crust formed in a leaky transform during phases of transtension and subsequently underplated by material flowing southwards from the Greenland-Iceland plume (Funck et al., 2007). Comparison with the 3D model (Figure 36) indicates that the latter overestimates the depth to Moho in areas away from the high velocity crust and that this discrepancy is too large to be explained by shortcomings in the cover sequence model. The latter shows a deep basin at 260 km, at the eastern edge of the zone of oceanic crust. There is an indication of this in seismic reflection data (Funck et al., 2007, their fig. 16) although the refraction interpretation suggests that there is only a modest velocity contrast with the rocks on either side (Funck et al., 2007, their fig. 11).

The NUGGET-2 seismic refraction profile extends from continental crust of the Davis Strait in the north to oceanic crust of the Labrador Sea in the south. The 3D model predicts a similar Moho depth in the south but there is divergence towards the north with the modelled Moho lying at greater depth (Figure 37). The discrepancy cannot be fully explained by an underestimate in sediment thickness, so the results from this profile join those from NUGGET-1 (Funck et al., 2007) and AWI-200807 (Suckro et al., 2013) in indicating that the Moho from the gravity model

lies at greater depth than the seismic Moho in the Davis Strait area. This does not apply a short distance to the east, where modelled Moho lies at similar or shallower depth to a high velocity zone at the base of the crust detected by Gohl and Smithson (1993) beneath a refraction profile close to the Greenland coast (Figures 33 and 38). The discrepancy is unlikely to be due to the crustal density assumed in the gravity modelling because that is towards the low end of the range of possibilities, given the evidence for underplating from the seismic experiments. A more likely explanation is that the upper mantle has a relatively low density beneath the Davis Strait. This might be either because it is hotter than assumed in the modelling or because it is more depleted (as a result of melt extraction). It may be possible to distinguish between these possibilities as more heat flow data become available. The very limited data currently in the public domain do not suggest a conspicuous heat flow anomaly: Goutorbe et al. (2007) estimated values of 36 mW/m^2 and 48 mW/m^2 respectively for the Ralegh N-18 in Gjoa G-37 wells which lie at 96 km and 286 km respectively along the NUGGET-1 profile.

The gravity model resolves a number of cover sequence structures along the east side of Davis Strait which have previously been identified from seismic reflection data (e.g. Dalhoff et al., 2003; Sorensen, 2006). For example the Sisimiut Basin (**SIB**), Kangâmiut Basin (**KB**), Nuuk Basin (**NB**) and Fylla West High (**FWH**) can be identified along the West Greenland margin. Toward the centre of the strait, the Davis Strait High (**DSH**) and Hecla High (**HH**) are clearly identifiable, but sediment thickness within the Lady Franklin Basin (**LFB**) is substantially underestimated (cf. Sorensen, 2006), primarily because of shortcomings in the initial sediment thickness model.

5.4 THE LABRADOR SEA MARGINS

Conjugate seismic refraction profiles 88R2 and 90R1 are key in defining the deep structure on the South-west Greenland and Labrador margins respectively (Figure 33; Chian and Louden, 1994; Chian et al., 1995a, b). Comparison with the 3D model (Figures 39 and 40) indicates that it has replicated the structure beneath these profiles reasonably well, although there is a mismatch in the crustal thickening at the north-eastern end of 88R2 which is partly due to an underestimate of sediment thickness in the 3D model and partly due to lack of ray coverage at the end of the seismic profile. The transition zone is well resolved as a zone of minimum modelled crustal thickness on line 90R1, but is less clear on 88R2. However, inspection of the map view (Figure 21) indicates conjugate zones of crustal thinning which coincide with the transition zones on these profiles and extend about 250 km to the north-west of both profiles before grading into thicker crust as the Davis Strait is approached. There is a contrasting gravity response on the two profiles. On 90R1, a major gravity high occurs over the thick sedimentary sequence on the south-western side of the profile, indicating that the younger sediments have been deposited on relatively strong lithosphere, which has supported them at a shallower level than they would occupy if they were in isostatic equilibrium. The coincidence of the eastern edge of the gravity high with the western edge of the transition zone may simply be a consequence of the present-day position of the shelf edge, but it is possible that lithospheric weakening associated with the serpentinisation in the transition zone also plays a role. On profile 88R2 there is little indication of a sediment loading gravity anomaly (the bipolar anomaly at the eastern end of the profile is interpreted as an edge effect associated with the rapid change in crustal thickness).

The oceanic crust is generally less than 8 km thick beneath the Labrador Sea (Figure 21), and is modelled to be thinnest beneath the extinct spreading axis, which is also marked by sedimentary thicknening (**LSA** in Figure 33). The early ocean crust beneath the north-western part of the Labrador Sea is relatively thick in the model (Figure 21), suggesting that the factor responsible for the first (Paleocene) phase of magmatism in the Davis Strait area (the proto Greenland-Iceland plume?) also influenced crustal production in the adjacent ocean basin. Thickening of the oceanic crust immediately south of southern Greenland appears to be due to a local volcanic plateau of this age (Nielsen et al., 2002). Farther south, on the opposite side of the ocean basin, comparison with the ocean age model (Figure 11) indicates zones of crustal thickening

associated with both the Paleocene and later (latest Paleocene – Early Eocene) magmatic phases, in the vicinity of the triple junction that developed at the mouth of the Labrador Sea.

The model indicates a striking asymmetry in the development of Mesozoic basins along the Labrador Sea margins. On the Canadian side are the major Saglek Basin (**SB**) and Hopedale Basin (**HB**), while on the Greenland side the basins are more modest. Chalmers and Pulvertaft (2001) explained this in terms of displacement of the axis of final breakup toward the Greenland margin. The gravity inversion has introduced a lot more detail into the structure of the Saglek and Hopedale basins than was present in the initial model (compares Figures 7 and 33). The optimised basin structure is noticeably simpler outboard of the Okak Arch (**OA**) and Cartwright Arch (**CA**) (Balkwill, 1987).

More exploration data are available for the Labrador Shelf than for other parts of the study area, allowing comparisons with seismic mapping (e.g. Bell, 1989; Martin, 2007) and well intersections (information available from http://www.cnlopb.nl.ca/well_intro.shtml). These suggest that the optimised model is inaccurate in the quantitative definition of depth to basement, but that it has resolved structural patterns that are corroborated by the available seismic mapping. The inaccuracy stems in part from the simplified and regional nature of the model, but there is also evidence of incipient instability in the inversion leading to exaggeration of basement topography.

The boundary between the Hopedale Basin and the Hawke Basin (**HWB**) lies at an east-north-east-trending transfer zone which appears to be the continental precursor of the oceanic Cartwright Fracture Zone (**CFZ** in Figure 33). Comparison with the basement geology (Figure 2) suggests that these may have been inherited from structures associated with the Grenville Front. An adjacent structure with a more easterly trend lies 50-100 km south of this lineament and is marked by an axis of modelled sedimentary thickening and a distinct magnetic low (Figure 34).

5.5 THE NORTHEAST NEWFOUNDLAND SHELF

Valuable seismic control across the Northeast Newfoundland Shelf is provided by the combination of seismic refraction (86-6, 86-8) and reflection (84-3) profiles interpreted by Chian et al. (2001), which extend from close to the Newfoundland coast to the continent-ocean boundary just south of Orphan Knoll (**OK**; Figures 41 and 42). The 3D model reproduces many of the features of their final composite interpretation (Figure 43), except for the zone of crustal thickening at c. 250 – 350 km. The conspicuous gravity anomaly high at 100-250 km is a sediment-loading anomaly, indicating relatively strong lithosphere, and this is compatible with a its thin crustal (relatively weak) component and correspondingly thicker, relatively strong upper mantle component.

Modelled Moho depths in the south-eastern extremity of the study area agree well with those interpreted at the north-western ends of the SCREECH (Study of Continental Rifting and Extension on the Eastern Canadian Shelf) seismic refraction profiles in the Grand Banks - Flemish Cap area (Funck et al., 2003; Van Avedonk et al., 2006; Lau et al., 2006).

Comparison of the sediment thickness model (Figure 41) with structural maps (Edwards et al., 2003; Enachescu, 2005) indicates that the gravity inversion has successfully resolved many of the key features in this area, including the major Mesozoic basins and aspects of their internal structure. This includes the West Orphan Basin (**WOB**) East Orphan Basin (**EOB**), Jeanne d'Arc Basin (**JB**) Flemish Pass Basin (**FPB**) and Flemish Cap Basin (**FCB**) (Figure 41). The Palaeozoic St Anthony Basin (**SAB**; Dietrich et al., 2011) is also detected, although the local apparent sedimentary thickening within it may be the result of instability in the inversion. Structures in the northern part of the Orphan Basin generally have a north to north-west strike whereas in the southern part of the basin there is a zone of east-west structures (e.g. the Cumberland Ridge, **CUR**). Comparison with the magnetic map (Figure 42) suggests that the east-west structures may have been inherited from the basement, as they closely follow a

magnetic anomaly belt which is probably associated with Neoproterozoic calc-alkaline plutons in the Avalonian basement (Haworth and Lefort, 1979).

5.6 GULF OF ST LAWRENCE

This area lies outside the main (Labrador Sea to Davis Strait) area of interest so only received limited attention. A simple (and poorly constrained) density model was assumed which assigned a fixed density of 2.5 Mg/m^3 to the low density (mainly Upper Palaeozoic) parts of the cover sequence and 'basement' density (2.75 Mg/m^3) to the remainder of this sequence. The model resolves the Magdalen (**MB**) and Sydney (**SB**) Upper Palaeozoic basins (Dietrich et al., 2011) and also a thickening of low density (mid Palaeozoic?) rocks adjacent to the Appalachian Structural Front in the Anticosti Basin (**AB**).

Seismic refraction and reflection data have used to interpret a high-velocity underplated zone beneath the central part of the Magdalen Basin, lying between depths of about 25 km and 43 km, whereas towards the north-west edge of the basin a simple Moho has been identified at a depth of about 36 km (Marillier and Reid 1990; Jackson, 2002). The Moho from the 3D model is shallower, lying at a depth of 27 km beneath the centre of the basin and 30-35 km beneath its north-west side.

5.7 SOUTH-EAST GREENLAND

Again, this was a low-priority area, but included because of the availability of deep seismic control. Comparison with results from the SIGMA 4 seismic profile (Holbrook et al., 2001; location shown in Figure 20) suggest good agreement over the oceanic crust in the east including thickening towards the continent-ocean boundary (Figure 44). Farther west on this profile the modelled Moho lies at greater depth than indicated by the seismic interpretation, in part because of lack of allowance for a thick basalt sequence in the cover sequence model. Comparison with the SIGMA-3 profile farther north also indicates a seismic Moho which is significantly shallower than predicted by the 3D model (Figure 45). This line lacks ray coverage at Moho depth west of about 80 km (Holbrook et al., 2001, their fig. 3), but there is still a disparity of up to c. 6 km in the constrained part of the model. There is thus a suggestion that the modelling assumptions are becoming invalid in this area, but this is not considered proven on the basis of comparison with seismic refraction profile DLC94-5, which is a strike line in the critical area (Figure 46; location shown in Figure 20). The 3D model shows a Moho at around 35 km, which lies within, or close to the top of, a zone of high-velocity lower crust identified in the seismic experiment (Dahl Jensen et al., 1998).

6 Conclusions and recommendations

This report describes the construction of a three-dimensional lithospheric model for the Labrador Sea – Davis Strait – Baffin Bay region based on gravity modelling and employing data sources that are in the public domain. The region includes magma-poor and magma-rich conjugate continental margins with a cumulative strike-length of more than 60000 km. The methodology was developed from that originally devised for the Passive Margins Modelling Project (PmmP; Kimbell, 2002; Kimbell et al., 2004), with the adaptations relating to changes in the computational platform and the geological regime.

Modifications to the modelling methodology involved incorporating the ability to construct a spatially varying thermal model of the continental lithosphere which took into account variations in pre-breakup lithospheric extension and/or surface heat flow. These have only been applied in a simple fashion in the current model – assuming a simple (instantaneous) mid-Cretaceous rifting episode and a constant heat flow away from the rifted margins – but they have proved stable in their application and have the potential for more ambitious implementations.

Model optimisation involved modifications to Moho and top basement interfaces based on the long and short wavelength components of the observed gravity field respectively. Variations in the depth of the resulting Moho interface are comparable to the results of seismic experiments across a range of environments, including cratonic basement, transitional (hyperextended, non-volcanic) zones on the continental margins, thicker crust on the volcanic margins and oceanic crust of different ages. In detail, there are departures from the Moho identified using seismic interpretation which can be ascribed to a variety of causes:

- Inaccuracies in the cover sequence model. For example, an underestimate in cover sequence thickness (perhaps because of lack of data or the influence of volcanic rocks on the original sediment thickness compilation) will lead to an overestimate in Moho depth.
- Variations in crustal density not allowed for in the gravity model. Examples of this occur over the low-density Nain Plutonic Suite on the eastern Labrador coast and in areas where high velocity lower crust is indicated by seismic experiments.
- Variations in upper mantle density not allowed for in the modelling. An example of this occurs beneath the Davis Strait, where an overestimate of Moho depth is ascribed to either an underestimate of mantle temperatures or a zone of relatively depleted upper mantle.
- Shortcomings in the seismic database. There are instances where comparisons with the 3D modelling results help to highlight inconsistencies between different seismic interpretations.

The first point noted above highlights the importance of the starting cover sequence model in investigations of this type. The starting model does not have to be detailed but it has to place the top basement interface at the right general level to produce an effective result. Large errors in the initial model will not be recovered by the optimisation process because they will be absorbed, at least in part, by distortion of the Moho interface (i.e. incorrect partitioning of the gravity response between the two optimised horizons). This may appear an impediment to the application of the method in true frontier areas, but in fact progress is often possible even where seismic control is very limited. Careful analysis of observed and residual gravity fields and an iterative approach to the development of the initial cover sequence model (perhaps testing several alternatives) can pay dividends. It is also important, when taking a more detailed approach, to refine the density model for the cover sequence, explicitly incorporating volcanic and/or overcompacted layers where appropriate. Comparison of more detailed investigations within the area of the original PmmP study (e.g. Kimbell et al., 2010 and several unpublished studies) indicates the progress that can be made, even in areas with severe deep seismic imaging problems such as the Hatton Basin.

The approach to modelling cover sequence thickness within the current project is at a comparable, simple level to that in the original PmmP study (Kimbell, 2002; Kimbell et al., 2004, 2005). There is evidence that the optimisation has resolved basin structures that were not present in the initial model, for example on the margins of Baffin Bay and in the Hopedale and Orphan basins, but the calibration of top basement depth is often inaccurate and resolution is poor in areas where volcanic rocks are present. From the published literature and recent/current activity in the area it is clear that the seismic and well database would allow a more detailed approach to the cover sequence, as outlined in the preceding paragraph, and this could perhaps focus on particular subareas in collaboration with researchers with local knowledge.

There is potential for a much more integrated approach to 3D modelling and seismic refraction interpretation and this could be used to address some of the discrepancies outlined above and help in the design of new seismic experiments. For example it would be straightforward to build a routine that would generate an input file for the commonly-used RAYINVR ray-tracing program (Zelt and Smith, 1992) along any line across the 3D model.

Given the capabilities of the PmmP routines and the areas over which they have been applied to date, there is a clear opportunity to extend them to an investigation of the East Greenland margin. North-east Greenland is a frontier area with developing seismic databases that is attracting considerable interest. There is an absence of well control but the methodology has built-in assumptions regarding sediment density and compaction trends that can be employed in the construction of reconnaissance models and tested by comparison with seismic observations. The South-east Greenland margin and Greenland-Iceland Ridge would hold less interest with regard to the investigation of Mesozoic basins but mapping of the oceanic crustal thickness pattern adjacent to this margin and comparison with its conjugate (Kimbell et al., 2005) could provide very valuable. Features which are mirrored across the ocean basin will have been formed synchronously at the mid-ocean ridge and thus allow reliable identification of temporal variations in magmatic productivity at different locations along the ridge. This can, in turn, be interpreted in terms of potential impact on the continental margins at different times during their evolution, for example through changes in differential gravitational potential energy (‘ridge-push’).

On a different theme, the developments to the modelling methodology makes it more adaptable to the investigation of the interiors of the continents as well as their margins, and would be an interesting companion to, for example, receiver function studies in the investigation of such regions. It would be possible, for example, to extend the models across Greenland to allow comparison of the cratonic area with the Caledonides and also investigate the influence of the possible ‘hot-spot’ beneath the centre of that country (Petrunin et al., 2013).

Appendix 1 Abbreviations for structural elements

The following abbreviations are employed in figures within this report and in a layer within the project GIS (see Appendix 2).

Code	Feature
64W	64 Degree West Fracture Zone
AB	Aasiaat Basin
ANB	Anticosti Basin
BP	Bonavista Platform
CA	Cartwright Arch
CB	Carey Basin
CBNR	Cape Breton - Newfoundland Ridge
CFZ	Cartwright Fracture Zone
CR	Central Ridge
CUR	Cumberland Ridge
DSH	Davis Strait High
EOB	East Orphan Basin
FC	Flemish Cap
FCB	Flemish Cap Basin
FPB	Flemish Pass Basin
FWH	Fylla West High
GB	Glacier Basin
HB	Hopedale Basin
HH	Hecla High
HSB	Hudson Strait Basin
HWB	Hawke Basin
JB	Jean d'Arc Basin
JSB	Jones Sound Basin
KB	Kangâmiut Basin
KS	Kangerluk Structure
KYB	Kap York Basin

Code	Feature
LAB	Lady Anne Basin
LFB	Lady Franklin Basin
LSA	Extinct spreading axis in the Labrador Sea
LSB	Lancaster Sound Basin
MB	Magdalen Basin
MBG	Melville Bay Graben
NB	Nuuk Basin
NKB	North Kivioq Basin
NKB	Northwater - Kiatak basins
NP	Nuuk Platform
NUB	North Ungava Basin
NUUB	Nuussuaq Basin
OA	Okak Arch
OK	Orphan Knoll
SA1	Extinct spreading axis in northern Baffin Bay
SA2	Extinct spreading axis in southern Baffin Bay
SAB	St Anthony Basin
SB	Saglek Basin
SG	Scott Graben
SIB	Sisimiut Basin
SKB	South Kivioq Basin
SMBG	Southern part of the Melville Bay Graben
SYB	Sydney Basin
WOB	West Orphan Basin

Appendix 2 GIS components

A GIS is included on the DVD produced by this project. It contains the elements used to create the map figures in this report, including gridded versions of the geophysical fields and model interfaces (allowing further manipulation and display of these by the user). The contents of the 'gis' folder should be copied to the user's system without altering their arrangement. The GIS can then be viewed by opening the file **pmmp_labrador_baffin.mxd** (compatible with ArcMap versions 9.3.1 and later). The model displays are organised in group layers containing the model grid, coloured as in the report figures, overlain by contours generated from this grid. The grids are at their original resolution (4 km node spacing) whereas interpolated versions were used when generating the report figures, which consequently have smoother colour boundaries.

The various GIS components (shapefiles, images and grids) are listed below, organised according to the subfolders into which they are organised in the file structure. Not all of these components are pre-loaded in the mxd supplied.

Shapefiles	
annotated_features.shp	Feature labels (abbreviations) as used in Figures 26, 27, 33, 34, 41 and 42 of this report (see Appendix 1)
basement_elements.shp	Main basement elements (Figure 2 of this report)
canadian_receiver_function.shp	Canadian receiver function sites (after Thompson et al., 2010)
coast.shp	Coastline, based on the Global Self-consistent Hierachical, High-resolution Shoreline (GSHHS, Version 1.3; Wessel and Smith, 1996).
cob.shp	Continent-ocean boundary (approximate)
greenland_receiver_function.shp	Greenland receiver function sites (after Kumar et al., 2007 and Dahl Jensen, 2003)
seismic_lines.shp	Seismic lines used for comparisons with the 3D modelling results
study_area.shp	Study area rectangle. Use with Data Frame Properties > Data Frame > Clip to Shape within the GIS if appropriate.
Geophysical grids	
gravity	Bouguer gravity anomalies onshore and free-air gravity anomalies offshore (mGal). See Section 2.2 for details of the data compilation.
icethk	Thickness of the Greenland Ice Sheet in metres (after Bamber et al., 2001)
mag_gammaa5	Total magnetic field grid (nT) based on the GAMMAA5 compilation (Verhoef et al., 1996)
mag_gsc	Total magnetic field grid (nT) based on data from the Canadian Aeromagnetic Database (Geological Survey of Canada)
ocean_age	Age of ocean crust (Ma; modified from Müller et al., 2008)
topography	Topographic grid (m) based on SRTM30_PLUS (Becker et al., 2009)
Geophysical images	
grav_csrw.jpg	Gravity image generated from above grid (Figure 4 in the report). Colour shaded-relief with illumination from the west.
grav_calc_csrw.jpg	Gravity field calculated from the 3D model (Figure 18 in the report). Colour shaded-relief with illumination from the west.
mag_gammaa5_csrw.jpg	Magnetic image generated from the GAMMAA5 compilation (Verhoef et al., 1996) (Figure 5 in the report). Colour shaded-relief with illumination from the west.
mag_gsc_csrw.jpg	Magnetic image based on the Canadian Aeromagnetic Database (Figure 6 in the report). Colour shaded-relief with illumination from the west.

topo_csrn.jpg	Topographic image generated from SRTM30_PLUS model (Becker et al., 2009) (Figure 1 in the report). Colour shaded-relief with illumination from the north.
Model contours	
crysthk_conts.shp	Contours of modelled thickness of crystalline crust (2000 m intervals)
moho_conts.shp	Contours of modelled Moho depth (2000 m intervals)
sedthk_init_conts.shp	Initial sediment thickness contours (1000 m intervals)
sedthk_opt_conts.shp	Optimised sediment thickness contours (1000 m intervals)
topbsmnt_init_conts.shp	Initial top basement contours (1000 m intervals)
topbsmnt_opt_conts.shp	Optimised top basement contours (1000 m intervals)
Model grids	
crysthk	Modelled thickness of crystalline crust (m)
grav_calc	Calculated gravity field (mGal)
grav_obs	Observed gravity field, including the indirect effect (mGal)
Moho	Modelled depth to Moho (m relative to datum)
sedthk_init	Initial sediment thickness (m)
sedthk_opt	Optimised sediment thickness (m)
topbsmnt_init	Initial top basement (m relative to datum)
topbsmnt_opt	Optimised top basement (m relative to datum)

References

British Geological Survey holds most of the references listed below, and copies may be obtained via the library service subject to copyright legislation (contact libuser@bgs.ac.uk for details). The library catalogue is available at: http://geolib.bgs.ac.uk.

BALKWILL, H R. 1987. Labrador Basin: structural and stratigraphic style. 17-43 in *Sedimentary basins and basin-forming mechanisms*. BEAUMONT, C, and TANKARD, A J (editors). *Memoir of the Canadian Society of Petroleum Geologists,* No. 12.

BAMBER, J L, LAYBERRY, R L, and GOGINENI, S P. 2001. A new ice thickness and bed data set for the Greenland ice sheet: 1. Measurement, data reduction, and errors. *Journal of Geophysical Research: Atmospheres*, Vol. 106, 33773-33780.

BECKER, J J, SANDWELL, D T, SMITH, W H F, BRAUD, J, BINDER, B, DEPNER, J, FABRE, D, FACTOR, J, INGALLS, S, KIM, S H, LADNER, R, MARKS, K, NELSON, S, PHARAOH, A, TRIMMER, R, VON ROSENBERG, J, WALLACE, G, and WEATHERALL, P. 2009. Global Bathymetry and Elevation Data at 30 Arc Seconds Resolution: SRTM30_PLUS. *Marine Geodesy*, Vol. 32, 355-371.

BELL, J S. 1989. *East Coast Basin Atlas Series. Volume 1: Labrador Sea*. (Halifax, Nova Scotia: Geological Survey of Canada.)

BERRY, M J, and FUCHS, K. 1973. Crustal structure of the Superior and Grenville provinces of the Northeastern Canadian Shield. *Bulletin of the Seismological Society of America*, Vol. 63, 1393-1432.

BIZZARRO, M, and STEVENSON, R. 2003. Major element composition of the lithospheric mantle under the North Atlantic craton: Evidence from peridotite xenoliths of the Sarfartoq area, southwestern Greenland. *Contributions to Mineralogy and Petrology*, Vol. 146, 223-240.

BONNEVILLE, A, and CAPOLSINI, P. 1999. THERMIC: a 2-D finite-element tool to solve conductive and advective heat transfer problems in Earth Sciences. *Computers & Geosciences*, Vol. 25, 1137-1148.

BRAUN, A, KIM, H R, CSATHO, B, and VON FRESE, R R B. 2007. Gravity-inferred crustal thickness of Greenland. *Earth and Planetary Science Letters*, Vol. 262, 138-158.

CHALMERS, J A. 1991. New evidence on the structure of the Labrador Sea/Greenland continental margin. *Journal of the Geological Society*, Vol. 148, 899-908.

CHALMERS, J A, and LAURSEN, K H. 1995. Labrador Sea - the extent of continental and oceanic-crust and the timing of the onset of sea-floor spreading. *Marine and Petroleum Geology*, Vol. 12, 205-217.

CHALMERS, J A, and PULVERTAFT, T C R. 2001. Development of the continental margins of the Labrador Sea: a review. *Geological Society, London, Special Publications*, Vol. 187, 77-105.

CHALMERS, J A, PULVERTAFT, T C R, MARCUSSEN, C, and PEDERSEN, A K. 1999. New insight into the structure of the Nuussuaq Basin, central West Greenland. *Marine and Petroleum Geology*, Vol. 16, 197-224.

CHAPMAN, M E, and BODINE, J H. 1979. Considerations of the indirect effect in marine gravity modeling. *Journal of Geophysical Research: Solid Earth*, Vol. 84, 3889-3892.

CHIAN, D P, and LOUDEN, K E. 1994. The continent-ocean crustal transition across the southwest Greenland margin. *Journal of Geophysical Research: Solid Earth*, Vol. 99, 9117-9135.

CHIAN, D P, KEEN, C, REID, I, and LOUDEN, K E. 1995a. Evolution of nonvolcanic rifted margins - new results from the conjugate margins of the Labrador Sea. *Geology*, Vol. 23, 589-592.

CHIAN, D P, LOUDEN, K E, and REID, I. 1995b. Crustal structure of the Labrador Sea conjugate margin and implications for the formation of nonvolcanic continental margins. *Journal of Geophysical Research: Solid Earth*, Vol. 100, 24239-24253.

CHRISTIANSEN, F G, BOJESEN-KOEFOED, J A, CHALMERS, J A, DALHOFF, F, MATHIESEN, A, SØNDERHOLM, M, DAM, G, GREGERSEN, U, MARCUSSEN, C, NØHR-HANSEN, H, PIASECKI, S, PREUSS, T, PULVERTAFT, T C R, RASMUSSEN, J A, and SHELDON, E. 2001. Petroleum geological activities in West Greenland in 2000. *Geology of Greenland Survey Bulletin*, Vol. 189, 24-33.

DABEK, Z K and WILLIAMSON, J P. 1999. Forward and inverse wavenumber formulae for the gravity and magnetic responses of layered models. *British Geological Survey Technical Report* WK/99/03C.

DAHL-JENSEN, T, THYBO, H, HOPPER, J, and ROSING, M. 1998. Crustal structure at the SE Greenland margin from wide-angle and normal incidence seismic data. *Tectonophysics*, Vol. 288, 191-198.

DAHL-JENSEN, T, LARSEN, T B, WOELBERN, I, BACH, T, HANKA, W, KIND, R, GREGERSEN, S, MOSEGAARD, K, VOSS, P, and GUDMUNDSSON, O. 2003. Depth to Moho in Greenland: receiver-function analysis suggests two Proterozoic blocks in Greenland. *Earth and Planetary Science Letters*, Vol. 205, 379-393.

DALHOFF, F, CHALMERS, J A, GREGERSEN, U, NØHR-HANSEN, H, AUDUN RASMUSSEN, J, and SHELDON, E. 2003. Mapping and facies analysis of Paleocene–Mid-Eocene seismic sequences, offshore southern West Greenland. *Marine and Petroleum Geology*, Vol. 20, 935-986.

DENLINGER, R P. 1992. A revised estimate for the temperature structure of the oceanic lithosphere. *Journal of Geophysical Research: Solid Earth*, Vol. 97, 7219-7222.

DICKIE, K, KEEN, C E, WILLIAMS, G L, and DEHLER, S A. 2011. Tectonostratigraphic evolution of the Labrador margin, Atlantic Canada. *Marine and Petroleum Geology*, Vol. 28, 1663-1675.

DIETRICH, J, LAVOIE, D, HANNIGAN, P, PINET, N, CASTONGUAY, S, GILES, P, and HAMBLIN, A. 2011. Geological setting and resource potential of conventional petroleum plays in Paleozoic basins in eastern Canada. *Bulletin of Canadian Petroleum Geology*, Vol. 59, 54-84.

EDWARDS, T, JAUER, C D, MOIR, P, and WIELENS, J B W. 2003. Tectonic elements, Grand Banks of Newfoundland (East Coast Basin Atlas Series). *Geological Survey of Canada, Open File* 1795 (ftp://ftp2.cits.rncan.gc.ca/pub/geott/ess_pubs/214/214599/of_1795.pdf).

ENACHESCU, M. 2005. Regional setting, representative transects and petroleum potential of the Orphan Basin, offshore Newfoundland and Labrador. http://www.pr-ac.ca/files/files/154_GeologicalSummary_Oct05.pdf.

FUNCK, T, and LOUDEN, K E. 1998. Wide-angle seismic imaging of pristine Archean crust in the Nain Province, Labrador. *Canadian Journal of Earth Sciences*, Vol. 35, 672-685.

FUNCK, T, LOUDEN, K E, and REID, I D. 2000. Wide-angle seismic imaging of a Mesoproterozoic anorthosite complex: The Nain Plutonic Suite in Labrador, Canada. *Journal of Geophysical Research: Solid Earth*, Vol. 105, 25693-25707.

FUNCK, T, LOUDEN, K E, and REID, I D. 2001. Crustal structure of the Grenville Province in southeastern Labrador from refraction seismic data: evidence for a high-velocity lower crustal wedge. *Canadian Journal of Earth Sciences*, Vol. 38, 1463-1478.

FUNCK, T, HOPPER, J R, LARSEN, H C, LOUDEN, K E, TUCHOLKE, B E, and HOLBROOK, W S. 2003. Crustal structure of the ocean-continent transition at Flemish Cap: Seismic refraction results. *Journal of Geophysical Research: Solid Earth*, Vol. 108, 2531.

FUNCK, T, JACKSON, H R, DEHLER, S A, and REID, I. 2006. A Refraction Seismic Transect from Greenland to Ellesmere Island, Canada: The Crustal Structure in Southern Nares Strait. *Polarforschung*, Vol. 74, 97-112.

FUNCK, T, JACKSON, H R, LOUDEN, K E, and KLINGELHOFER, F. 2007. Seismic study of the transform-rifted margin in Davis Strait between Baffin Island (Canada) and Greenland: What happens when a plume meets a transform. *Journal of Geophysical Research: Solid Earth*, Vol. 112.

FUNCK, T, HANSEN, A K, REID, I D, and LOUDEN, K E. 2008. The crustal structure of the southern Nain and Makkovik provinces of Labrador derived from refraction seismic data. *Canadian Journal of Earth Sciences*, Vol. 45, 465-481.

FUNCK, T, GOHL, K, DAMM, V, and HEYDE, I. 2012. Tectonic evolution of southern Baffin Bay and Davis Strait: Results from a seismic refraction transect between Canada and Greenland. *Journal of Geophysical Research: Solid Earth*, Vol. 117, B04107.

GERLINGS, J, FUNCK, T, JACKSON, H R, LOUDEN, K E, and KLINGELHOFER, F. 2009. Seismic evidence for plume-derived volcanism during formation of the continental margin in southern Davis Strait and northern Labrador Sea. *Geophysical Journal International*, Vol. 176, 980-994.

GOHL, K, and SMITHSON, S B. 1993. Structure of Archean crust and passive margin of southwest Greenland from seismic wide-angle data. *Journal of Geophysical Research: Solid Earth*, Vol. 98, 6623-6638.

GOUTORBE, B, DRAB, L, LOUBET, N, and LUCAZEAU, F. 2007. Heat flow of the eastern Canadian rifted continental margin revisited. *Terra Nova*, Vol. 19, 381-386.

GRANT, A C. 1988. Depth to basement of the Continental Margin of Eastern Canada. 1:5 000 000. *Geological Survey of Canada Map* 1707A.

GRASBY, S E, MAJOROWICZ, J, and KO, M. 2009. Geothermal Maps of Canada. *Geological Survey of Canada, Open File Report*, 6167.

GREGERSEN, U, and BIDSTRUP, T. 2008. Structures and hydrocarbon prospectivity in the northern Davis Strait area, offshore West Greenland. *Petroleum Geoscience*, Vol. 14, 151-166.

GUILLOU-FROTTIER, L, MARESCHAL, J-C, JAUPART, C, GARIÉPY, C, LAPOINTE, R, and BIENFAIT, G. 1995. Heat flow variations in the Grenville Province, Canada. *Earth and Planetary Science Letters*, Vol. 136, 447-460.

HAWORTH, R T, and LEFORT, J P. 1979. Geophysical evidence for the extent of the Avalon zone in Atlantic Canada. *Canadian Journal of Earth Sciences*, Vol. 16, 552-567.

HINZE, W J, AIKEN, C, BROZENA, J, COAKLEY, B, DATER, D, FLANAGAN, G, FORSBERG, R, HILDENBRAND, T, KELLER, G R, KELLOGG, J, KUCKS, R, LEE, X, MAINVILLE, A, MORIN, R, PILKINGTON, M, PLOUFF, D, RAVAT, D, ROMAN, D, URRUTIA-FUCUGAUCHI, J, VÉRONNEAU, M, WEBRING, M, and WINESTER, D. 2005. New standards for reducing gravity data: The North American gravity database. *Geophysics*, Vol. 70, J25-J32.

HOFMEISTER, A M. 1999. Mantle values of thermal conductivity and the geotherm from phonon lifetimes. *Science*, Vol. 283, 1699-1706.

HOLBROOK, W S, LARSEN, H C, KORENAGA, J, DAHL-JENSEN, T, REID, I D, KELEMEN, P B, HOPPER, J R, KENT, G M, LIZARRALDE, D, BERNSTEIN, S, and DETRICK, R S. 2001. Mantle thermal structure and active upwelling during continental breakup in the North Atlantic. *Earth and Planetary Science Letters*, Vol. 190, 251-266.

HUGHES, S, HALL, J, and LUETGERT, J H. 1994. The seismic velocity structure of the Newfoundland Appalachian orogen. *Journal of Geophysical Research: Solid Earth*, Vol. 99, 13633-13653.

JACKSON, H R. 2002. Seismic refraction profiles in the Gulf of Saint Lawrence and implications for extent of continuous Grenville lower crust. *Canadian Journal of Earth Sciences*, Vol. 39, 1-17.

JACKSON, H R, DICKIE, K, and MARILLIER, F. 1992. A seismic reflection study of northern Baffin Bay: implication for tectonic evolution. *Canadian Journal of Earth Sciences*, Vol. 29, 2353-2369.

JAPSEN, P, GREEN, P F, and CHALMERS, J A. 2005. Separation of Palaeogene and Neogene uplift on Nuussuaq, West Greenland. *Journal of the Geological Society*, Vol. 162, 299-314.

JAPSEN, P, BONOW, J M, GREEN, P F, CHALMERS, J A, and LIDMAR-BERGSTRÖM, K. 2006. Elevated, passive continental margins: Long-term highs or Neogene uplifts? New evidence from West Greenland. *Earth and Planetary Science Letters*, Vol. 248, 330-339.

JAUER, C D, and BUDKEWITSCH, P. 2010. Old marine seismic and new satellite radar data: Petroleum exploration of north west Labrador Sea, Canada. *Marine and Petroleum Geology*, Vol. 27, 1379-1394.

KAWAKATSU, H, KUMAR, P, TAKEI, Y, SHINOHARA, M, KANAZAWA, T, ARAKI, E, and SUYEHIRO, K. 2009. Seismic evidence for sharp lithosphere-asthenosphere boundaries of oceanic plates. *Science*, Vol. 324, 499-502.

KENYON, S, FORSBERG, R, and COAKLEY, B. 2008. New gravity field for the Arctic. *Eos, Transactions American Geophysical Union*, Vol. 89, 289-290.

KIMBELL, G S. 2002. Regional three-dimensional modelling of the NE Atlantic margin. *British Geological Survey Commissioned Report*, CR/02/093.

KIMBELL, G S. 2008. The new Passive Margins Modelling Project GIS. *British Geological Survey Commissioned Report*, CR/08/096.

KIMBELL, G S, GATLIFF, R W, RITCHIE, J D, WALKER, A S D, and WILLIAMSON, J P. 2002. The Passive Margins Modelling Project: overview report. *British Geological Survey Commissioned Report*, CR/02/095.

KIMBELL, G S, GATLIFF, R W, RITCHIE, J D, WALKER, A S D, and WILLIAMSON, J P. 2004. Regional three-dimensional gravity modelling of the NE Atlantic margin. *Basin Research*, Vol. 16, 259-278.

KIMBELL, G S, RITCHIE, J D, JOHNSON, H, and GATLIFF, R W. 2005. Controls on the structure and evolution of the NE Atlantic margin revealed by regional potential field imaging and 3D modelling. 933-945 in *Petroleum Geology: North-West Europe and Global Perspectives - Proceedings of the 6th Petroleum Geology Conference*. Doré, A G and Vining, B (editors). (London: The Geological Society.)

KIMBELL, G S, RITCHIE, J D, and HENDERSON, A F. 2010. Three-dimensional gravity and magnetic modelling of the Irish sector of the NE Atlantic margin. *Tectonophysics*, Vol. 486, 36-54.

KUKKONEN, I T. 1998. Temperature and heat flow density in a thick cratonic lithosphere: The SVEKA transect, central Fennoscandian Shield. *Journal of Geodynamics*, Vol. 26, 111-136.

KUMAR, P, KIND, R, HANKA, W, WYLEGALLA, K, REIGBER, C, YUAN, X, WOELBERN, I, SCHWINTZER, P, FLEMING, K, DAHL-JENSEN, T, LARSEN, T B, SCHWEITZER, J, PRIESTLEY, K, GUDMUNDSSON, O, and WOLF, D. 2005. The lithosphere–asthenosphere boundary in the North-West Atlantic region. *Earth and Planetary Science Letters*, Vol. 236, 249-257.

KUMAR, P, KIND, R, PRIESTLEY, K, and DAHL-JENSEN, T. 2007. Crustal structure of Iceland and Greenland from receiver function studies. *Journal of Geophysical Research: Solid Earth*, Vol. 112, B03301.

LARSEN, L M, HEAMAN, L M, CREASER, R A, DUNCAN, R A, FREI, R, and HUTCHINSON, M. 2009. Tectonomagmatic events during stretching and basin formation in the Labrador Sea and the Davis Strait: evidence from age and composition of Mesozoic to Palaeogene dyke swarms in West Greenland. *Journal of the Geological Society*, Vol. 166, 999-1012.

LAU, K W H, LOUDEN, K E, FUNCK, T, TUCHOLKE, B E, HOLBROOK, W S, HOPPER, J R, and CHRISTIAN LARSEN, H C. 2006. Crustal structure across the Grand Banks–Newfoundland Basin Continental Margin – I. Results from a seismic refraction profile. *Geophysical Journal International*, Vol. 167, 127-156.

LOUDEN, K E, TUCHOLKE, B E, and OAKEY, G N. 2004. Regional anomalies of sediment thickness, basement depth and isostatic crustal thickness in the North Atlantic Ocean. *Earth and Planetary Science Letters*, Vol. 224, 193-211.

MCKENZIE, D. 1978. Some remarks on the development of sedimentary basins. *Earth and Planetary Science Letters*, Vol. 40, 25-32.

MCKENZIE, D, JACKSON, J, and PRIESTLEY, K. 2005. Thermal structure of oceanic and continental lithosphere. *Earth and Planetary Science Letters*, Vol. 233, 337-349.

MARESCHAL, J C, POIRIER, A, ROLANDONE, F, BIENFAIT, G, GARIEPY, C, LAPOINTE, R, and JAUPART, C. 2000. Low mantle heat flow at the edge of the North American continent, Voisey Bay, Labrador. *Geophysical Research Letters*, Vol. 27, 823-826.

MARILLIER, F, and REID, I. 1990. Crustal underplating beneath the Carboniferous Magdalen Basin (Eastern Canada): evidence from seismic reflection and refraction. 209–218 in *The Potential of Deep Seismic Profiling for Hydrocarbon Exploration*. PINET, B, and BOIS, C (editors). (Paris: Editions Technip.)

MARILLIER, F, HALL, J, HUGHES, S, LOUDEN, K, REID, I, ROBERTS, B, CLOWES, R, COTÉ, T, FOWLER, J, GUEST, S, LU, H, LUETGERT, J, QUINLAN, G, SPENCER, C, and WRIGHT, J. 1994. LITHOPROBE East onshore-offshore seismic refraction survey — constraints on interpretation of reflection data in the Newfoundland Appalachians. *Tectonophysics*, Vol. 232, 43-58.

MARTIN, M R. 2007. Seismic stratigraphy and tectono-structural framework of the Bjarni area, Hopedale Basin, Labrador Sea. Unpublished MSc Thesis, Department of Earth Sciences, Memorial University of Newfoundland.

MÜLLER, R D, SDROLIAS, M, GAINA, C, and ROEST, W R. 2008. Age, spreading rates, and spreading asymmetry of the world's ocean crust. *Geochemistry, Geophysics, Geosystems*, Vol. 9, Q04006.

NEBEN, S, DAMM, V, BRENT, T, and TESSENSOHN, F. 2006. New multi-channel seismic reflection data from Northwater Bay, Nares Strait: indications for pull-apart tectonics. *Polarforschung*, Vol. 74, 77-96.

NIELSEN, T K, LARSEN, H C, and HOPPER, J R. 2002. Contrasting rifted margin styles south of Greenland: implications for mantle plume dynamics. *Earth and Planetary Science Letters*, Vol. 200, 271-286.

OAKEY, G N, and CHALMERS, J A. 2012. A new model for the Paleogene motion of Greenland relative to North America: Plate reconstructions of the Davis Strait and Nares Strait regions between Canada and Greenland. *Journal of Geophysical Research: Solid Earth*, Vol. 117, B10401.

PAVLIS, N K, HOLMES, S A, KENYON, S C, and FACTOR, J K. 2012. The development and evaluation of the Earth Gravitational Model 2008 (EGM2008). *Journal of Geophysical Research: Solid Earth*, Vol. 117, B04406.

PERRY, H K C, JAUPART, C, MARESCHAL, J C, and SHAPIRO, N M. 2006. Upper mantle velocity-temperature conversion and composition determined from seismic refraction and heat flow. *Journal of Geophysical Research: Solid Earth*, Vol. 111, B07301.

PERRY, C, ROSIEANU, C, MARESCHAL, J-C, and JAUPART, C. 2010. Thermal regime of the lithosphere in the Canadian. *Canadian Journal of Earth Sciences*, Vol. 47, 389-408.

PETRUNIN, A G, ROGOZHINA, I, VAUGHAN, A P M, KUKKONEN, I T, KABAN, M K, KOULAKOV, I, and THOMAS, M. 2013. Heat flux variations beneath central Greenland's ice due to anomalously thin lithosphere. *Nature Geoscience*, advance online publication.

PHILLIPS, J D. 2007. Geosoft eXecutables (GX's) developed by the U.S. Geological Survey, Version 2.0, with notes on GX development from Fortran code. *USGS Open-File Report* 2007-1355.

PINET, C, JAUPART, C, MARESCHAL, J-C, GARIEPY, C, BIENFAIT, G, and LAPOINTE, R. 1991. Heat flow and structure of the lithosphere in the Eastern Canadian Shield. *Journal of Geophysical Research: Solid Earth*, Vol. 96, 19941-19963.

POLLACK, H N, and CHAPMAN, D S. 1977. On the regional variation of heat flow, geotherms, and lithospheric thickness. *Tectonophysics*, Vol. 38, 279-296.

REID, I, and JACKSON, H R. 1997. Crustal structure of northern Baffin Bay: Seismic refraction results and tectonic implications. *Journal of Geophysical Research: Solid Earth*, Vol. 102, 523-542.

REITER, M, and JESSOP, A M. 1985. Estimates of terrestrial heat flow in offshore eastern Canada. *Canadian Journal of Earth Sciences*, Vol. 22, 1503-1517.

RESTON, T J, and PÉREZ-GUSSINYÉ, M. 2007. Lithospheric extension from rifting to continental breakup at magma-poor margins: rheology, serpentinisation and symmetry. *International Journal of Earth Sciences*, Vol. 96, 1033-1046.

ROEST, W R, and SRIVASTAVA, S P. 1989. Sea-floor spreading in the Labrador Sea: A new reconstruction. *Geology*, Vol. 17, 1000-1003.

ST-ONGE, M R, VAN GOOL, J A M, GARDE, A A, and SCOTT, D J. 2009. Correlation of Archaean and Palaeoproterozoic units between northeastern Canada and western Greenland: constraining the pre-collisional upper plate accretionary history of the Trans-Hudson orogen. *Geological Society, London, Special Publications*, Vol. 318, 193-235.

SAND, K K, WAIGHT, T E, PEARSON, D G, NIELSEN, T F D, MAKOVICKY, E, and HUTCHISON, M T. 2009. The lithospheric mantle below southern West Greenland: A geothermobarometric approach to diamond potential and mantle stratigraphy. *Lithos*, Vol. 112, Supplement 2, 1155-1166.

SANDWELL, D T, and SMITH, W H F. 1997. Marine gravity anomaly from Geosat and ERS 1 satellite altimetry. *Journal of Geophysical Research: Solid Earth*, Vol. 102, 10039-10054.

SASS, J H, NIELSEN, B L, WOLLENBERG, H A, and MUNROE, R J. 1972. Heat flow and surface radioactivity at two sites in South Greenland. *Journal of Geophysical Research: Solid Earth*, Vol. 77, 6435-6444.

SCLATER, J G, and CHRISTIE, P A F. 1980. Continental stretching: An explanation of the Post-Mid-Cretaceous subsidence of the central North Sea Basin. *Journal of Geophysical Research: Solid Earth*, Vol. 85, 3711-3739.

SKAARUP, N, JACKSON, H R, and OAKEY, G. 2006. Margin segmentation of Baffin Bay/Davis Strait, eastern Canada based on seismic reflection and potential field data. *Marine and Petroleum Geology*, Vol. 23, 127-144.

SMITH, W H F, and SANDWELL, D T. 1997. Global Sea Floor Topography from Satellite Altimetry and Ship Depth Soundings. *Science*, Vol. 277, 1956-1962.

SORENSEN, A B. 2006. Stratigraphy, structure and petroleum potential of the Lady Franklin and Maniitsoq Basins, offshore southern West Greenland. *Petroleum Geoscience*, Vol. 12, 221-234.

SRIVASTAVA, S P. 1978. Evolution of the Labrador Sea and its bearing on the early evolution of the North Atlantic. *Geophysical Journal of the Royal Astronomical Society*, Vol. 52, 313-357.

SRIVASTAVA, S P, and ROEST, W R. 1999. Extent of oceanic crust in the Labrador Sea. *Marine and Petroleum Geology*, Vol. 16, 65-84.

STOREY, M, DUNCAN, R A, PEDERSEN, A K, LARSEN, L M, and LARSEN, H C. 1998. 40Ar/39Ar geochronology of the West Greenland Tertiary volcanic province. *Earth and Planetary Science Letters*, Vol. 160, 569-586.

SUCKRO, S K, GOHL, K, FUNCK, T, HEYDE, I, EHRHARDT, A, SCHRECKENBERGER, B, GERLINGS, J, DAMM, V, and JOKAT, W. 2012. The crustal structure of southern Baffin Bay: implications from a seismic refraction experiment. *Geophysical Journal International*, Vol. 190, 37-58.

SUCKRO, S K, GOHL, K, FUNCK, T, HEYDE, I, SCHRECKENBERGER, B, GERLINGS, J, and DAMM, V. 2013. The Davis Strait crust - a transform margin between two oceanic basins. *Geophysical Journal International*, Vol. 193, 78-97.

TARASOV, L, and PELTIER, W R. 2003. Greenland glacial history, borehole constraints, and Eemian extent. *Journal of Geophysical Research: Solid Earth*, Vol. 108, 2143.

TESAURO, M, KABAN, M K, and CLOETINGH, S A P L. 2009. A new thermal and rheological model of the European lithosphere. *Tectonophysics*, Vol. 476, 478-495.

TESSENSOHN, F, JACKSON, H R, and REID, I. 2006. The tectonic evolution of Nares Strait: implications of new data. *Polarforschung*, Vol. 74, 191-198.

THOMPSON, D A, BASTOW, I D, HELFFRICH, G, KENDALL, J M, WOOKEY, J, SNYDER, D B, and EATON, D W. 2010. Precambrian crustal evolution: Seismic constraints from the Canadian Shield. *Earth and Planetary Science Letters*, Vol. 297, 655-666.

VAN AVENDONK, H J A, HOLBROOK, W S, NUNES, G T, SHILLINGTON, D J, TUCHOLKE, B E, LOUDEN, K E, LARSEN, H C, and HOPPER, J R. 2006. Seismic velocity structure of the rifted margin of the eastern Grand Banks of Newfoundland, Canada. *Journal of Geophysical Research: Solid Earth*, Vol. 111.

WHITTAKER, R C, HAMANN, N E, and PULVERTAFT, T C R. 1997. A new frontier province offshore northwest Greenland: Structure, basin development, and petroleum potential of the Melville Bay area. *AAPG Bulletin-American Association of Petroleum Geologists*, Vol. 81, 978-998.

WIELENS, J, JAUER, C, and WILLIAMS, G. 2006. First results of 4-D modelling of Saglek Basin, Labrador Shelf. *Abstract of paper presented at 2006 CSPG-CSEG-CWLS Convention.*

VERHOEF, J, ROEST, W R, MACNAB, R, ARKANI-HAMED, J, ET AL. 1996. Magnetic anomalies of the Arctic and North Atlantic Oceans and adjacent land areas. *Geological Survey of Canada Open File Report*, No. 3125a.

WESSEL, P, and SMITH, W H F. 1996. A Global, Self-consistent, Hierarchical, High-Resolution Shoreline Database. *Journal of Geophysical Research: Solid Earth*, Vol. 101, 8741-8743.

XU, Y, SHANKLAND, T J, LINHARDT, S, RUBIE, D C, LANGENHORST, F, and KLASINSKI, K. 2004. Thermal diffusivity and conductivity of olivine, wadsleyite and ringwoodite to 20 GPa and 1373 K. *Physics of the Earth and Planetary Interiors*, Vol. 143–144, 321-336.

ZELT, C A, and SMITH, R B. 1992. Seismic traveltime inversion for 2-D crustal velocity structure. *Geophysical Journal International*, Vol. 108, 16-34.

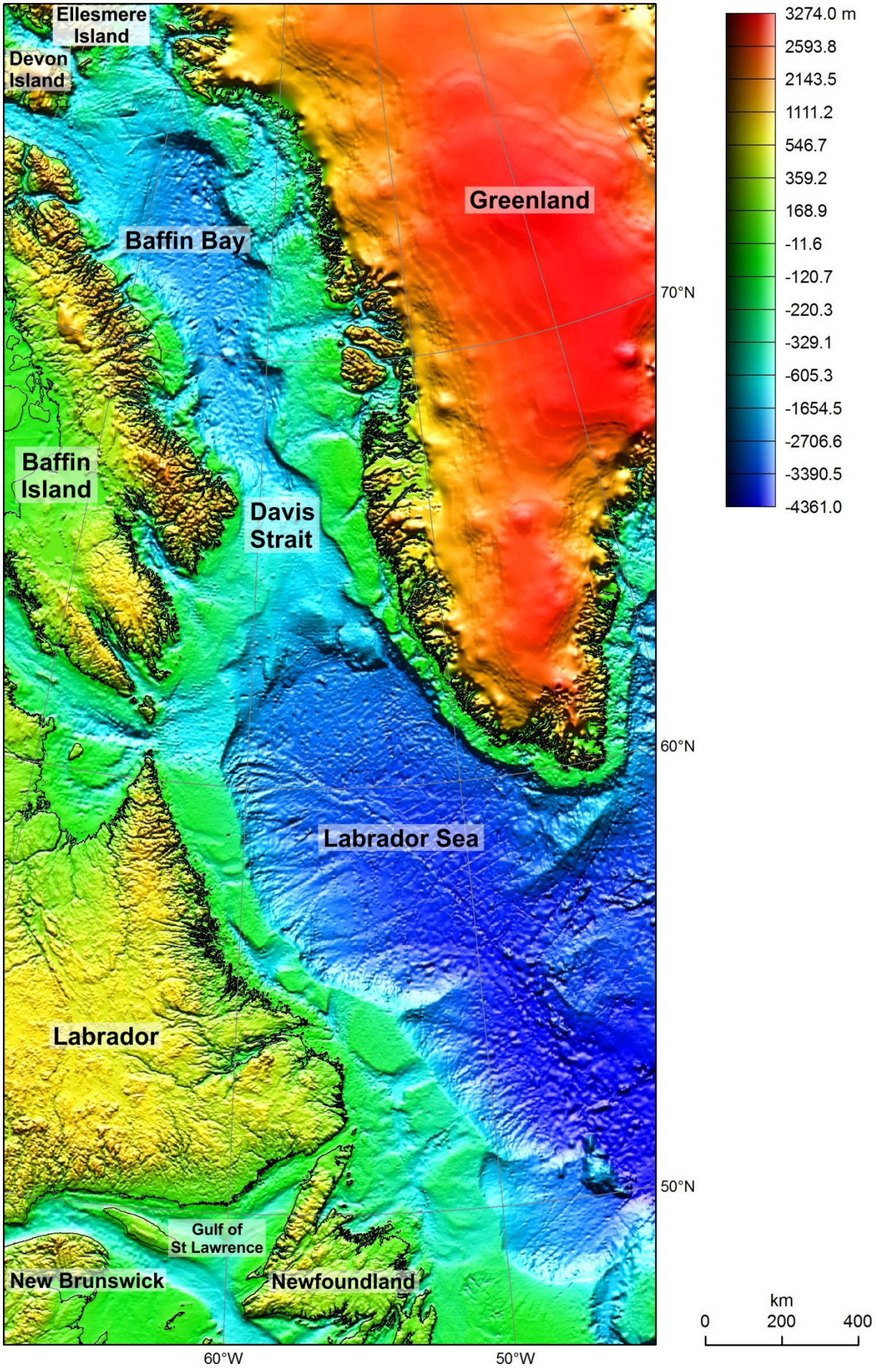

Figure 1 Topographic image, based on the SRTM30_PLUS global bathymetry and elevation model (Becker et al., 2009; Smith and Sandwell, 1997)

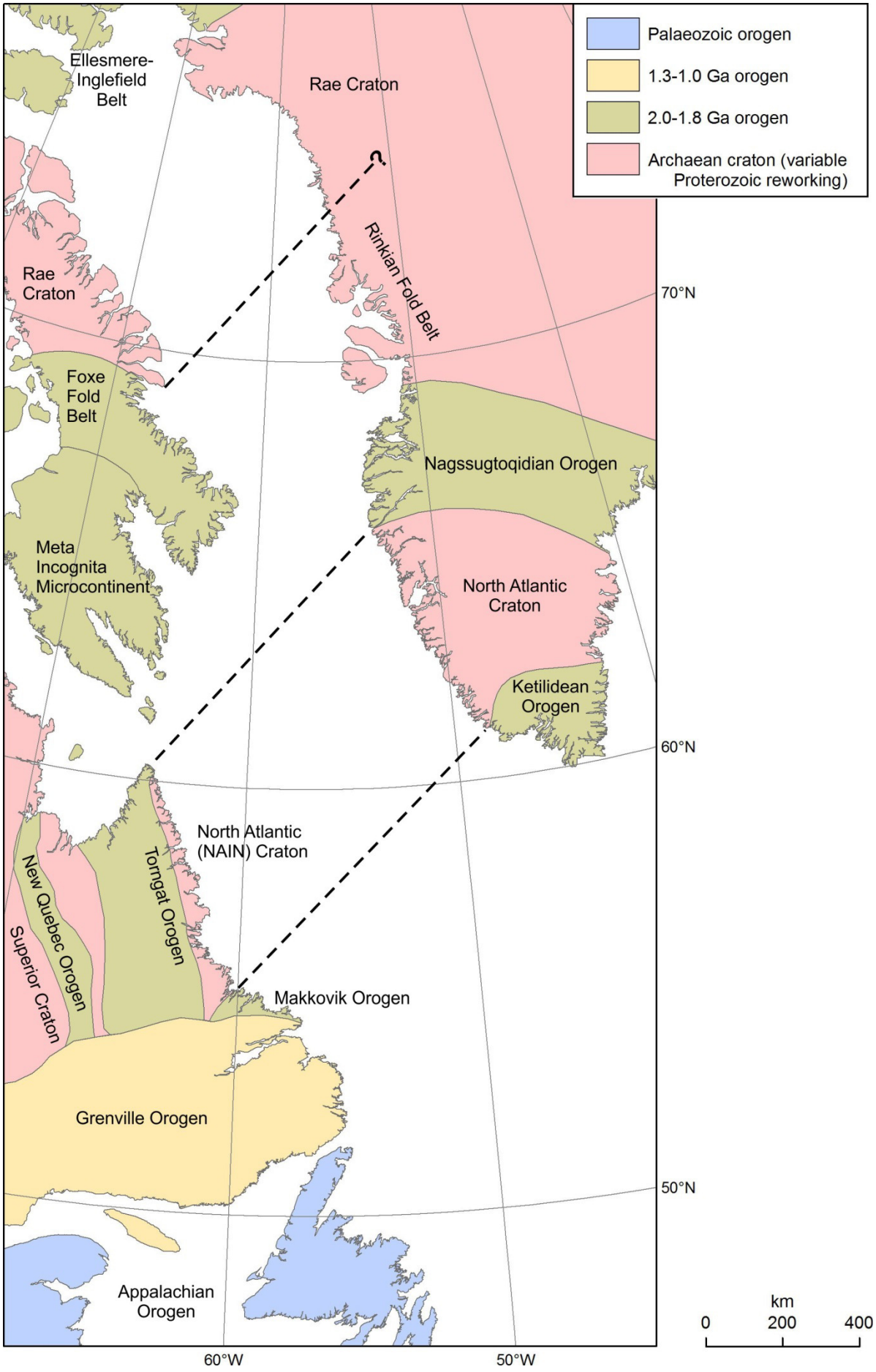

Figure 2 Sketch of basement elements (mainly after St-Onge et al., 2013). Baffin Island and the units between the Superior and NAIN cratons in Labrador form part of the Churchill Province

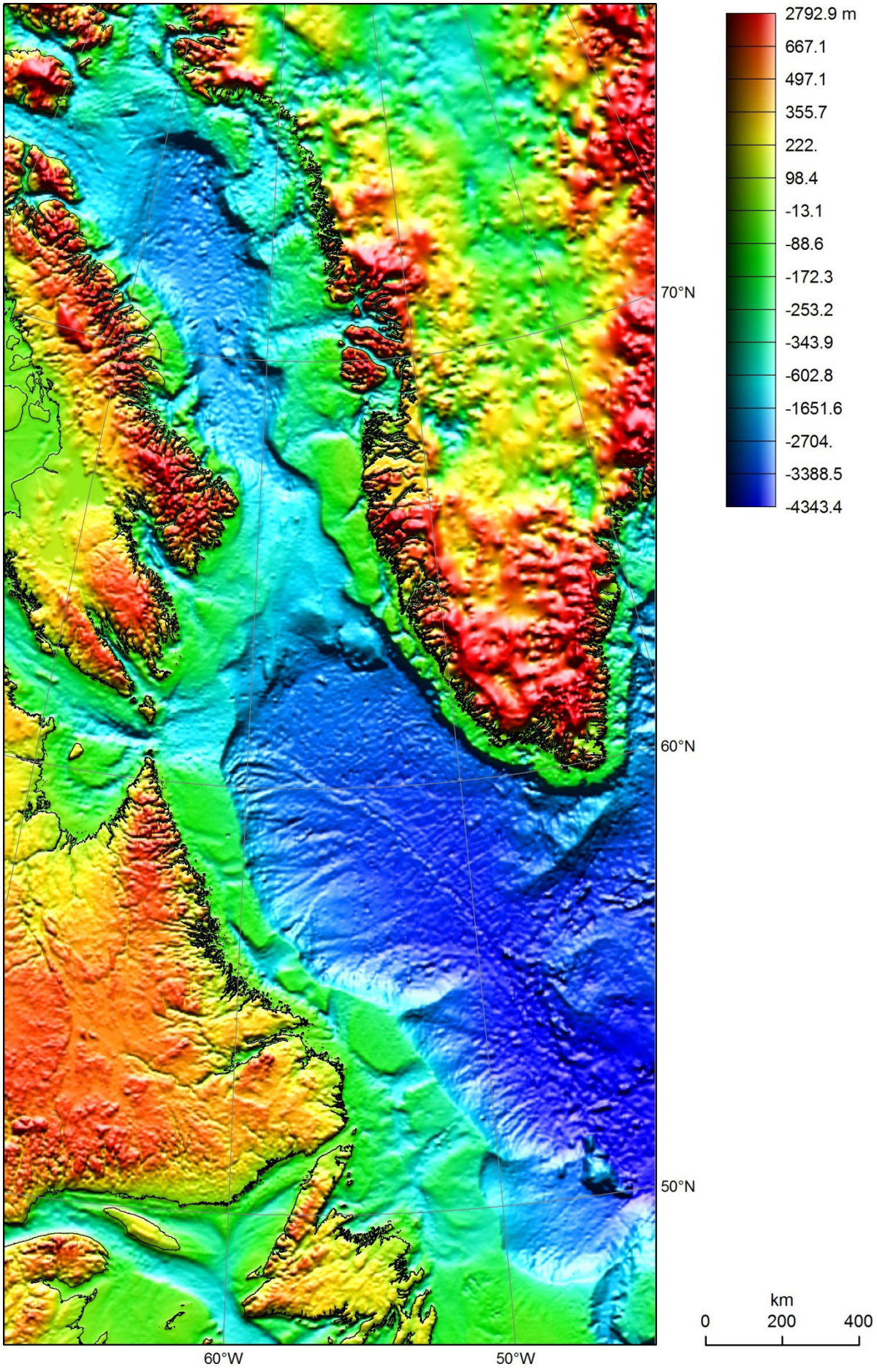

Figure 3 Bedrock topography after removal of the Greenland ice sheet

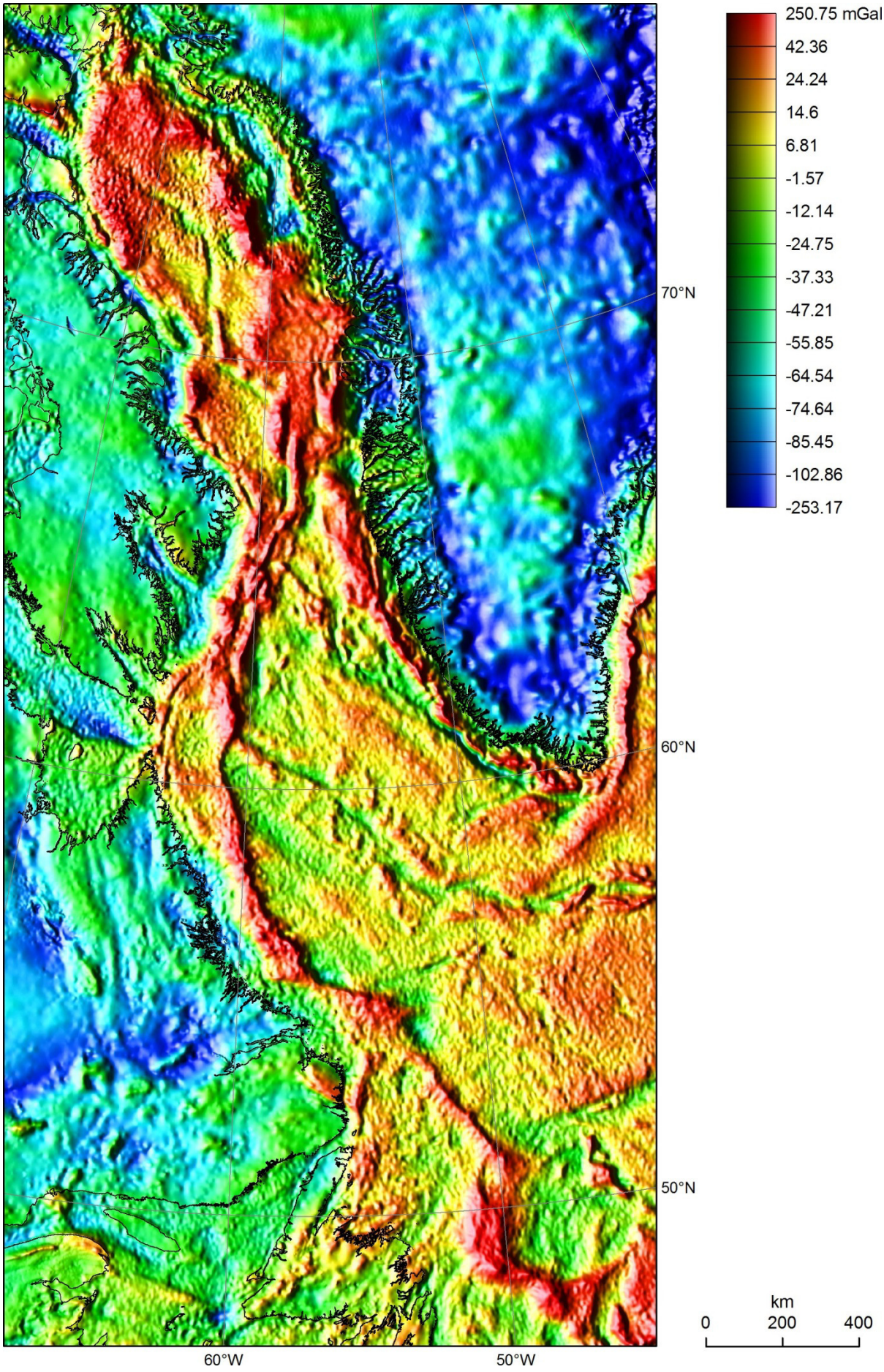

Figure 4 Gravity image (free-air anomalies offshore and Bouguer anomalies onshore). Colour shaded-relief with illumination from the west. See text for details of the data sources

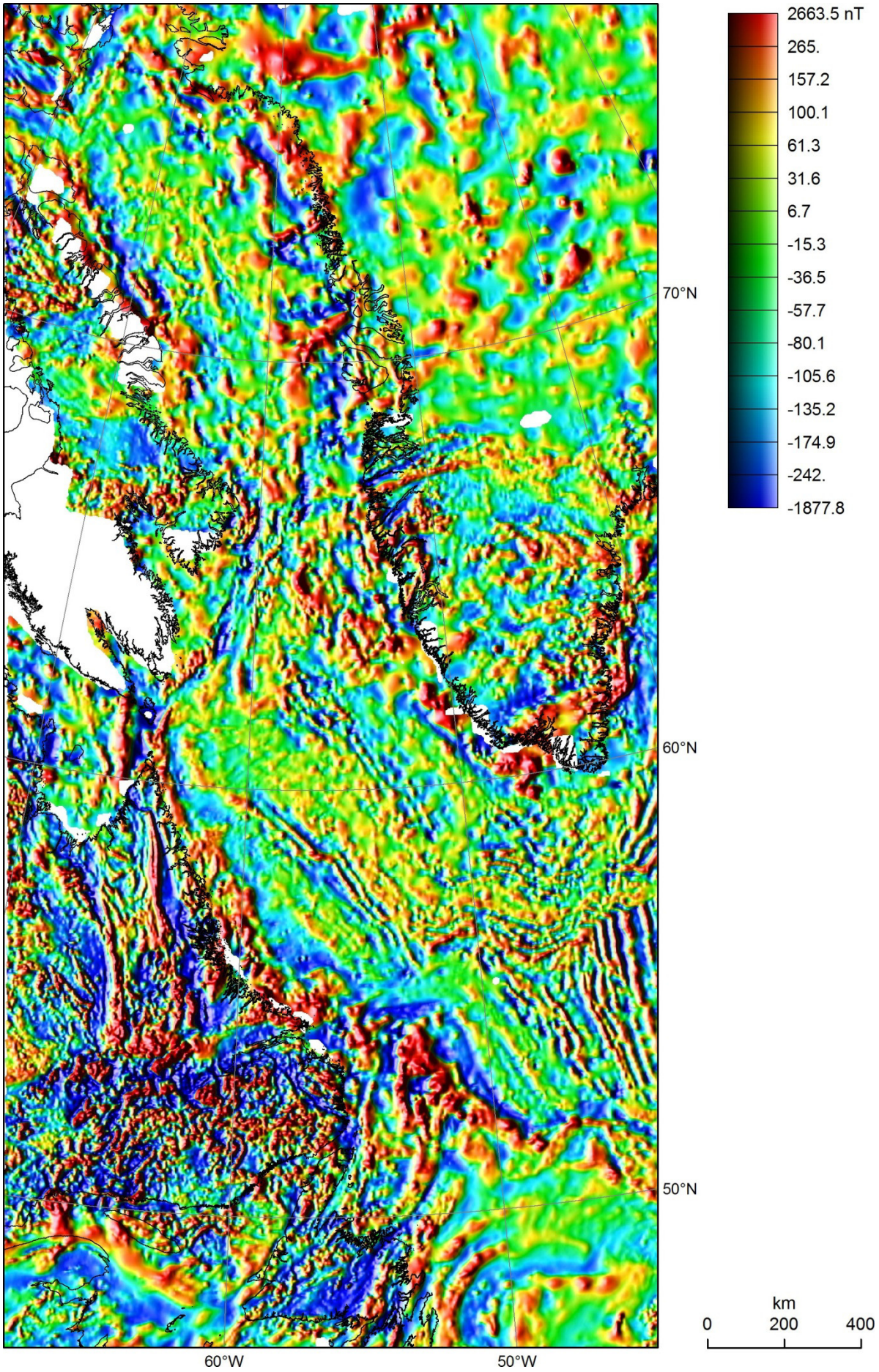

Figure 5 Magnetic image (total magnetic field) based on the GAMMAA5 compilation (Verhoef et al., 1996). Colour shaded-relief with illumination from the west

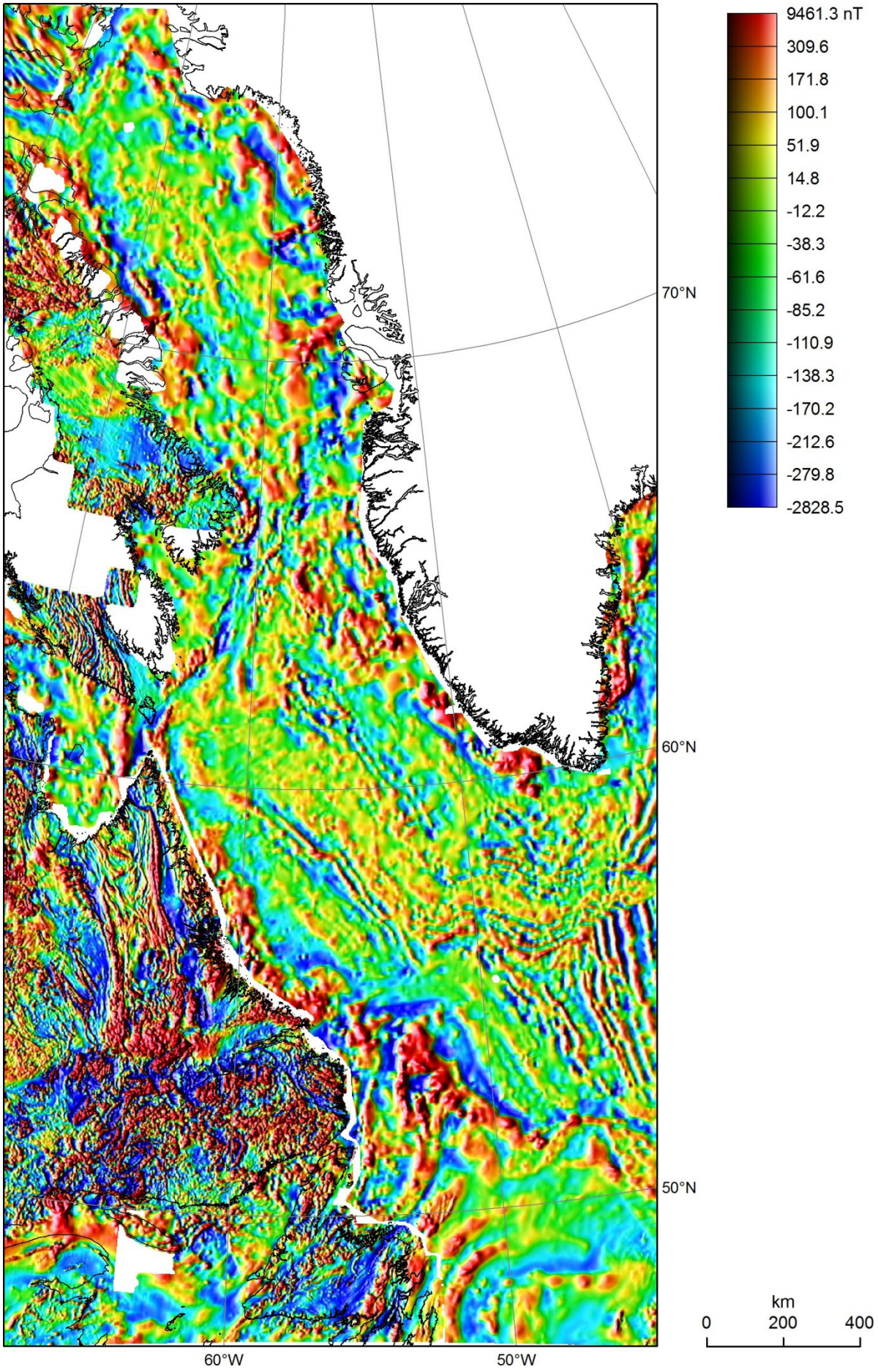

Figure 6 Magnetic image based on data compiled by the Geological Survey of Canada (© Department of Natural Resources Canada. All rights reserved).

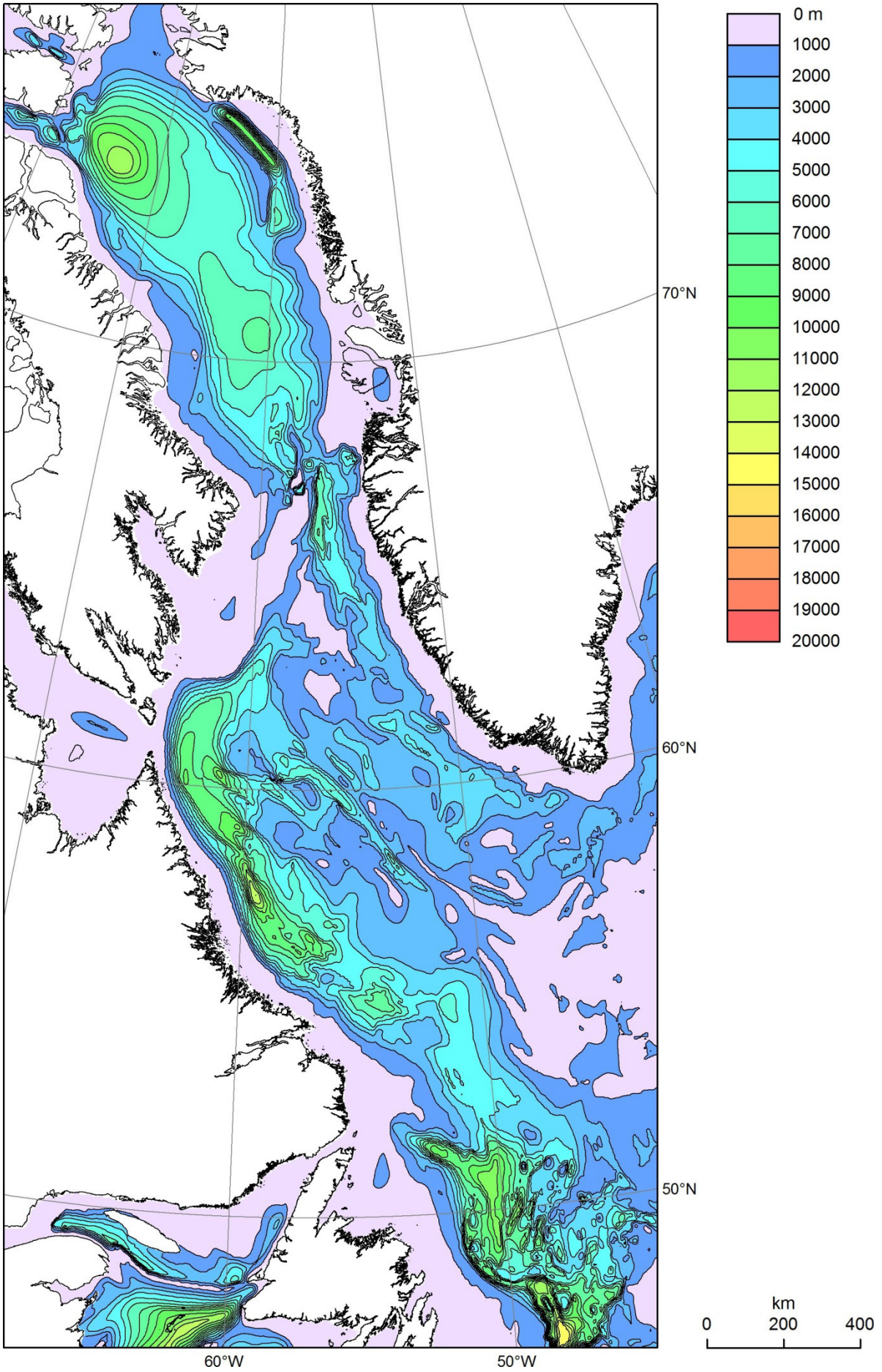

Figure 7 Initial sediment thickness model, based primarily on Louden et al. (2004) and Grant (1988)

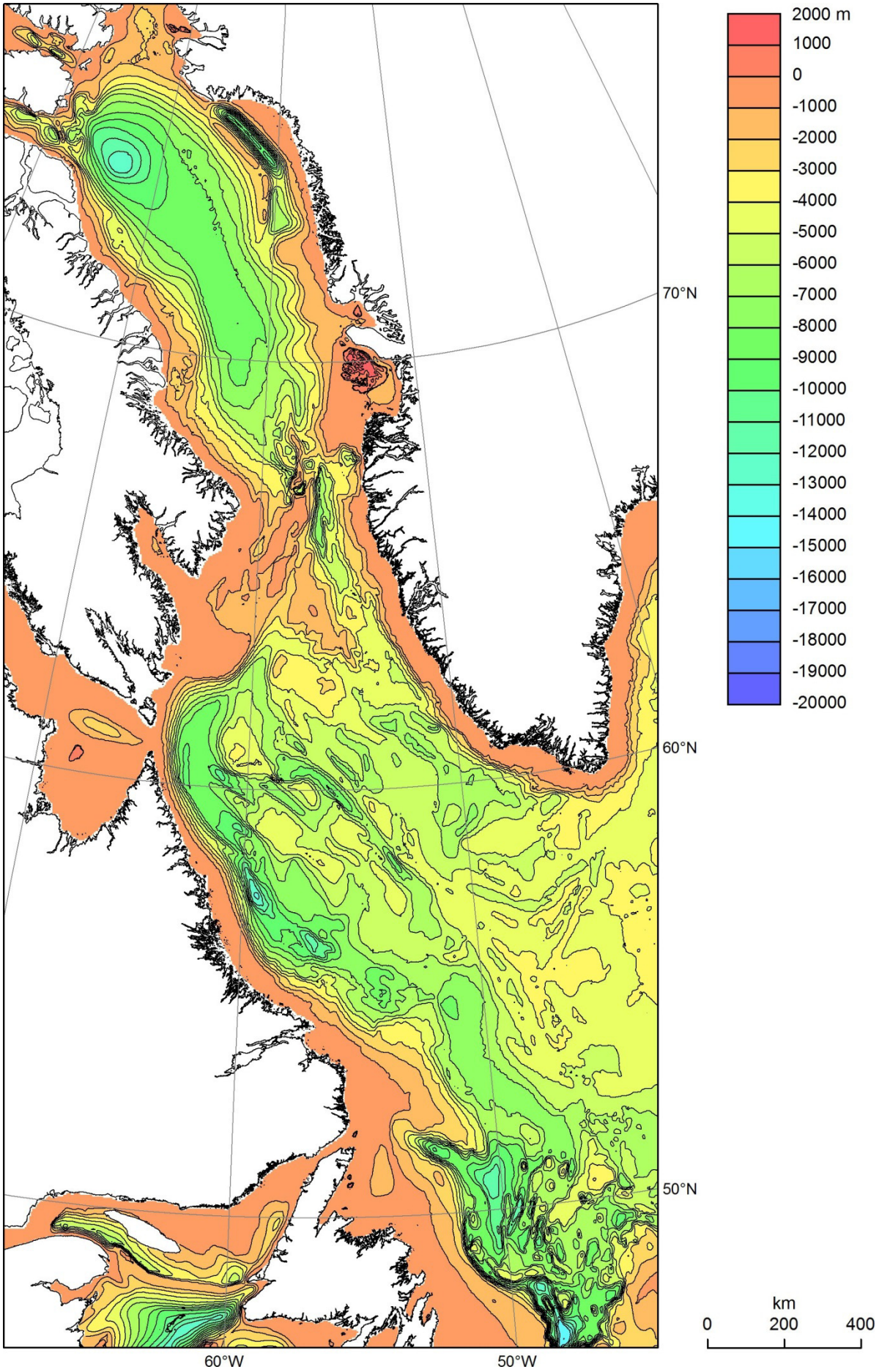

Figure 8 Initial model of depth to top basement (relative to datum)

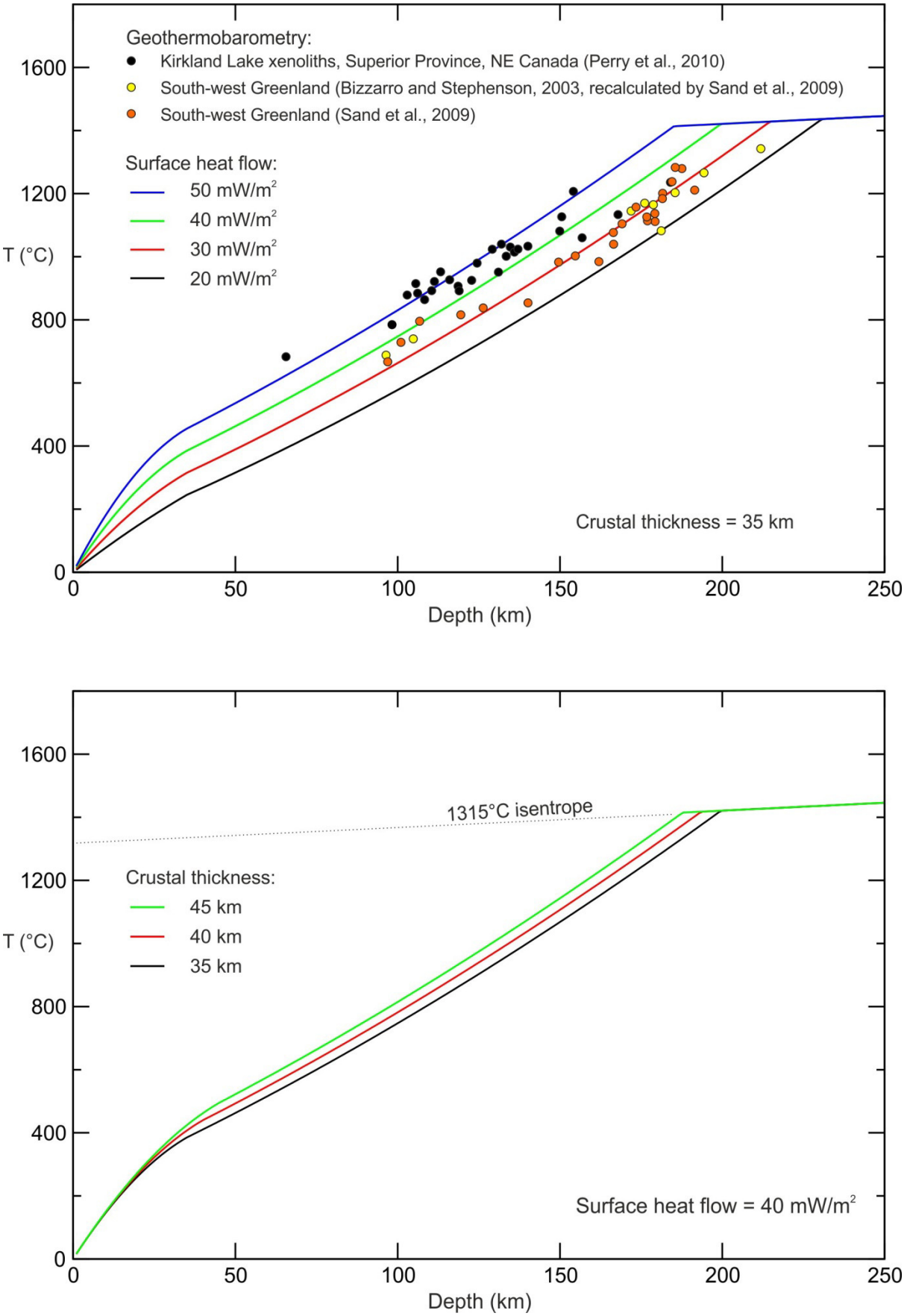

Figure 9 Predicted continental geotherms calculated using the methods described in the text and illustrating the sensitivity to heat flow (top panel) and crustal thickness (bottom panel). Geothermobarometric estimates have been added to the top panel for comparison. The mantle isentrope is after McKenzie et al. (2005)

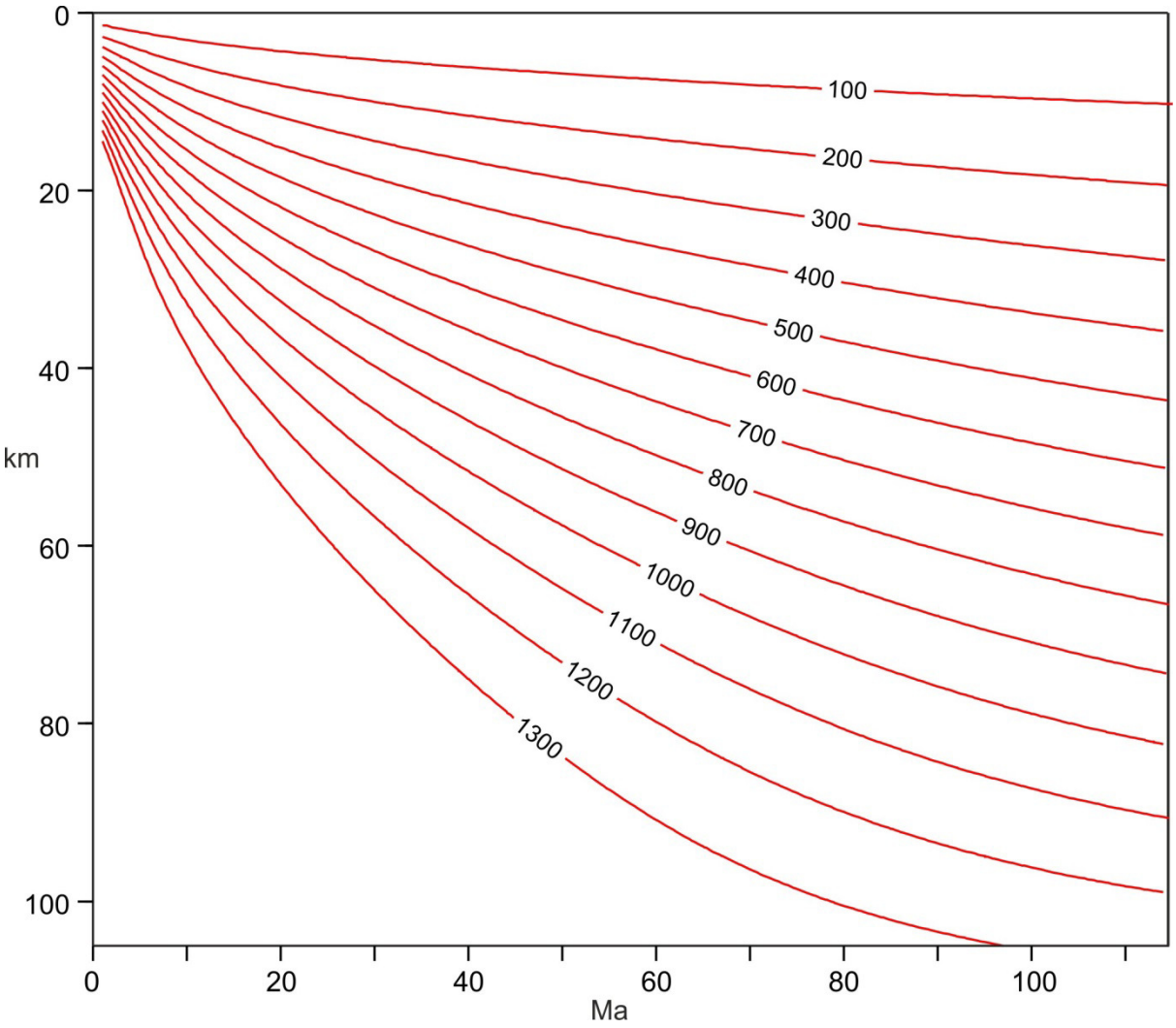

Figure 10 Predicted variation of the temperature of oceanic lithosphere with depth and age (conductive heat transfer only). Red lines are isotherms at 100ºC intervals

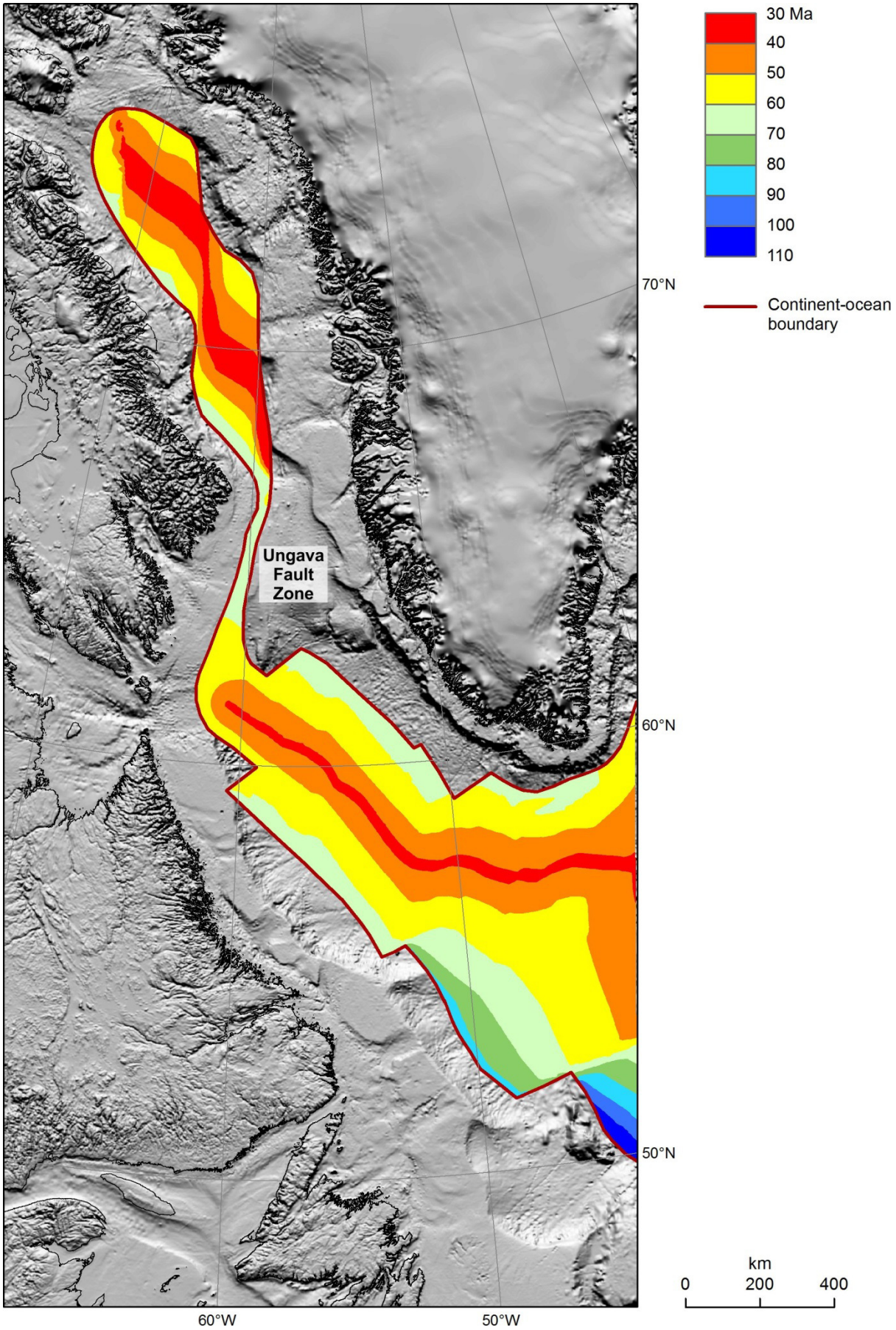

Figure 11 Assumed age of ocean crust within the study area, based on Müller et al. (2008), with modifications to the continent-ocean boundary

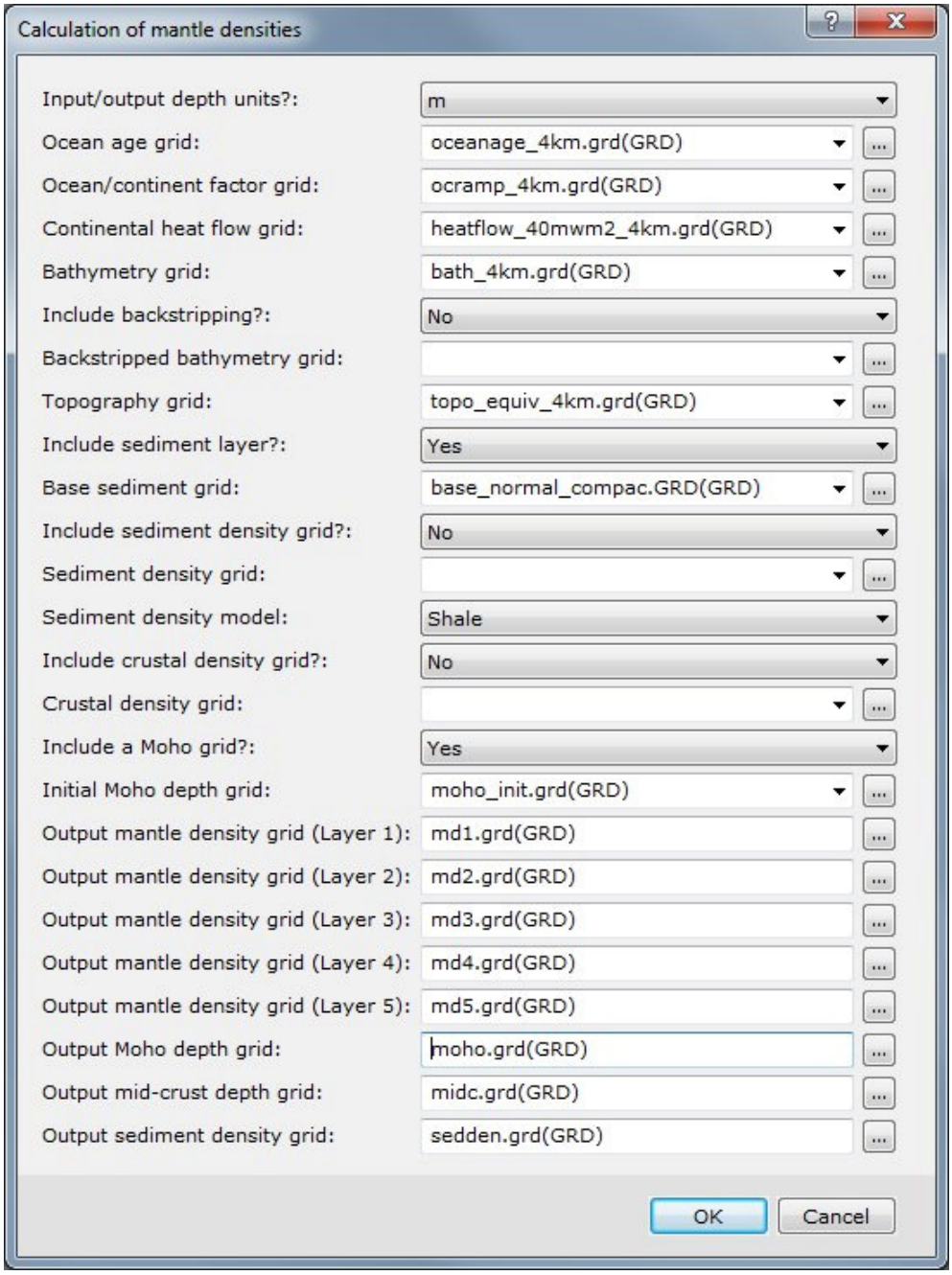

Figure 12 The interface to the customised routine developed for use within Geosoft Oasis montaj

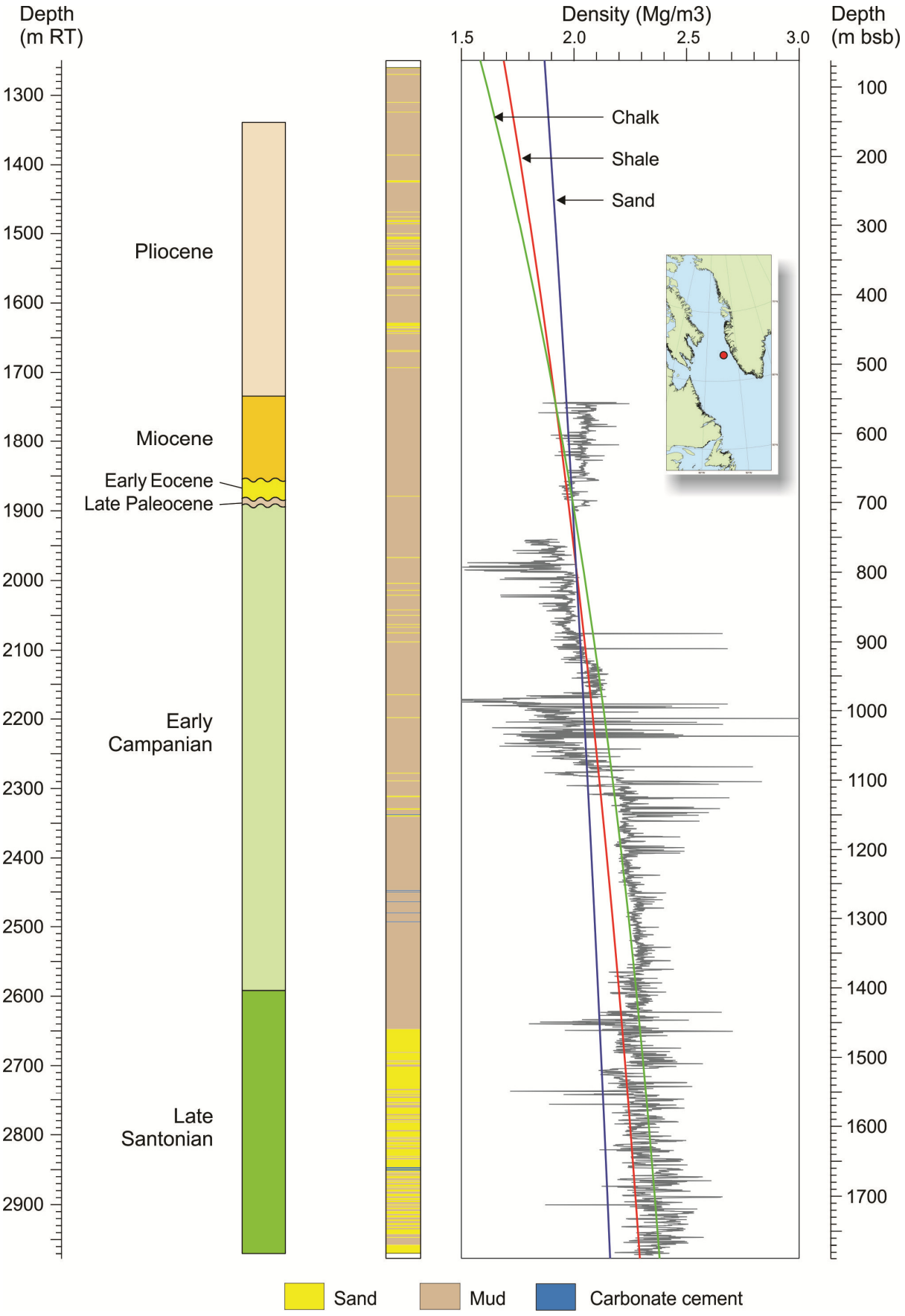

Figure 13 Density log from the Qulleq-1 well. Modified from Fig. 4 in Christiansen et al. (2001) Copyright: Geological Survey of Denmark and Greenland (GEUS)

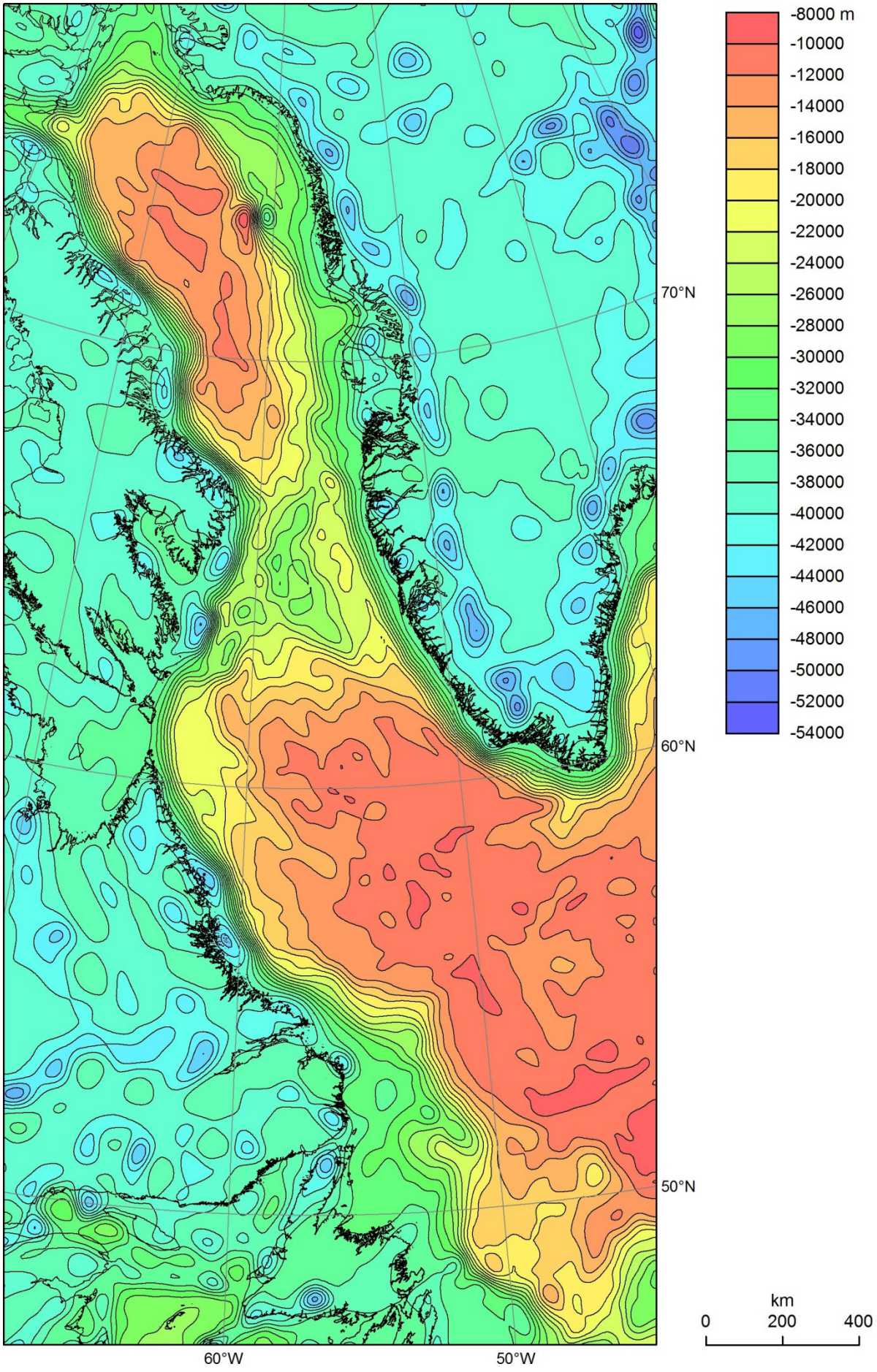

Figure 14 Modelled depth to optimised Moho (relative to datum)

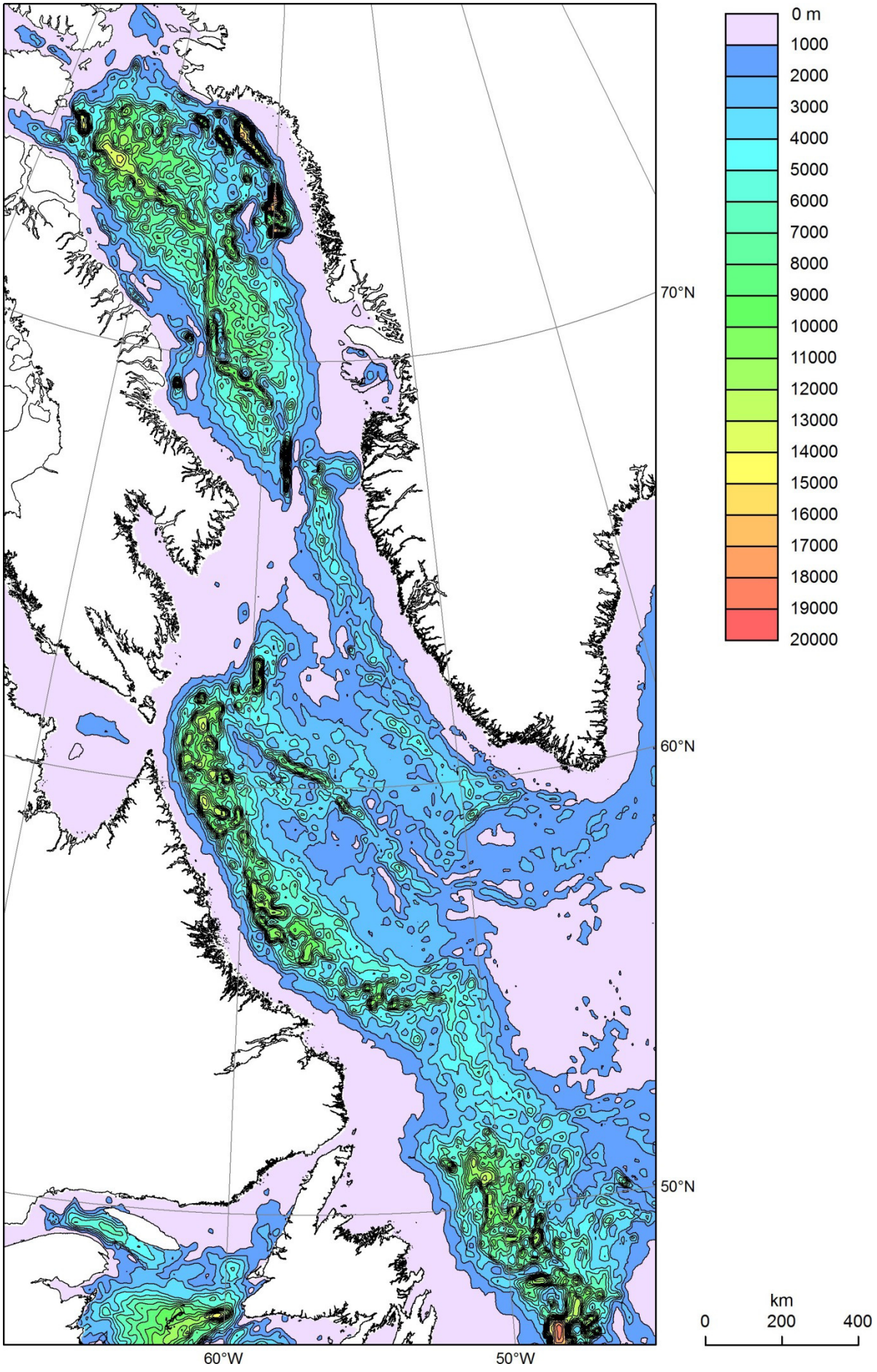

Figure 15 Optimised sediment thickness

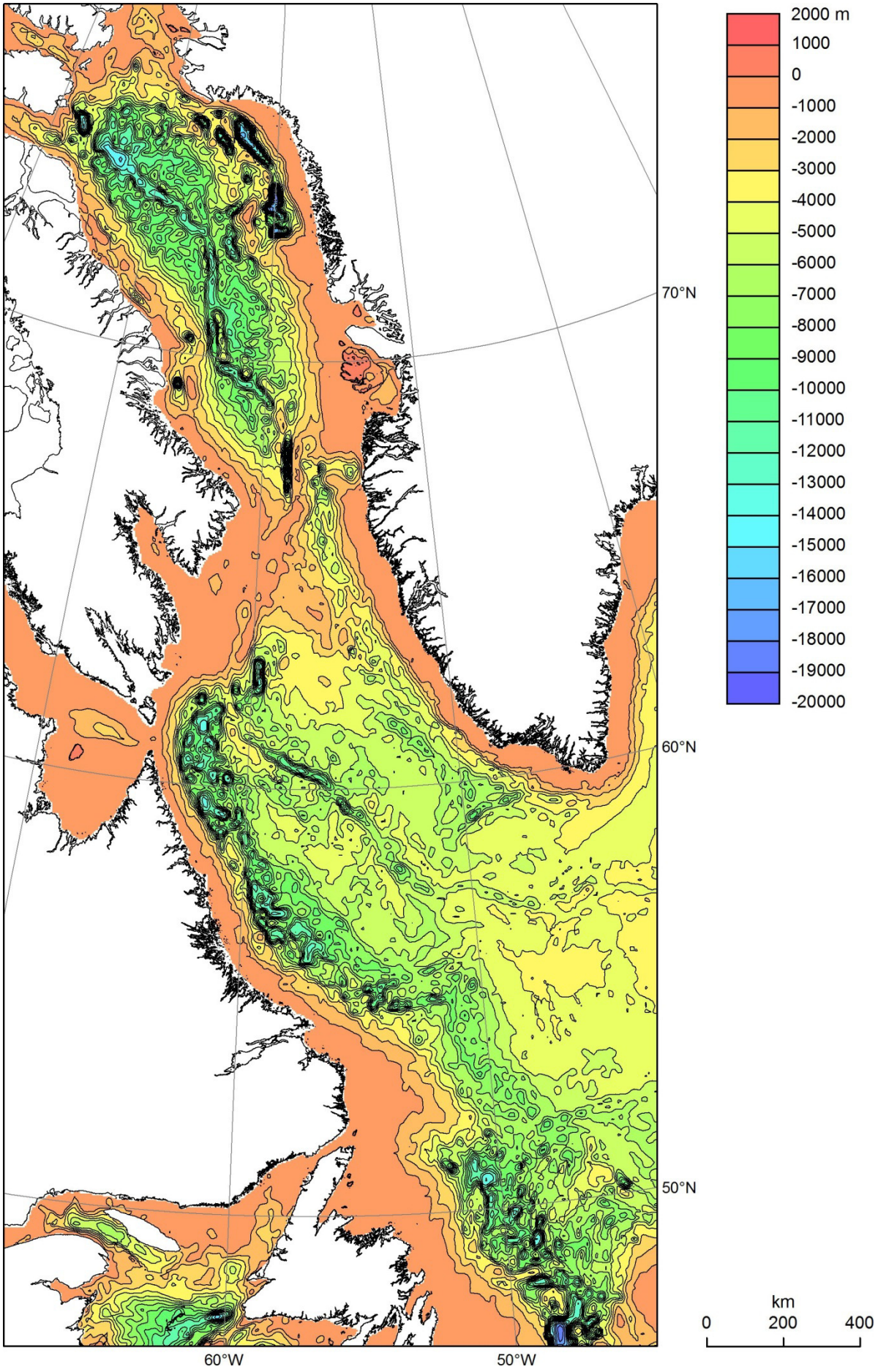

Figure 16 Depth to top basement (relative to datum) in the optimised model

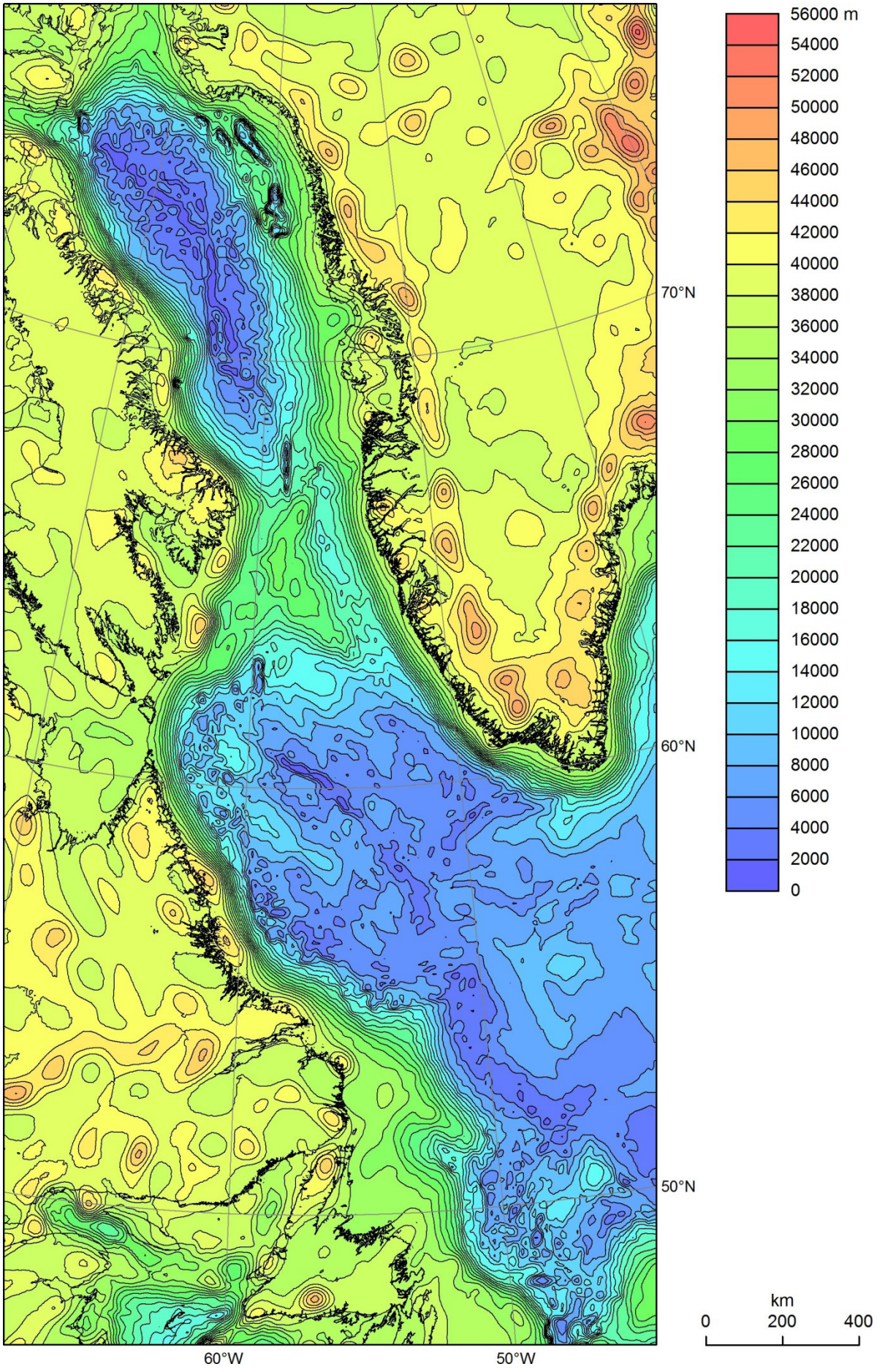

Figure 17 Thickness of crystalline crust in the optimised model

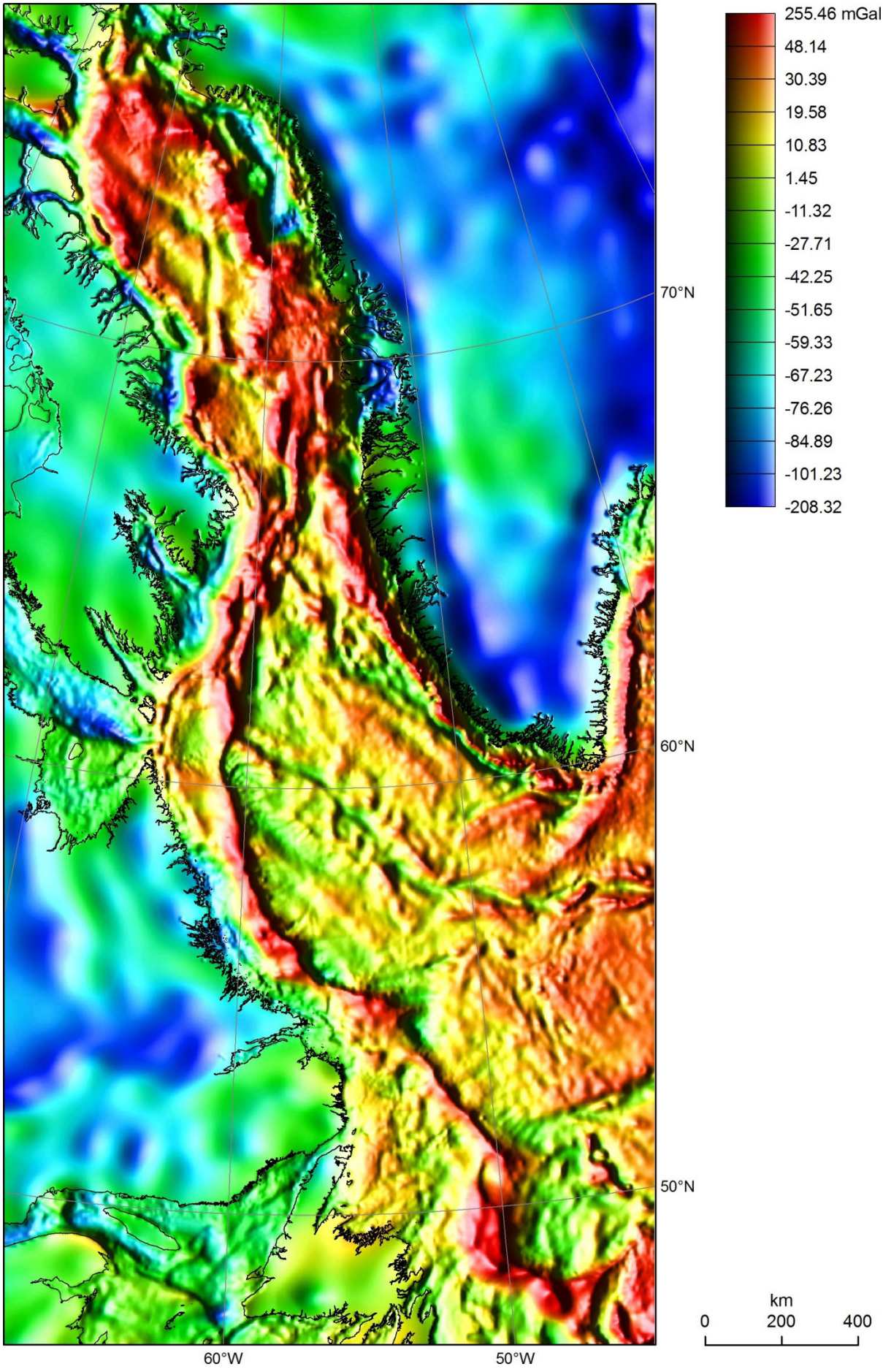

Figure 18 Calculated gravity field over the optimised model. Colour shaded-relief image, illuminated from the west

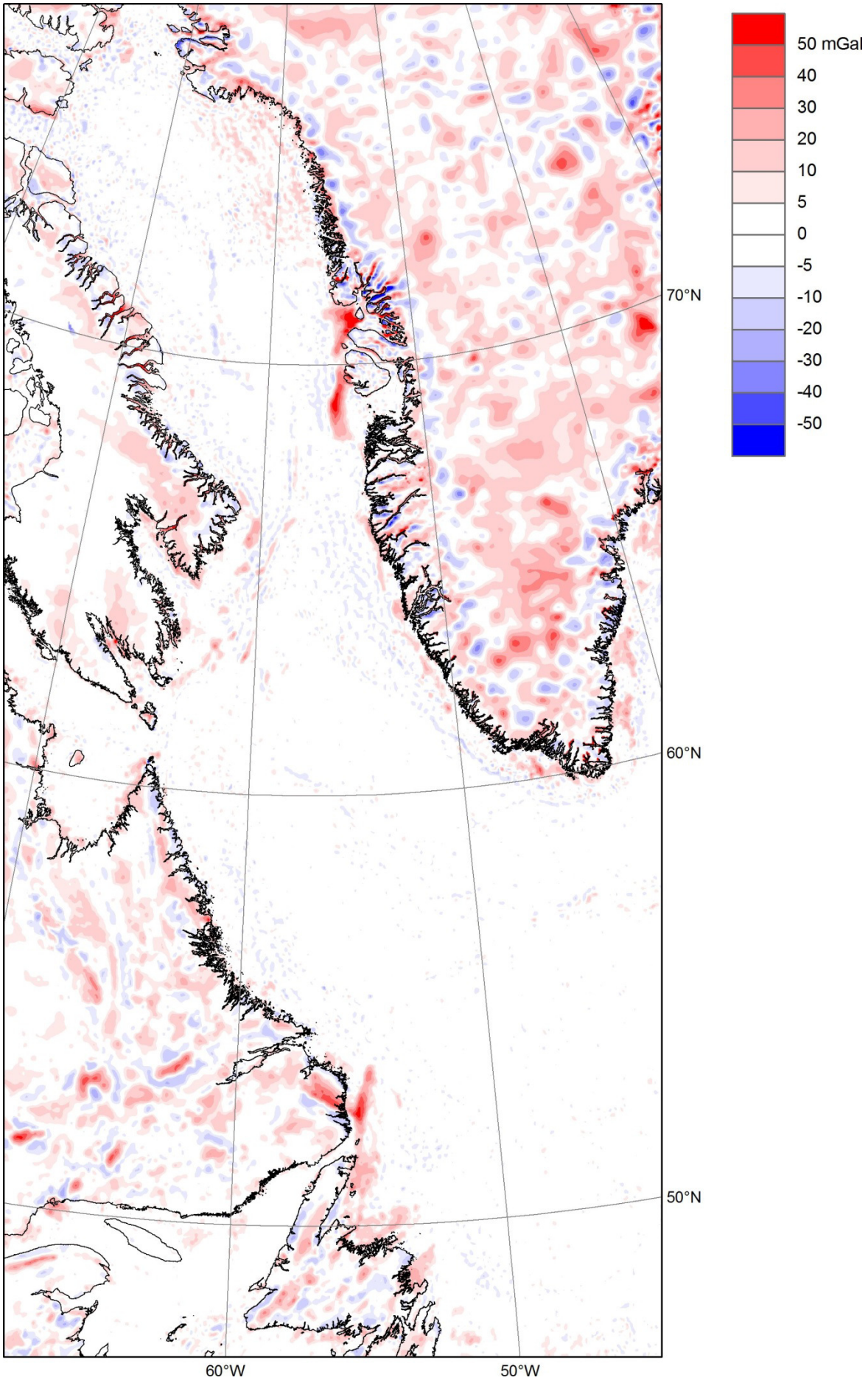

Figure 19 Residual (observed – calculated) gravity field, coloured where the values are outside ± 5 mGal

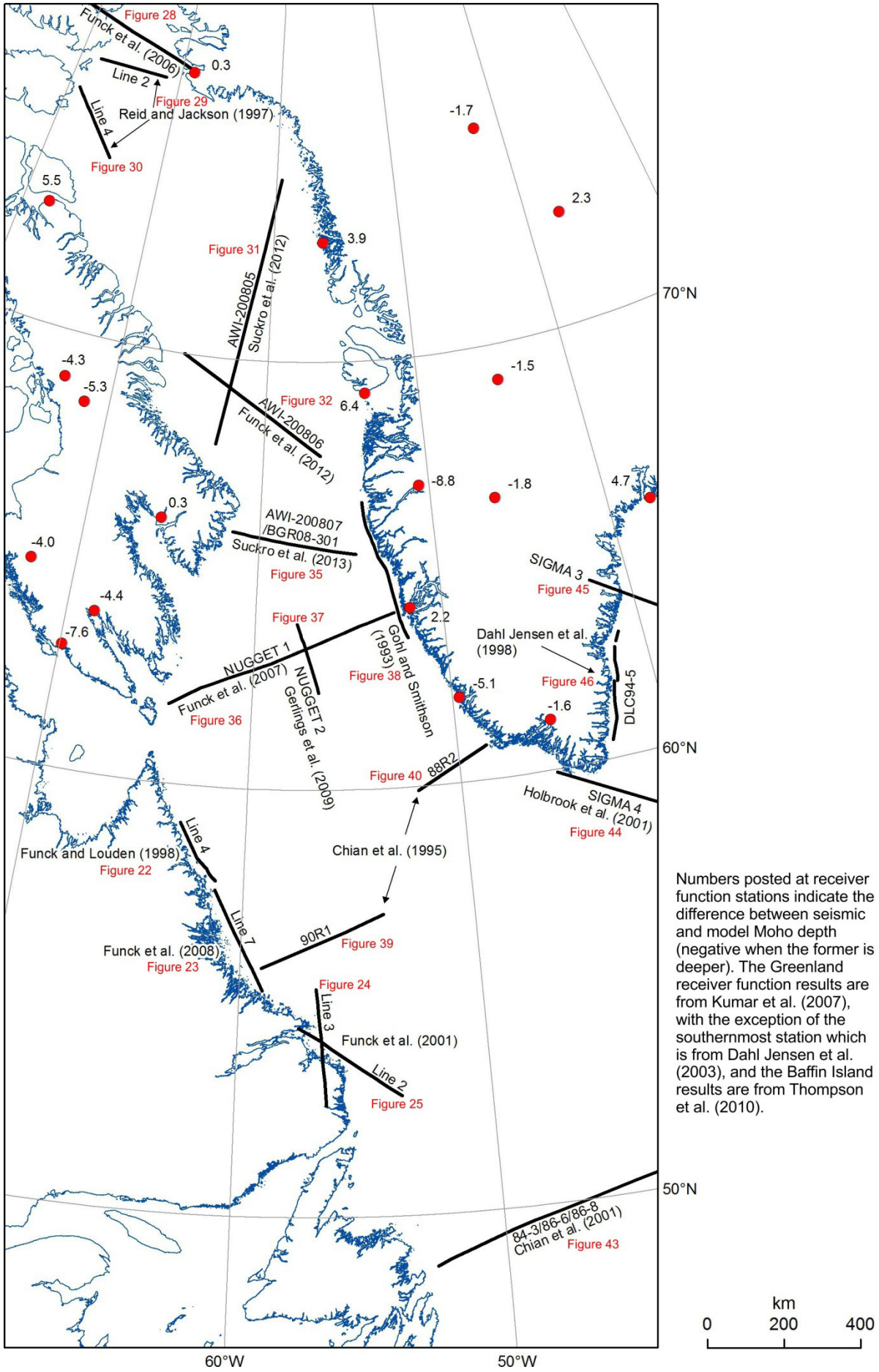

Numbers posted at receiver function stations indicate the difference between seismic and model Moho depth (negative when the former is deeper). The Greenland receiver function results are from Kumar et al. (2007), with the exception of the southernmost station which is from Dahl Jensen et al. (2003), and the Baffin Island results are from Thompson et al. (2010).

Figure 20 Locations of deep seismic refraction experiments (heavy black lines) and receiver function studies (red circles) used for comparison with the modelling results

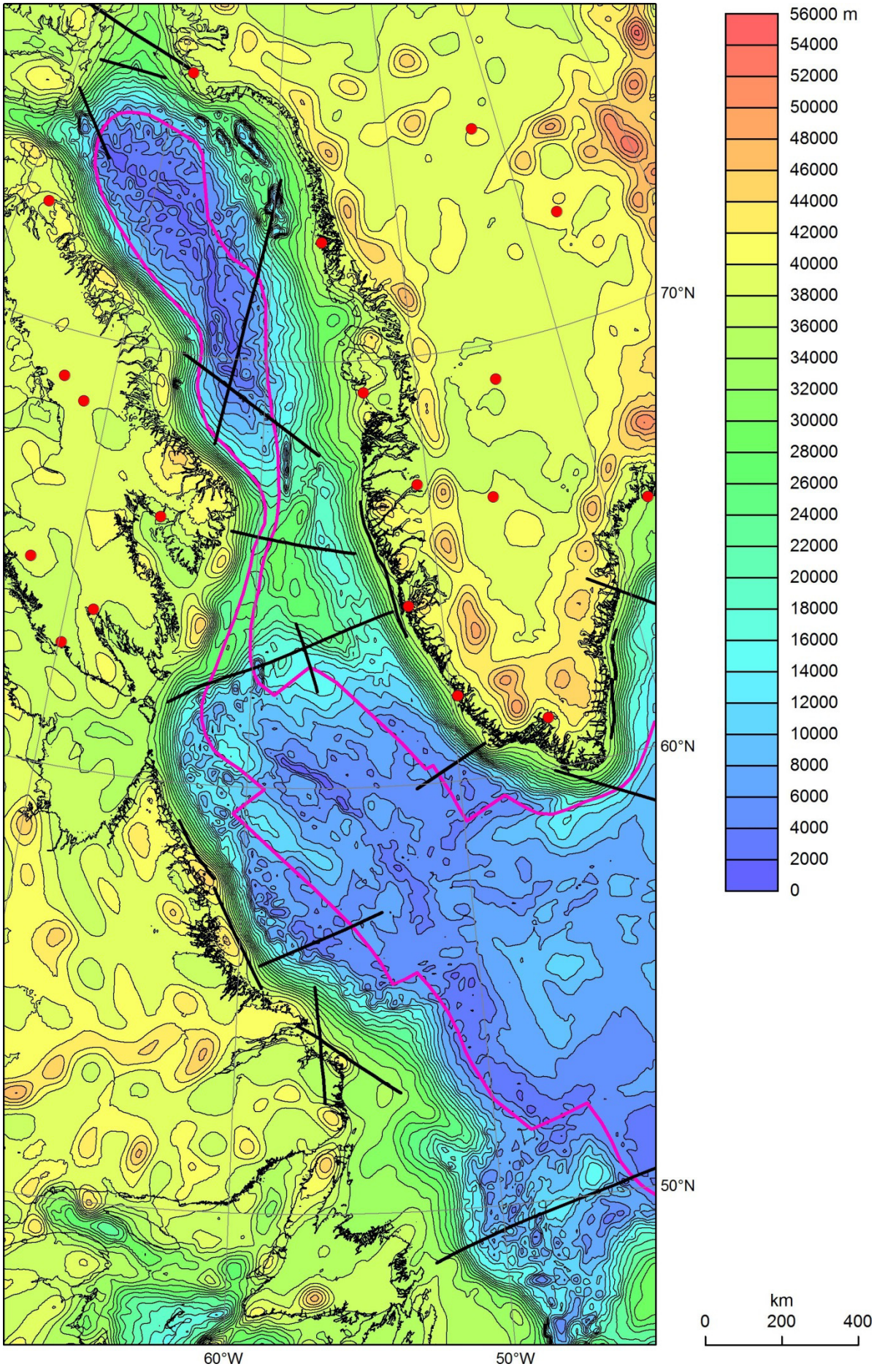

Figure 21 Location of seismic experiments superimposed on crystalline crustal thickness (for profile identification see Figure 20)

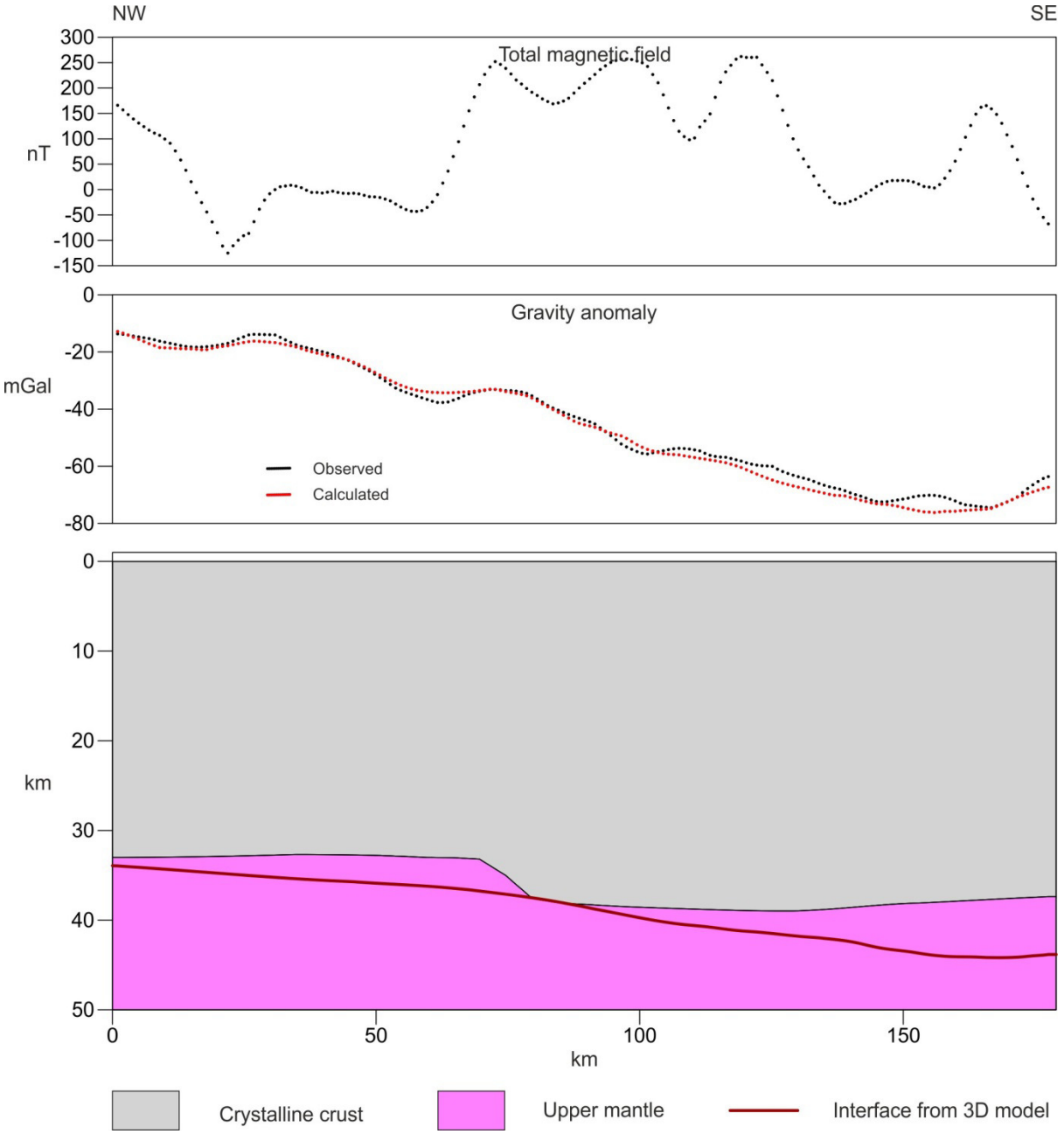

Figure 22 Moho interface from the 3D model superimposed on a simplified version of the published interpretation of seismic refraction line 4 of Funck and Louden (1998)

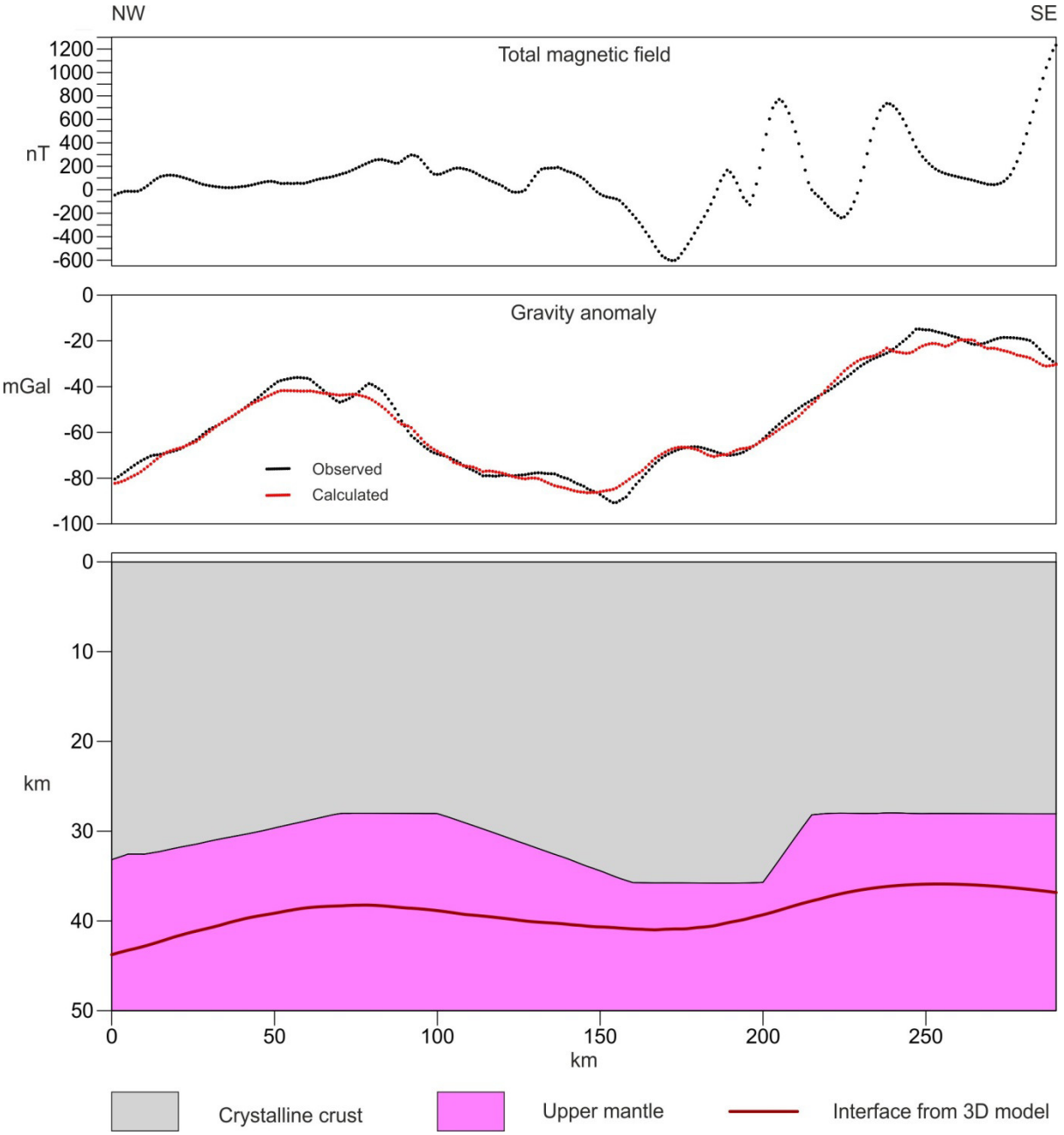

Figure 23 Moho interface from the 3D model superimposed on a simplified version of the published interpretation of seismic refraction line 7 of Funck et al. (2008)

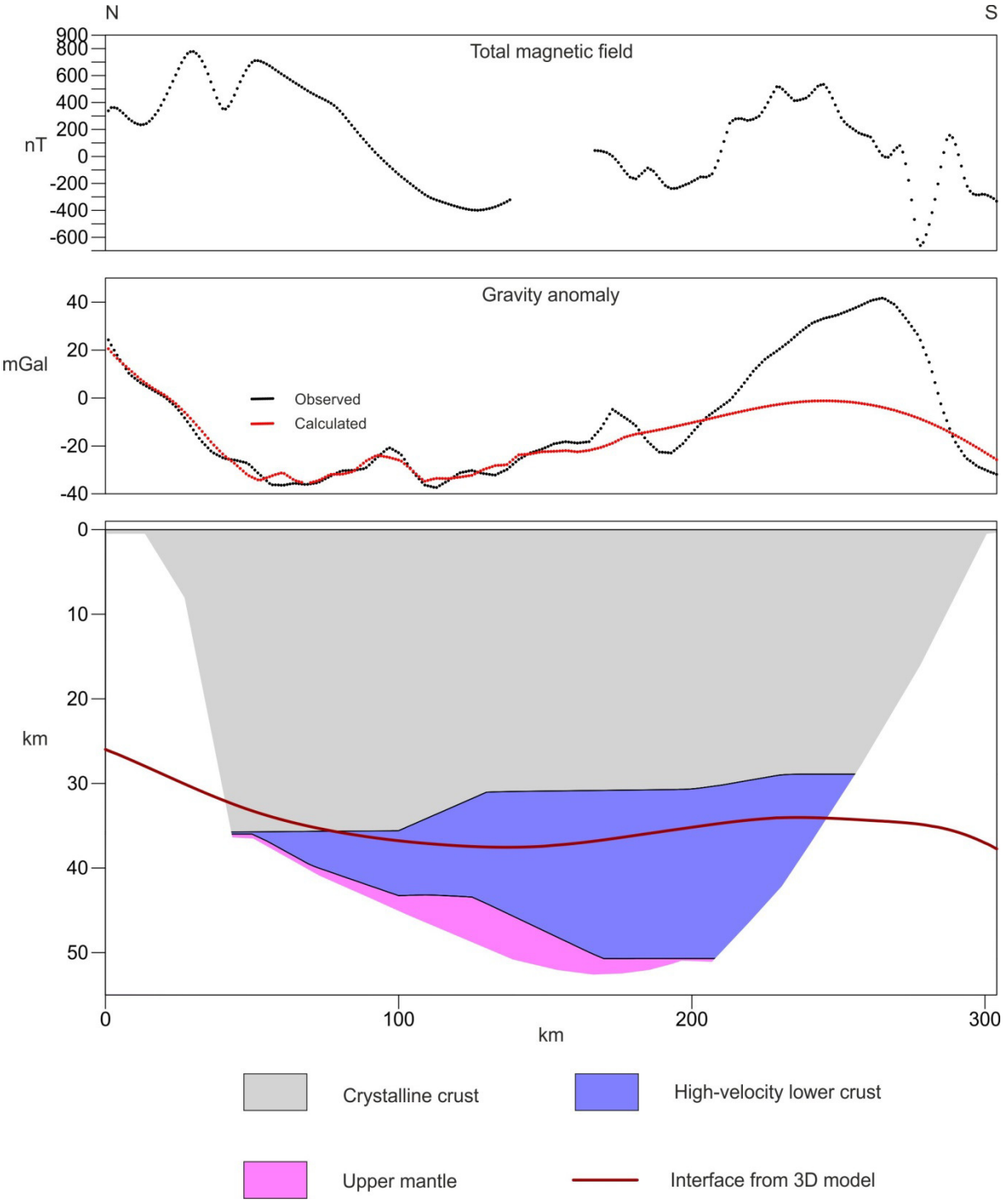

Figure 24 Moho interface from the 3D model superimposed on a simplified version of the published interpretation of seismic refraction line 3 of Funck et al. (2001)

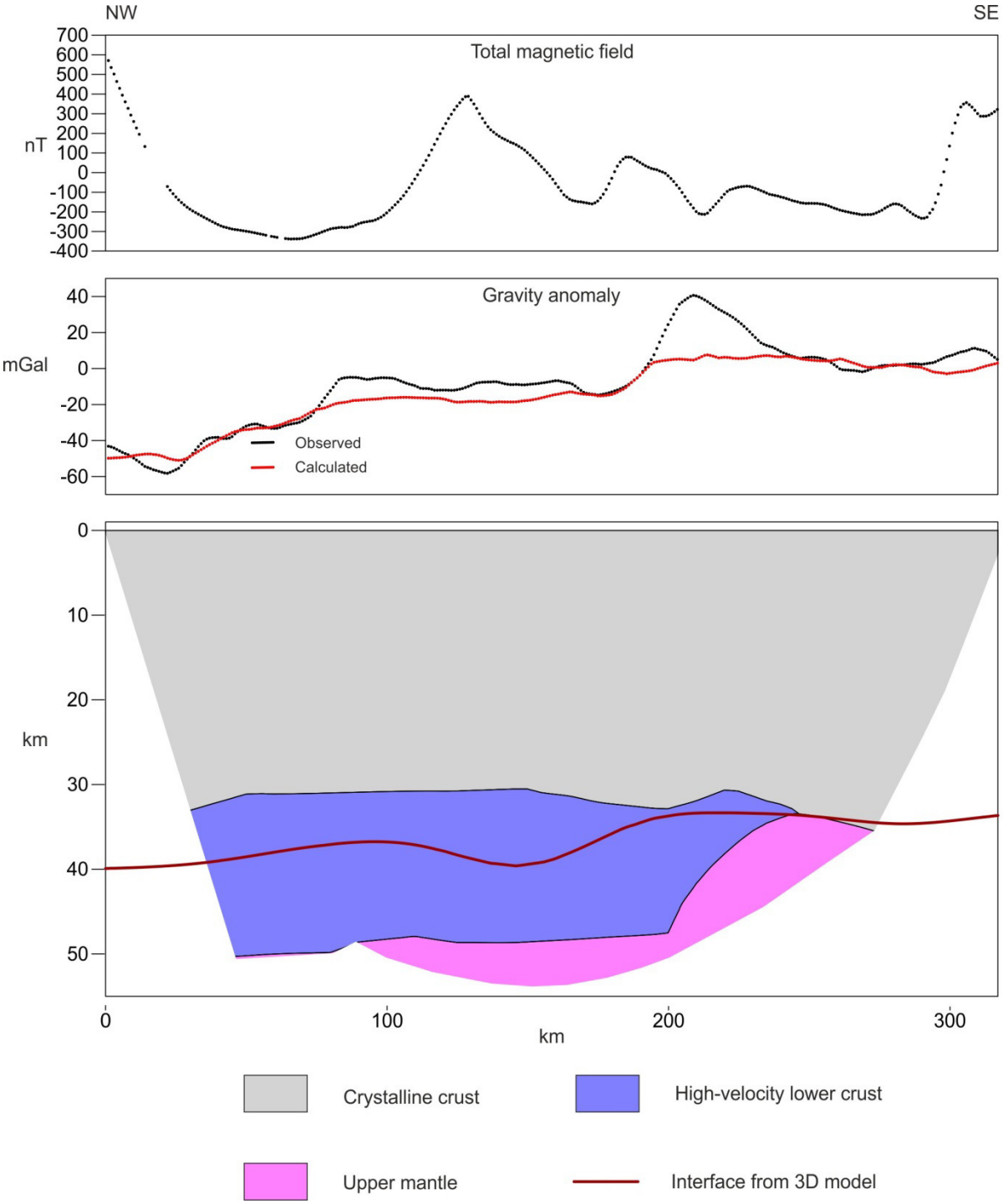

Figure 25 Moho interface from the 3D model superimposed on a simplified version of the published interpretation of seismic refraction line 2 of Funck et al. (2001)

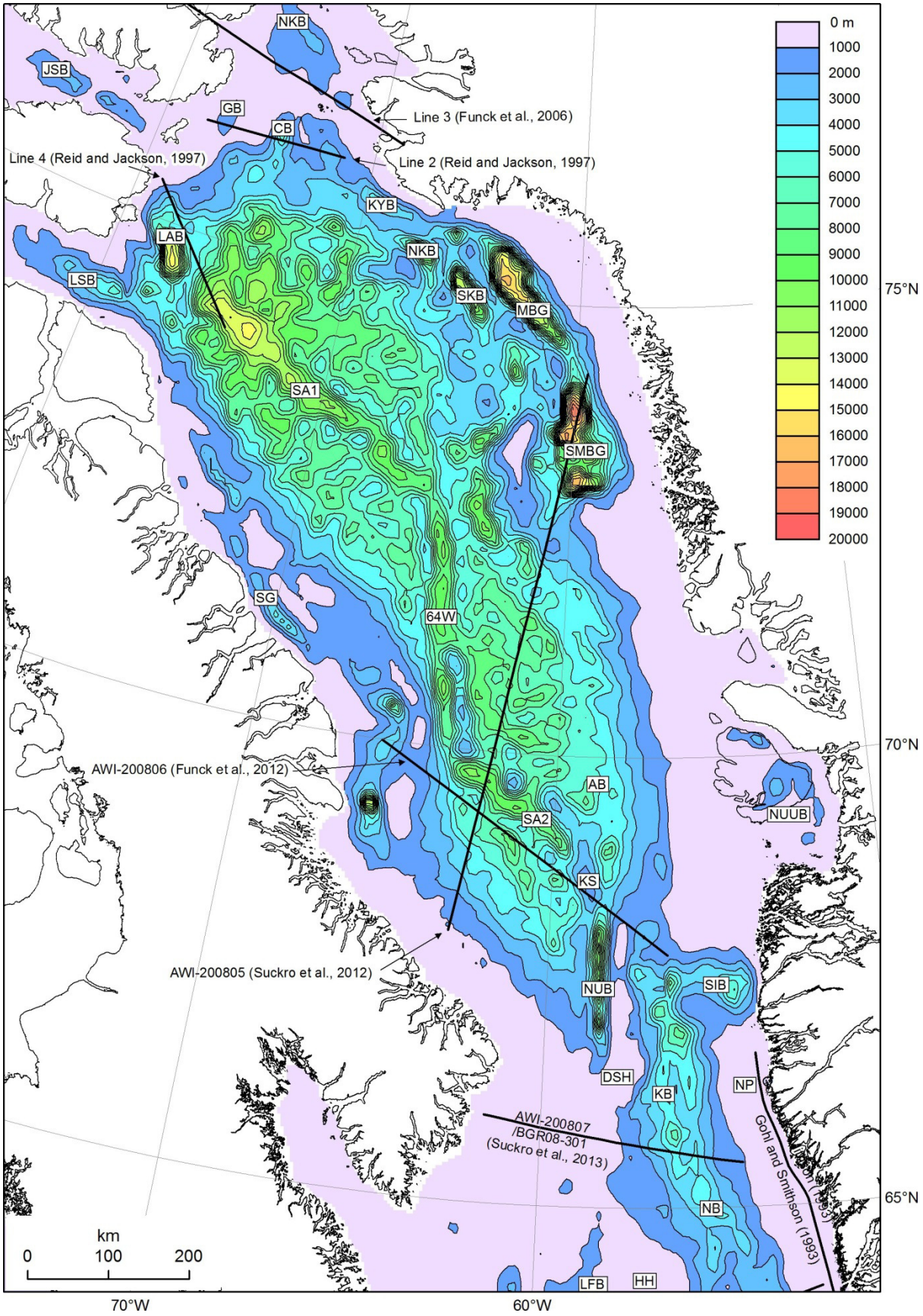

Figure 26 Optimised sediment thickness in the northern part of the study area.
64W - 64 Degree West Fracture Zone; AB - Aasiaat Basin; CB - Carey Basin; DSH - Davis Strait High; GB - Glacier Basin; HH - Hecla High; JSB - Jones Sound Basin; KB - Kangâmiut Basin; KS - Kangerluk Structure; KYB - Kap York Basin; LAB - Lady Anne Basin; LFB - Lady Franklin Basin; LSB - Lancaster Sound Basin; MBG - Melville Bay Graben; NB - Nuuk Basin; NKB - North Kivioq Basin; NP - Nuuk Platform; NUB - North Ungava Basin; NUUB - Nuussuaq Basin; SA1 - Extinct spreading axis in northern Baffin Bay; SA2 - Extinct spreading axis in southern Baffin Bay; SG - Scott Graben; SIB - Sisimiut Basin; SKB - South Kivioq Basin; SMBG - Southern part of the Melville Bay Graben

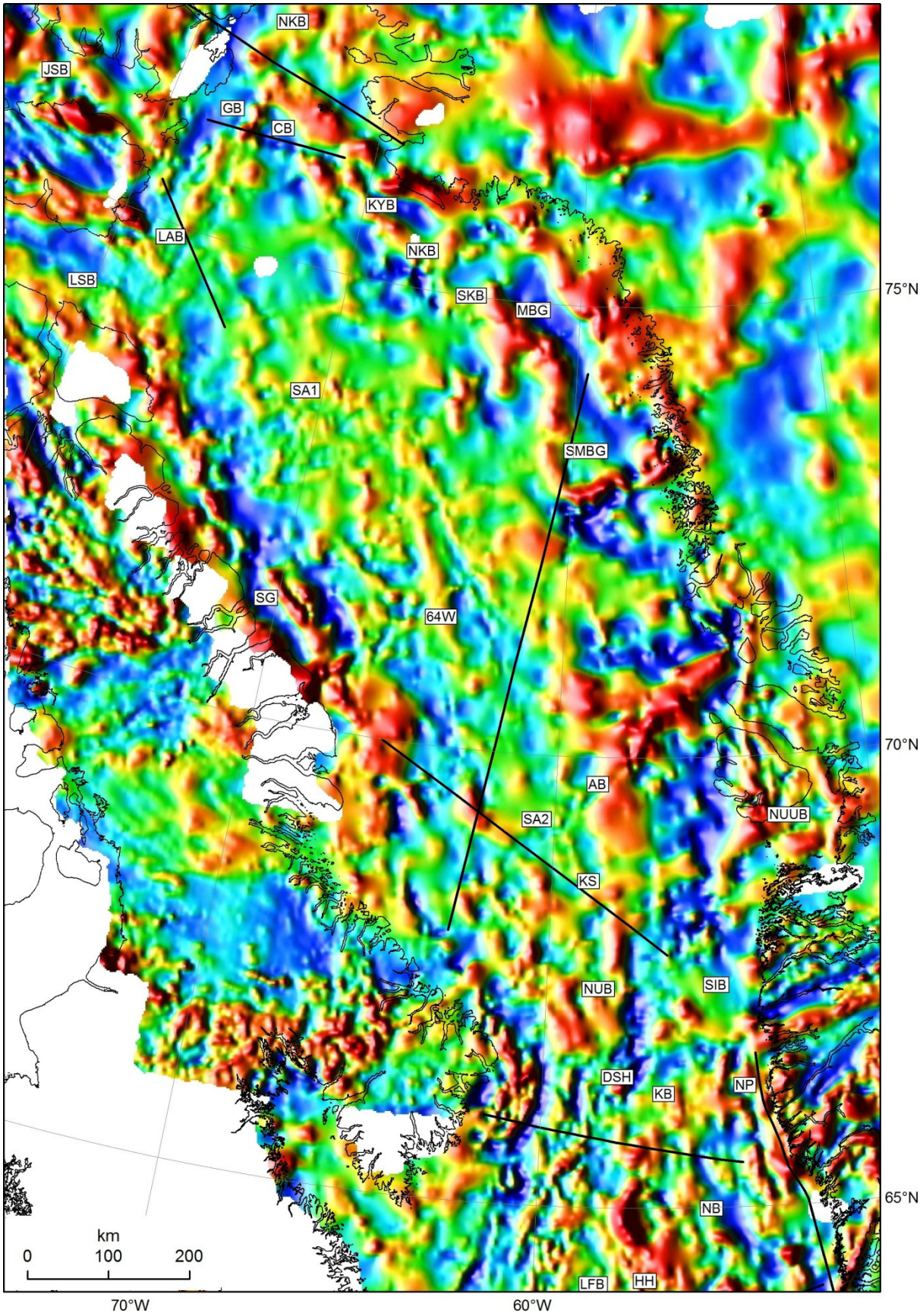

Figure 27 Total magnetic field over the area shown in Figure 21, based on the GAMMAA5 compilation (Verhoef et al., 1996). For key to abbreviations see Figure 26

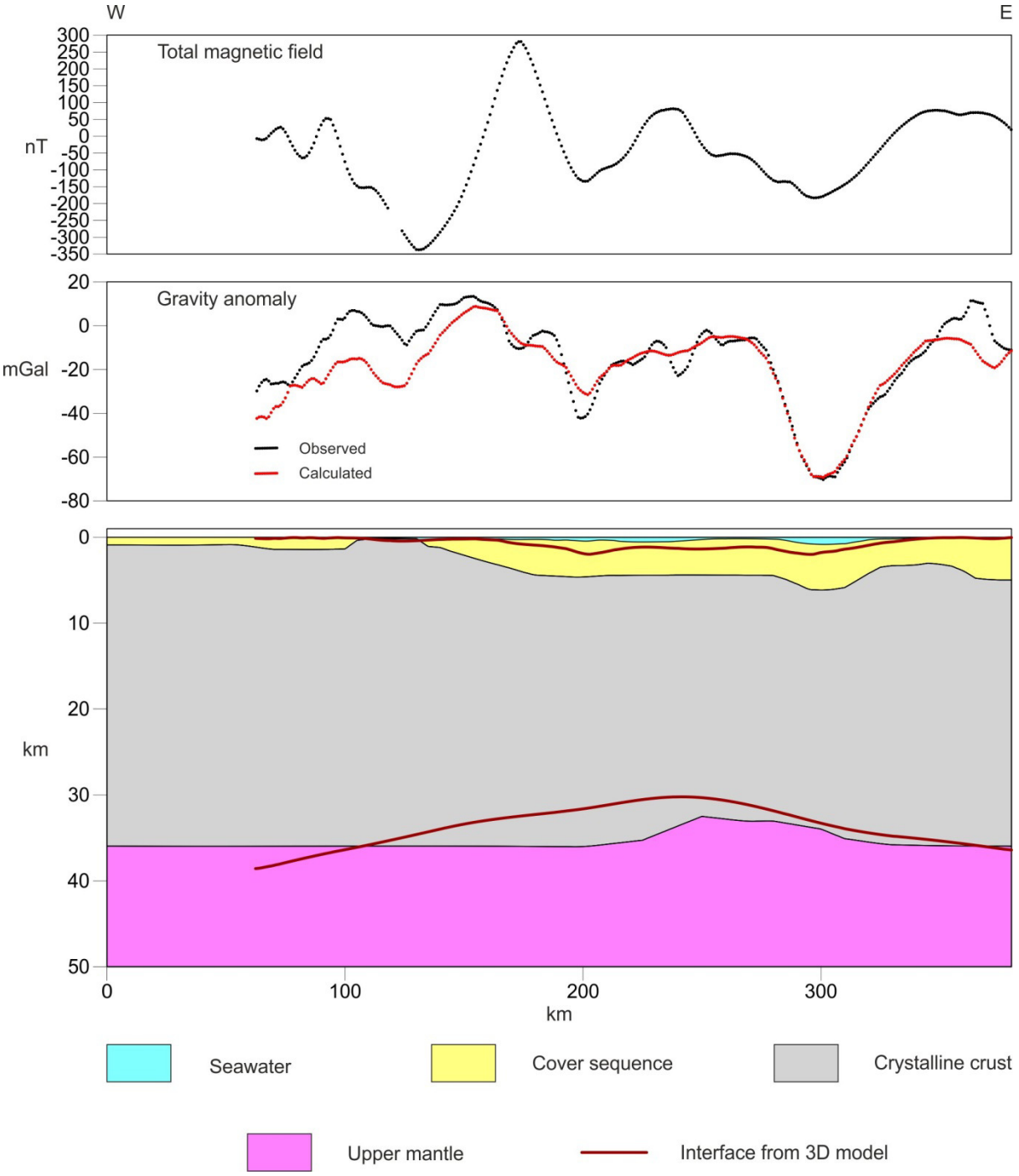

Figure 28 Top basement and Moho interfaces from the 3D model superimposed on a simplified version of the published interpretation of seismic refraction line 3 of Funck et al. (2006). Note that the cover sequence in the latter model mainly comprises the Proterozoic Thule Group, which was effectively assigned to 'basement' in the gravity model

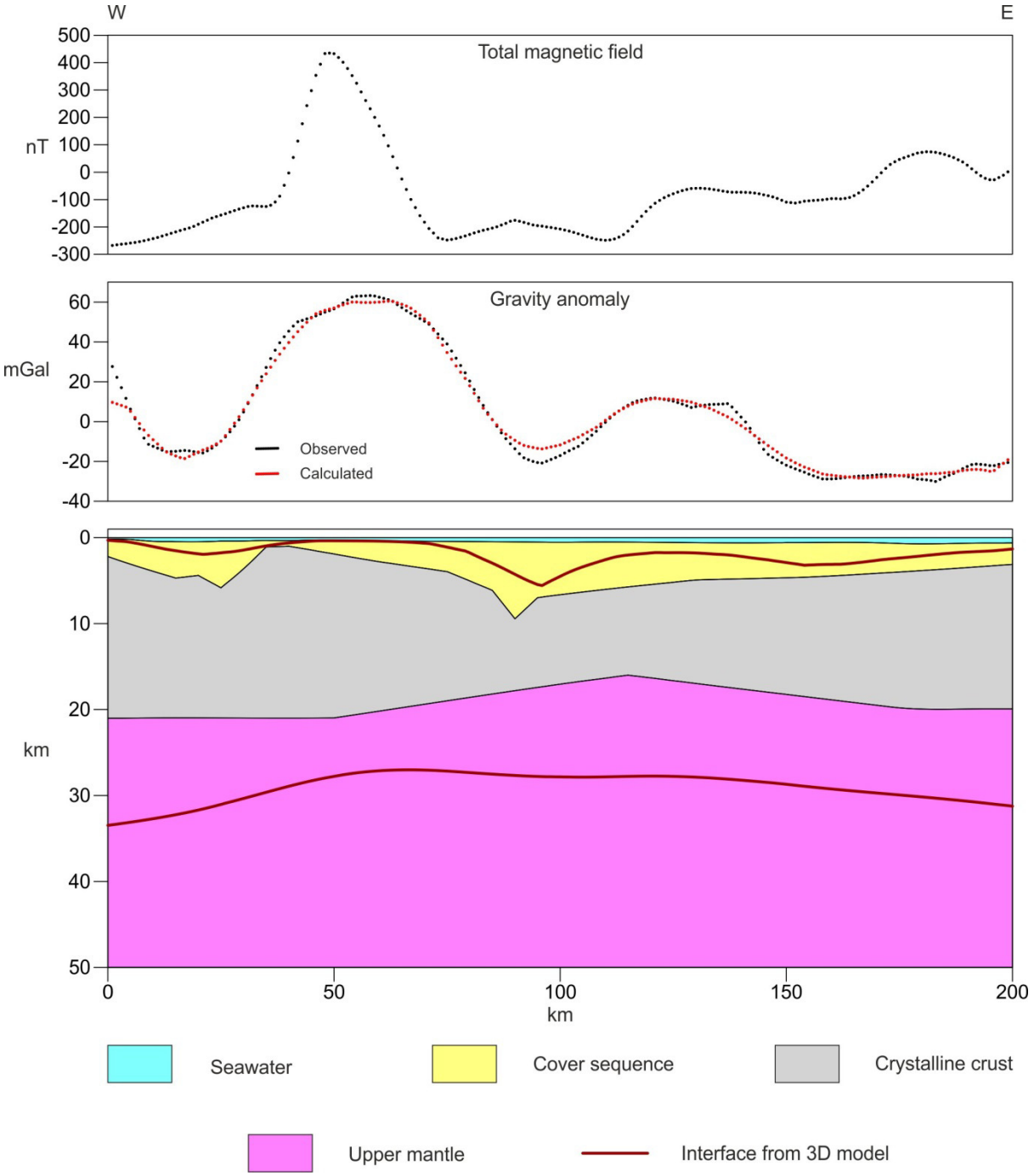

Figure 29 Top basement and Moho interfaces from the 3D model superimposed on a simplified version of the published interpretation of seismic refraction line 2 of Reid and Jackson (1997)

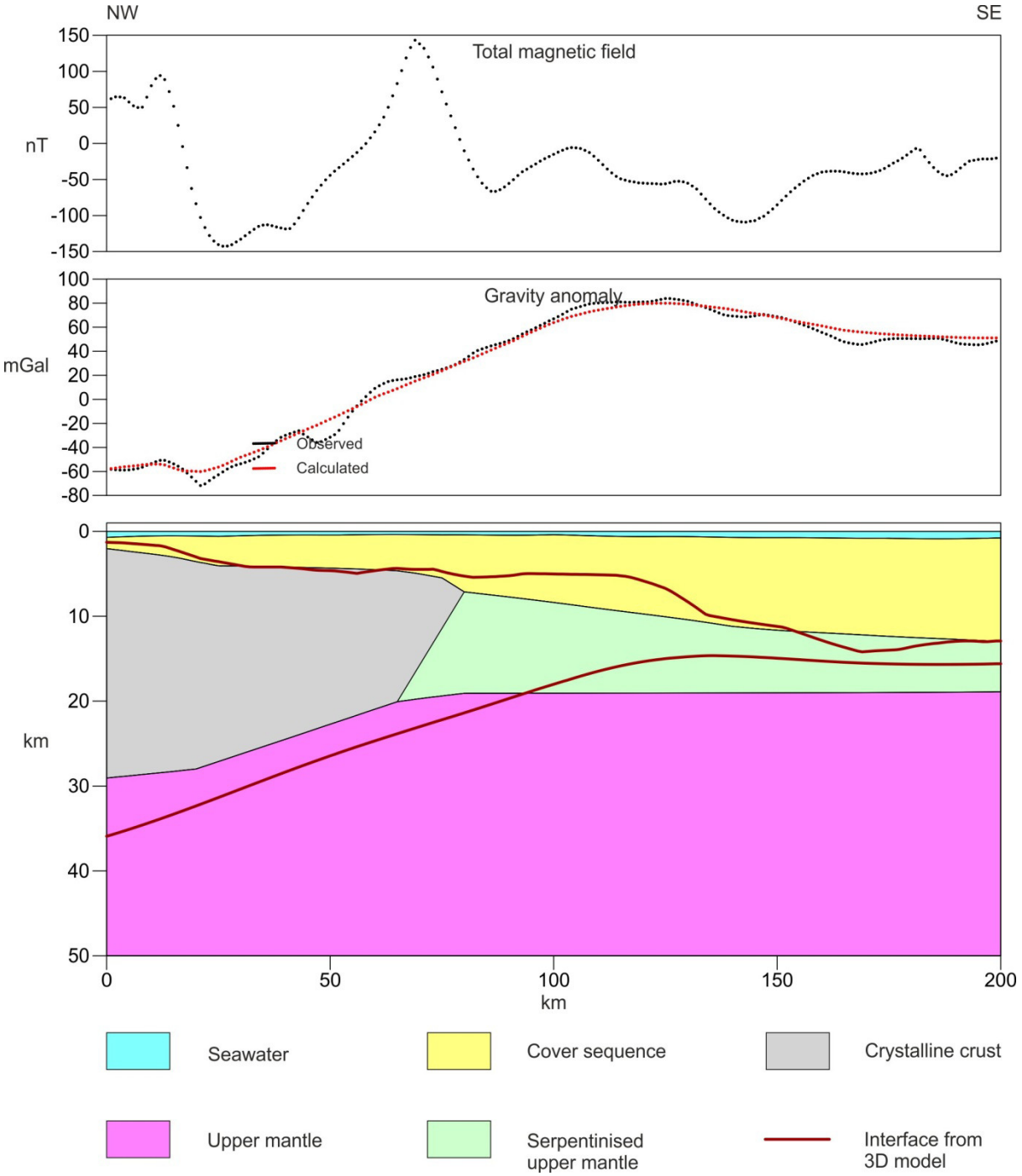

Figure 30 Top basement and Moho interfaces from the 3D model superimposed on a simplified version of the published interpretation of seismic refraction line 4 of Reid and Jackson (1997)

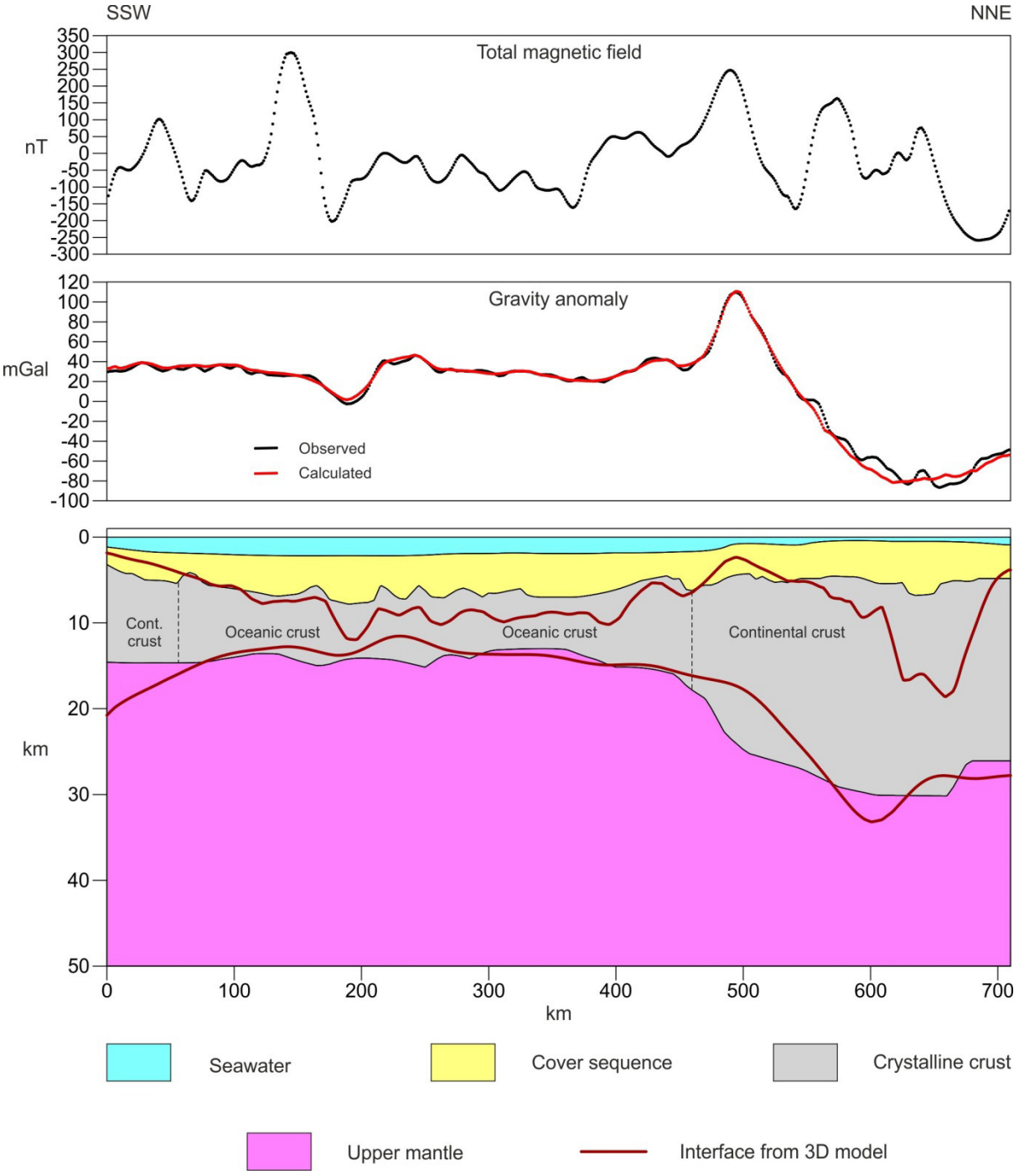

Figure 31 Top basement and Moho interfaces from the 3D model superimposed on a simplified version of the published interpretation of seismic refraction line AWI-200805 (Suckro et al., 2012)

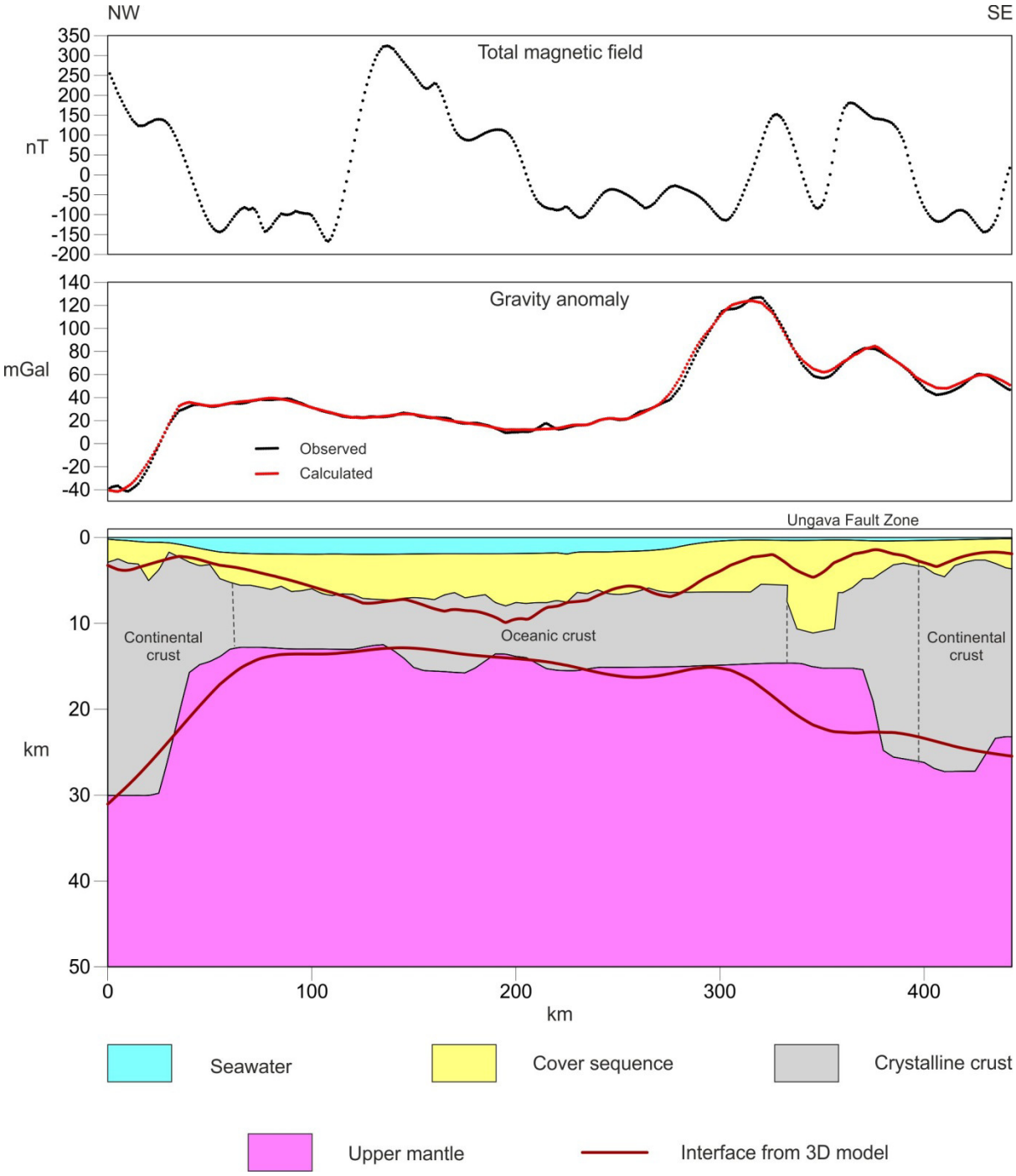

Figure 32 Top basement and Moho interfaces from the 3D model superimposed on a simplified version of the published interpretation of seismic refraction line AWI-200806 (Funck et al., 2012)

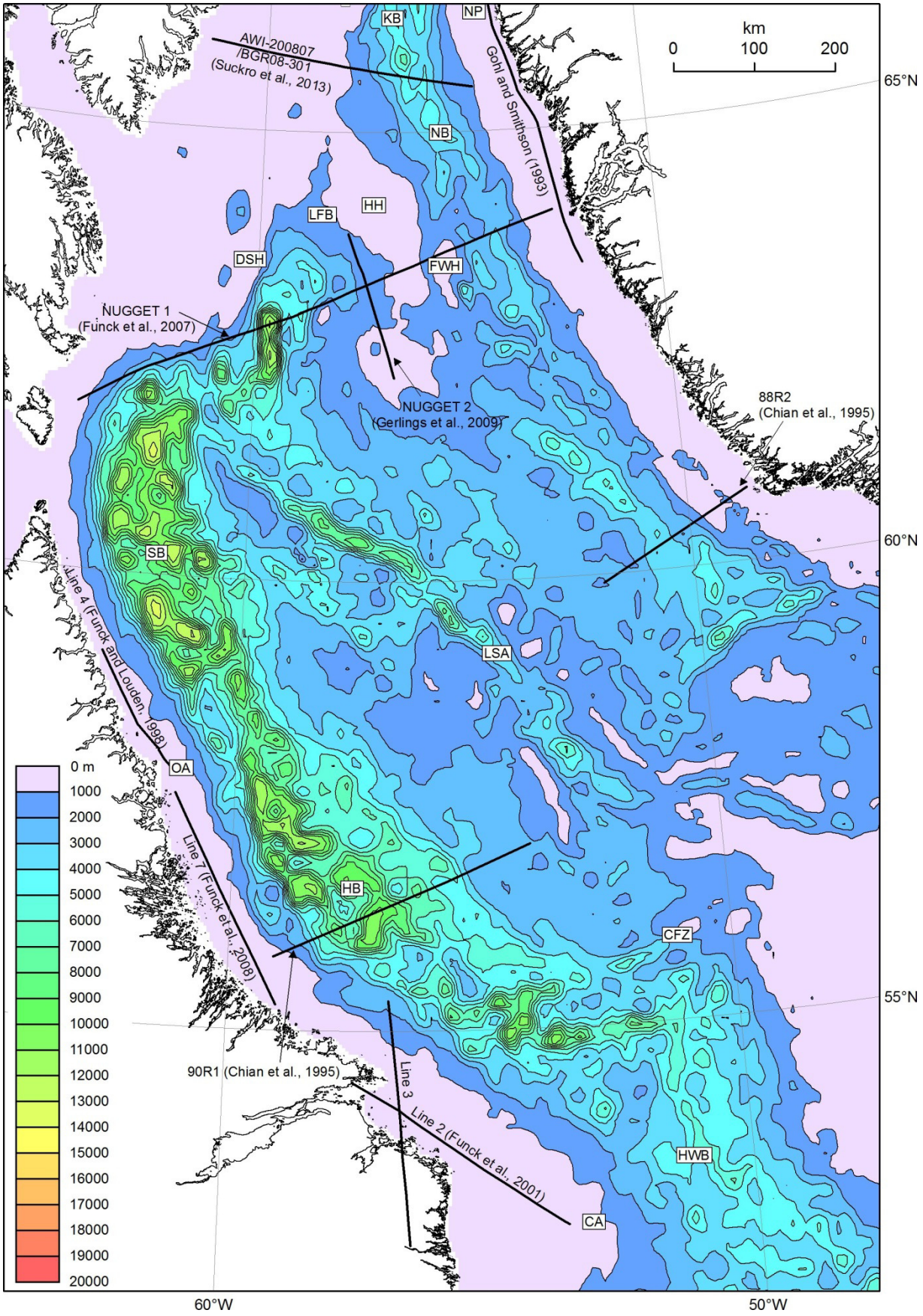

Figure 33 Optimised sediment thickness in the central part of the study area.
CA - Cartwright Arch; CFZ - Cartwright Fracture Zone; DSH - Davis Strait High; FWH - Fylla West High; HB - Hopedale Basin; HH - Hecla High; HWB - awke Basin; KB - Kangâmiut Basin; LFB - Lady Franklin Basin; NB - Nuuk Basin; NP - Nuuk Platform; OA - Okak Arch; SB - Saglek Basin

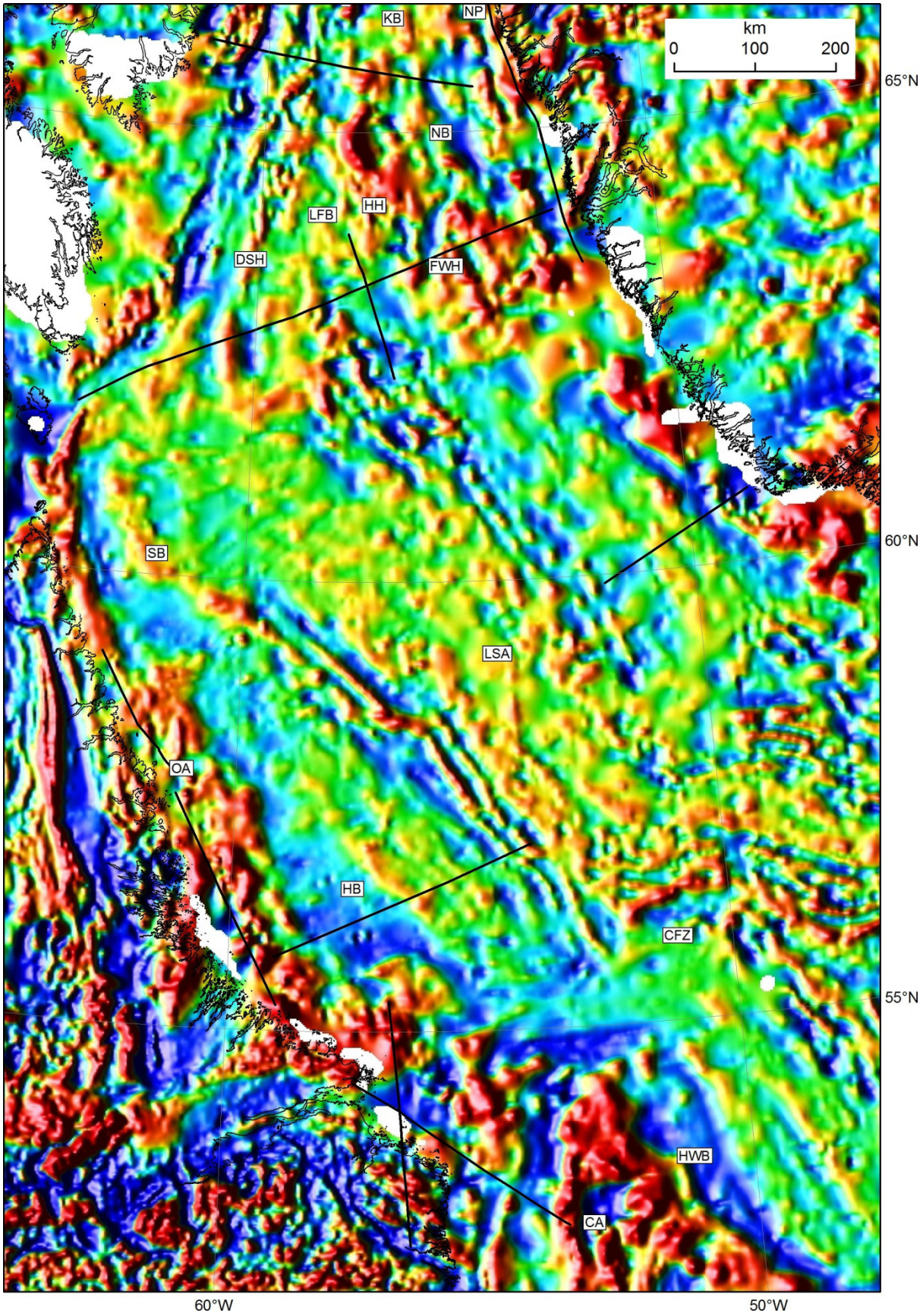

Figure 34 Total magnetic field over the area shown in Figure 33, based on the GAMMAA5 compilation (Verhoef et al., 1996). For key to abbreviations see Figure 33

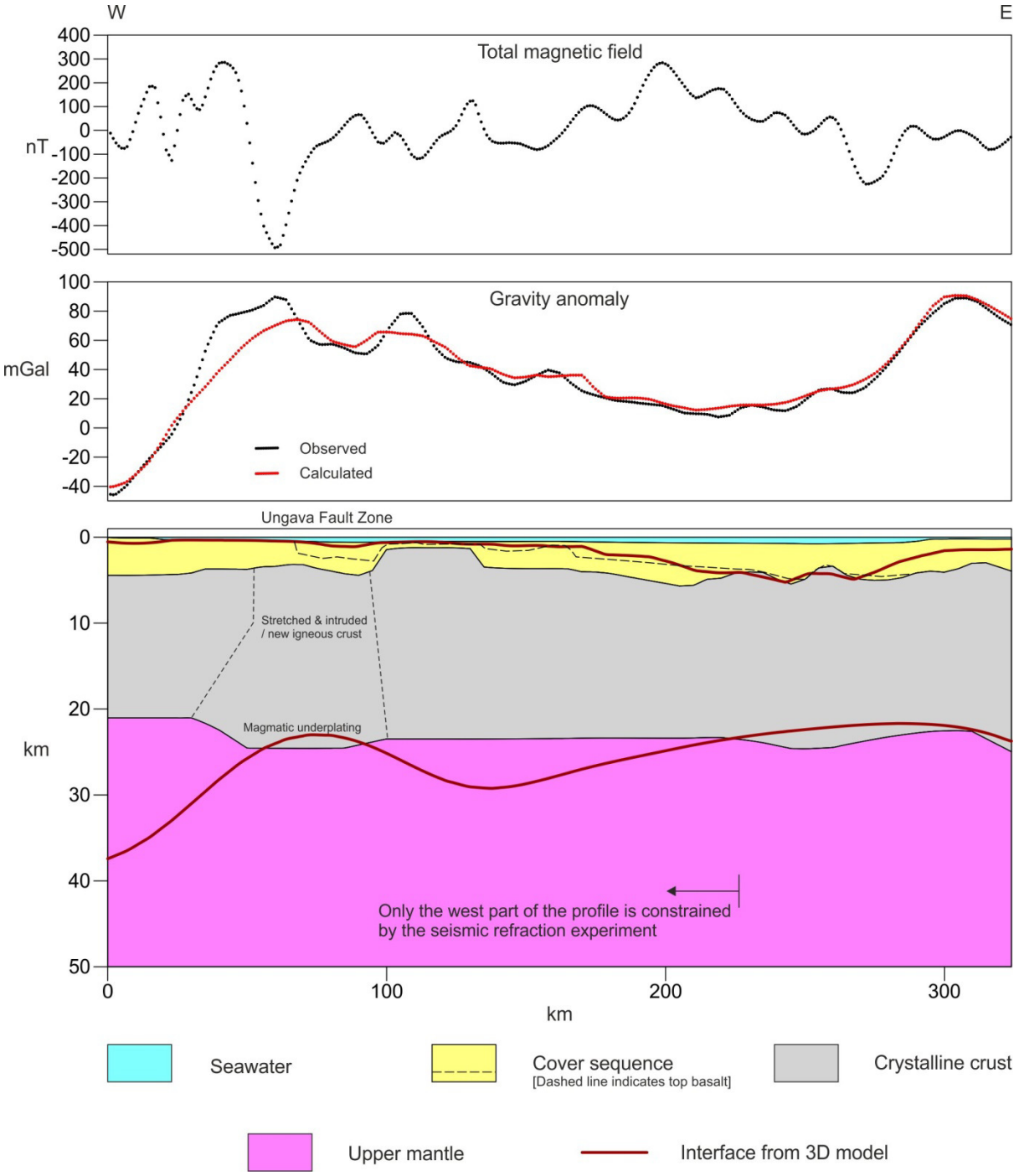

Figure 35 Top basement and Moho interfaces from the 3D model superimposed on a simplified version of the published interpretation of seismic refraction line AWI-200807 (+ BGR08-301) (Suckro et al., 2013)

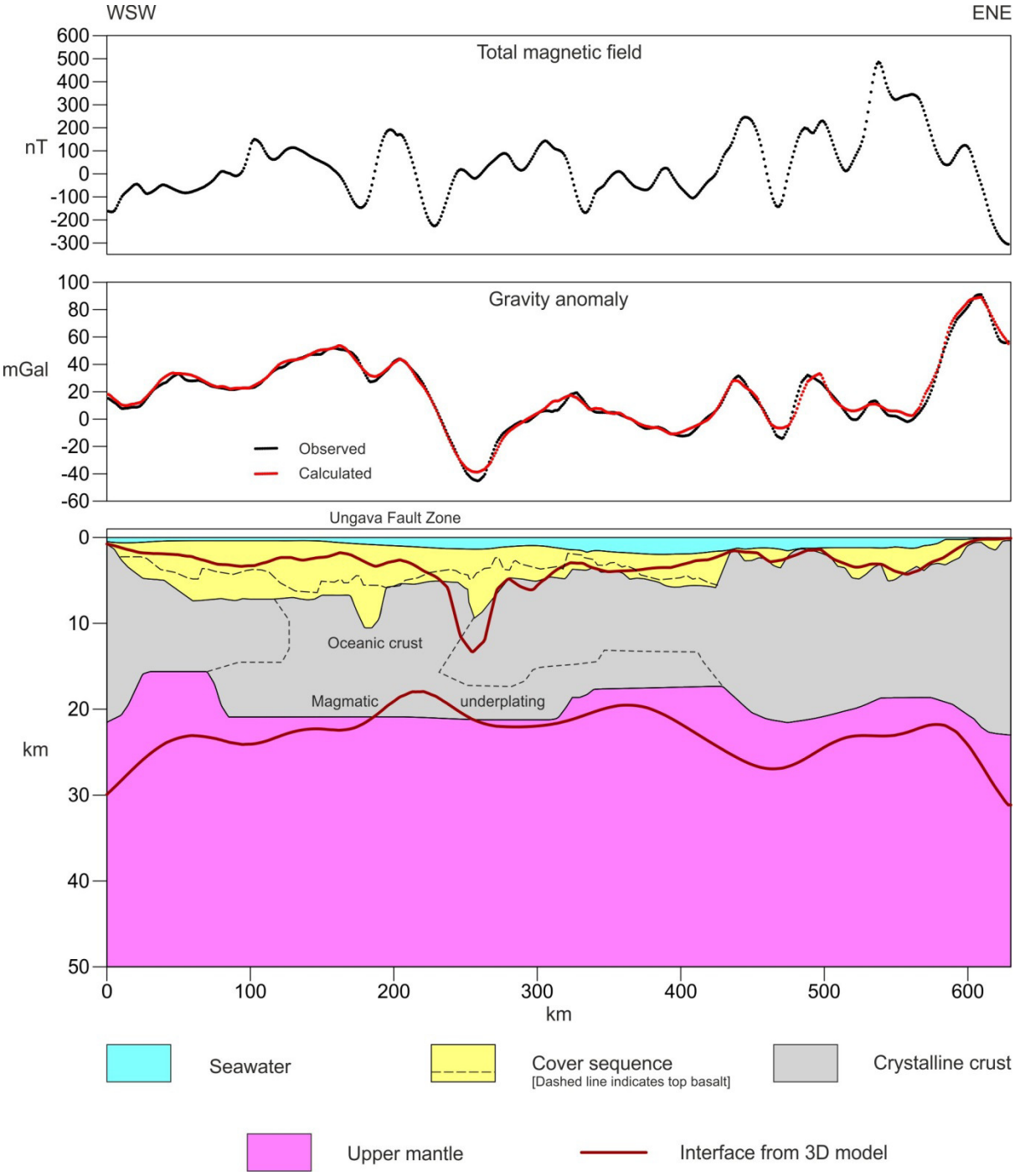

Figure 36 Moho interface from the 3D model superimposed on a simplified version of the published interpretation of seismic refraction line NUGGET-1 (Funck et al., 2007)

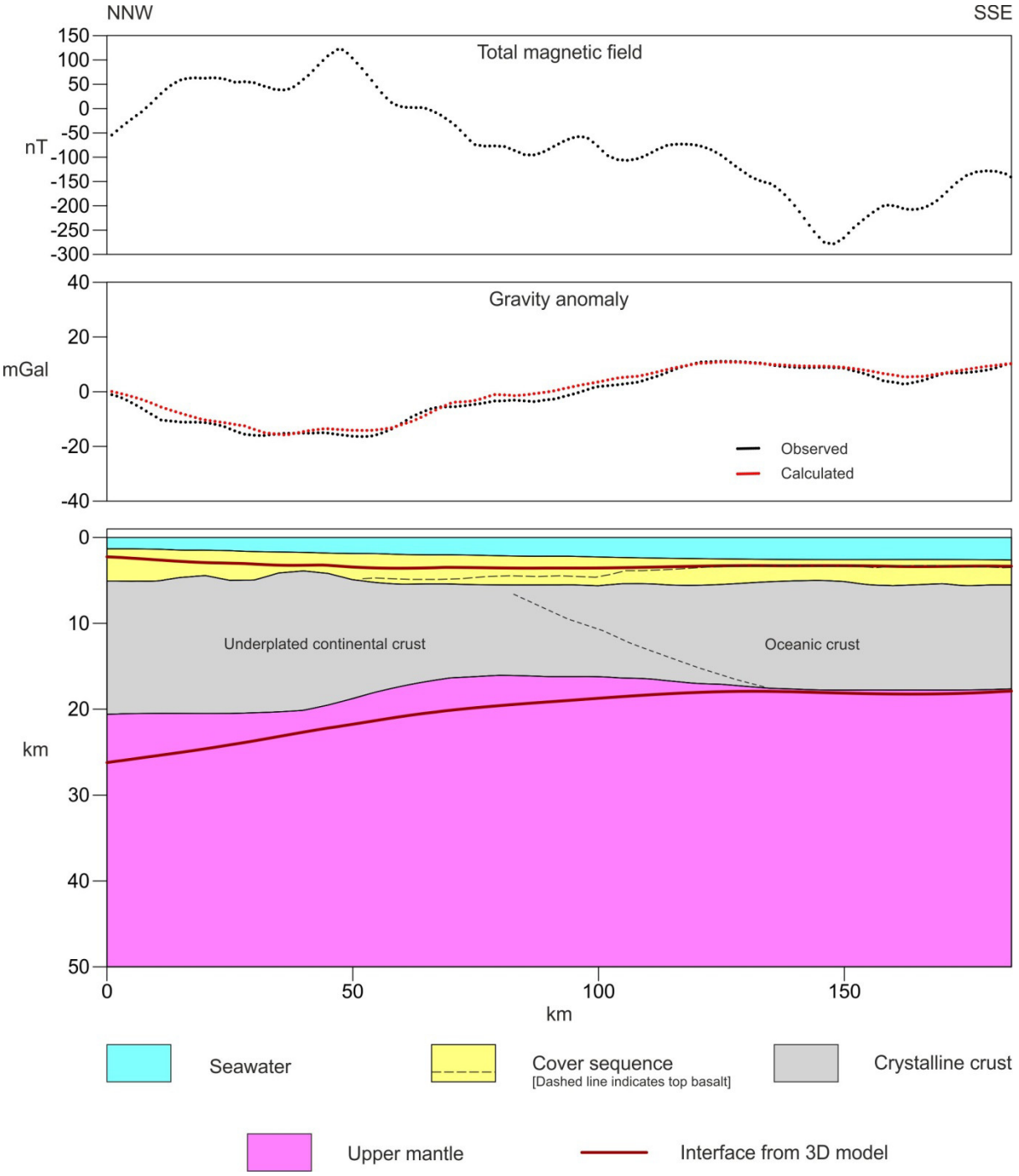

Figure 37 Top basement and Moho interfaces from the 3D model superimposed on a simplified version of the published interpretation of seismic refraction line NUGGET-2 (Gerlings et al., 2009)

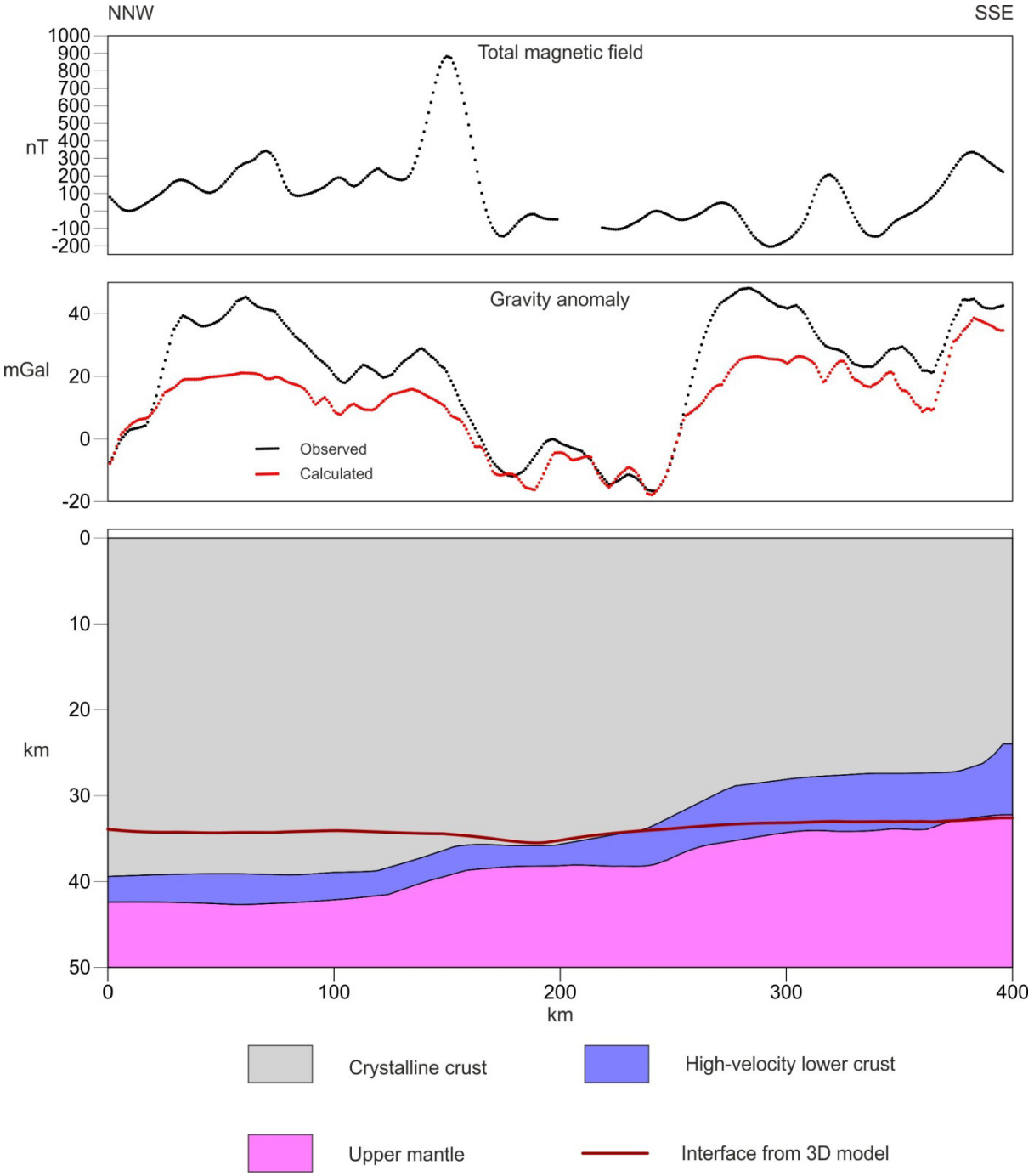

Figure 38 Top basement and Moho interfaces from the 3D model superimposed on a simplified version of the published interpretation of seismic refraction line of Gohl and Smithson (1993)

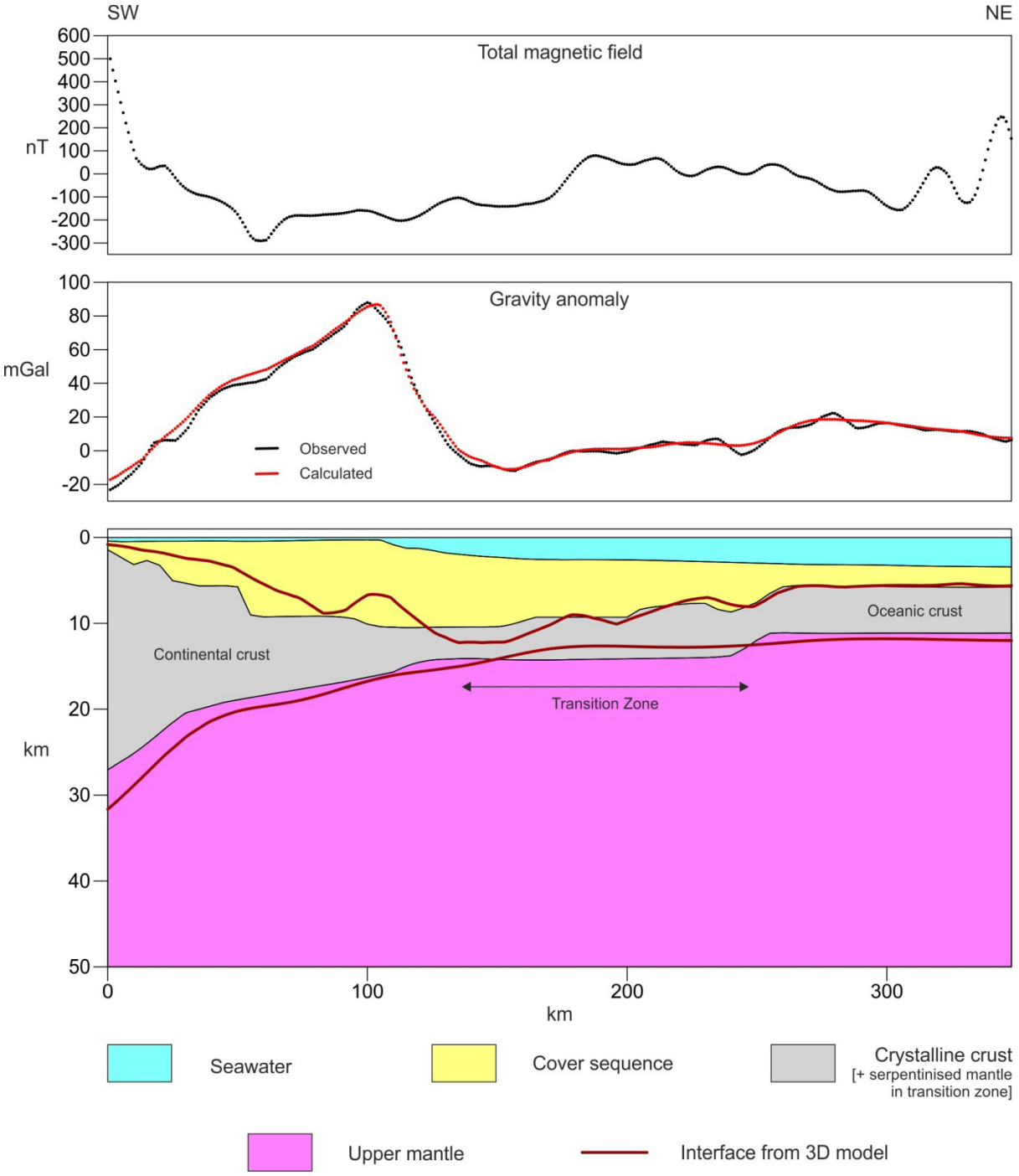

Figure 39 Top basement and Moho interfaces from the 3D model superimposed on a simplified version of the published interpretation of seismic refraction line 90R1 (Chian et al., 1995a,b)

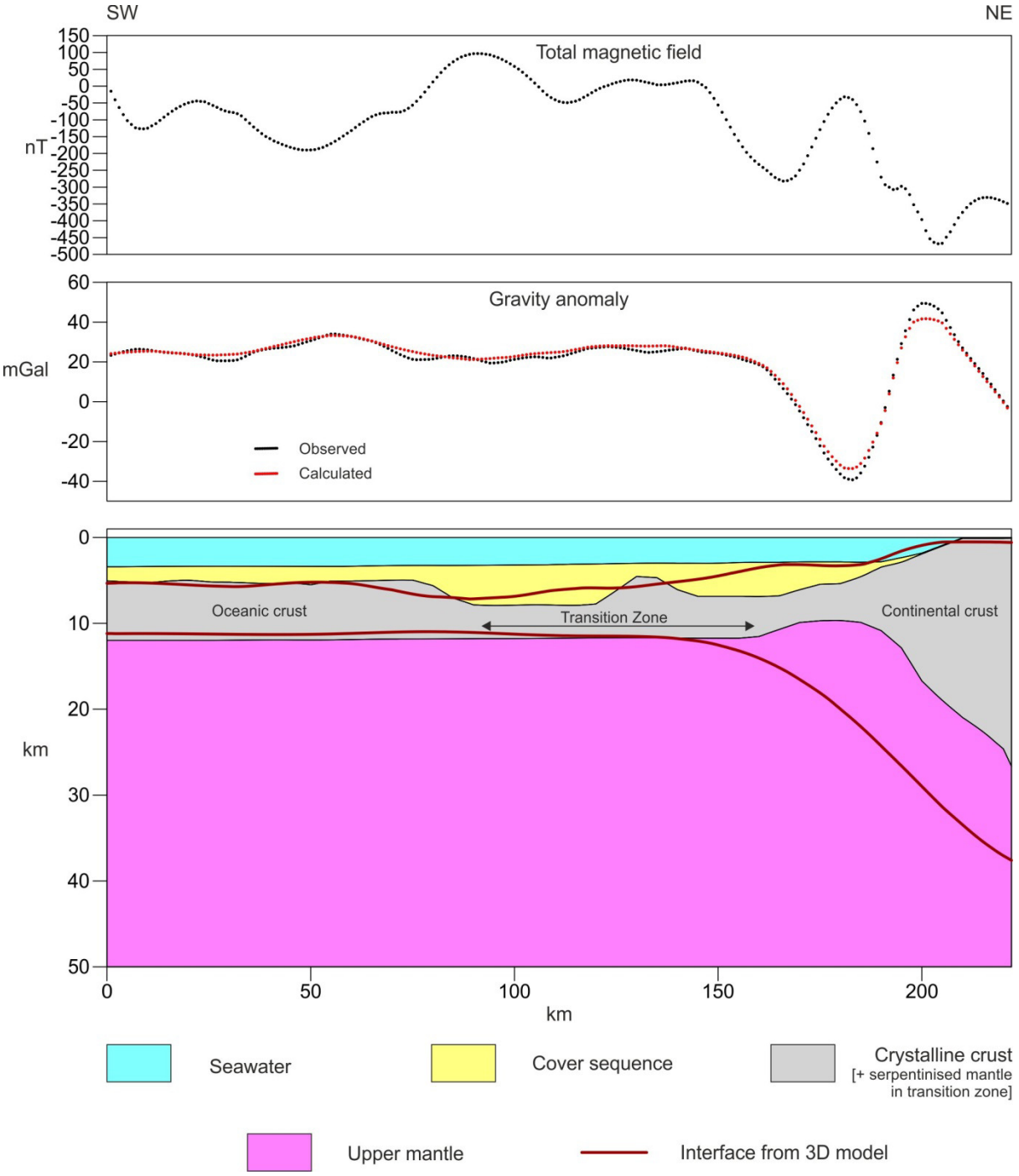

Figure 40 Top basement and Moho interfaces from the 3D model superimposed on a simplified version of the published interpretation of seismic refraction line 88R2 (Chian and Louden, 1994)

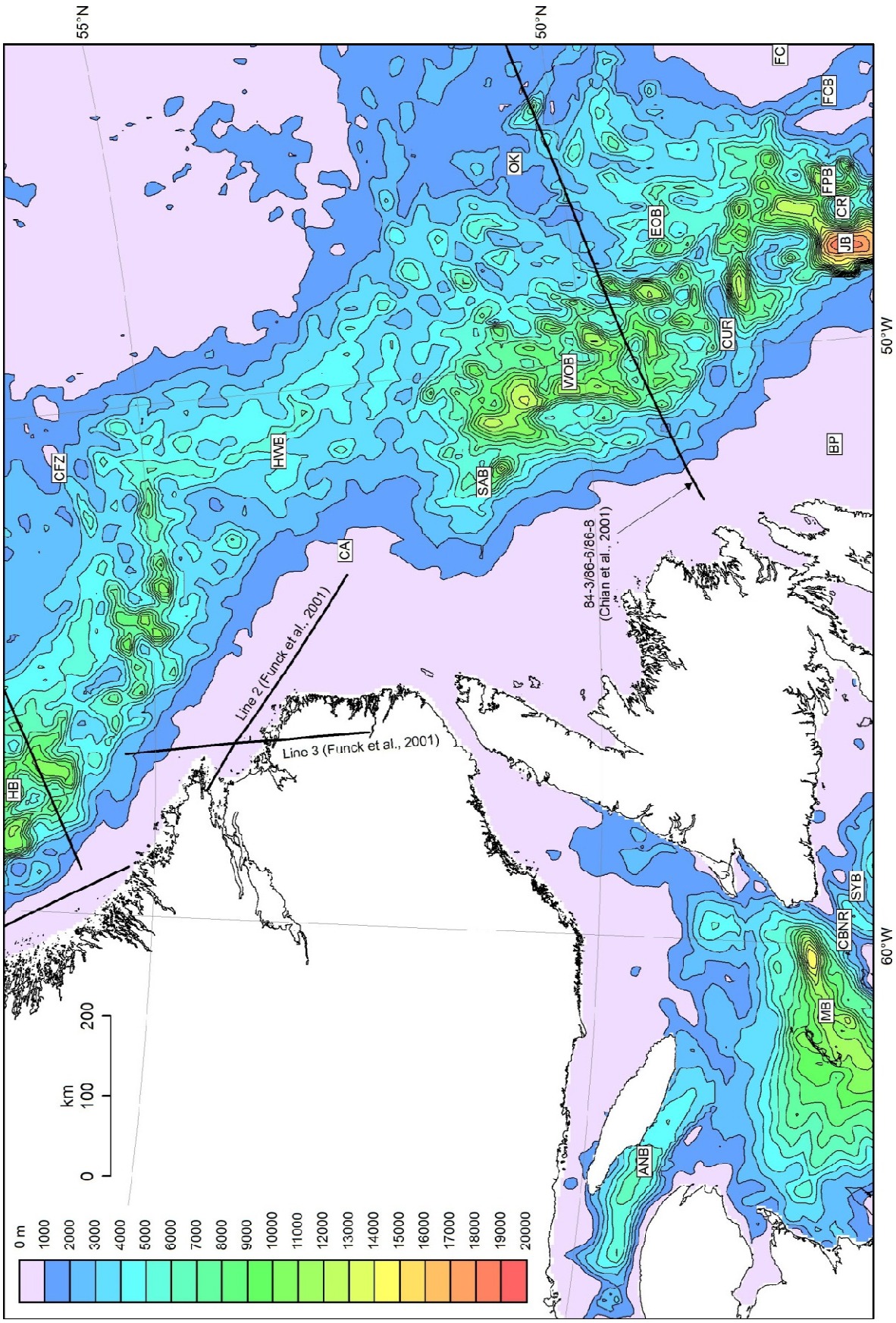

Figure 41 Optimised sediment thickness in the southern part of the study area.
ANB - Anticosti Basin; BP - Bonavista Platform; CA - Cartwright Arch; CBNR - Cape Breton - Newfoundland Ridge; CFZ - Cartwright Fracture Zone; CR - Central Ridge; CUR - Cumberland Ridge; EOB - East OIphan Basin; FC - Flemish Cap; FCB - Flemish Cap Basin; FPB - Flemish Pass Basin; HB - Hopedale Basin; HWB - Hawke Basin; JB - Jean d'Arc Basin; MB - Magdalen Basin; OK - Orphan Knoll; SAB - St Anthony Basin; SYB - Sydney Basin; WOB - West Orphan Basin

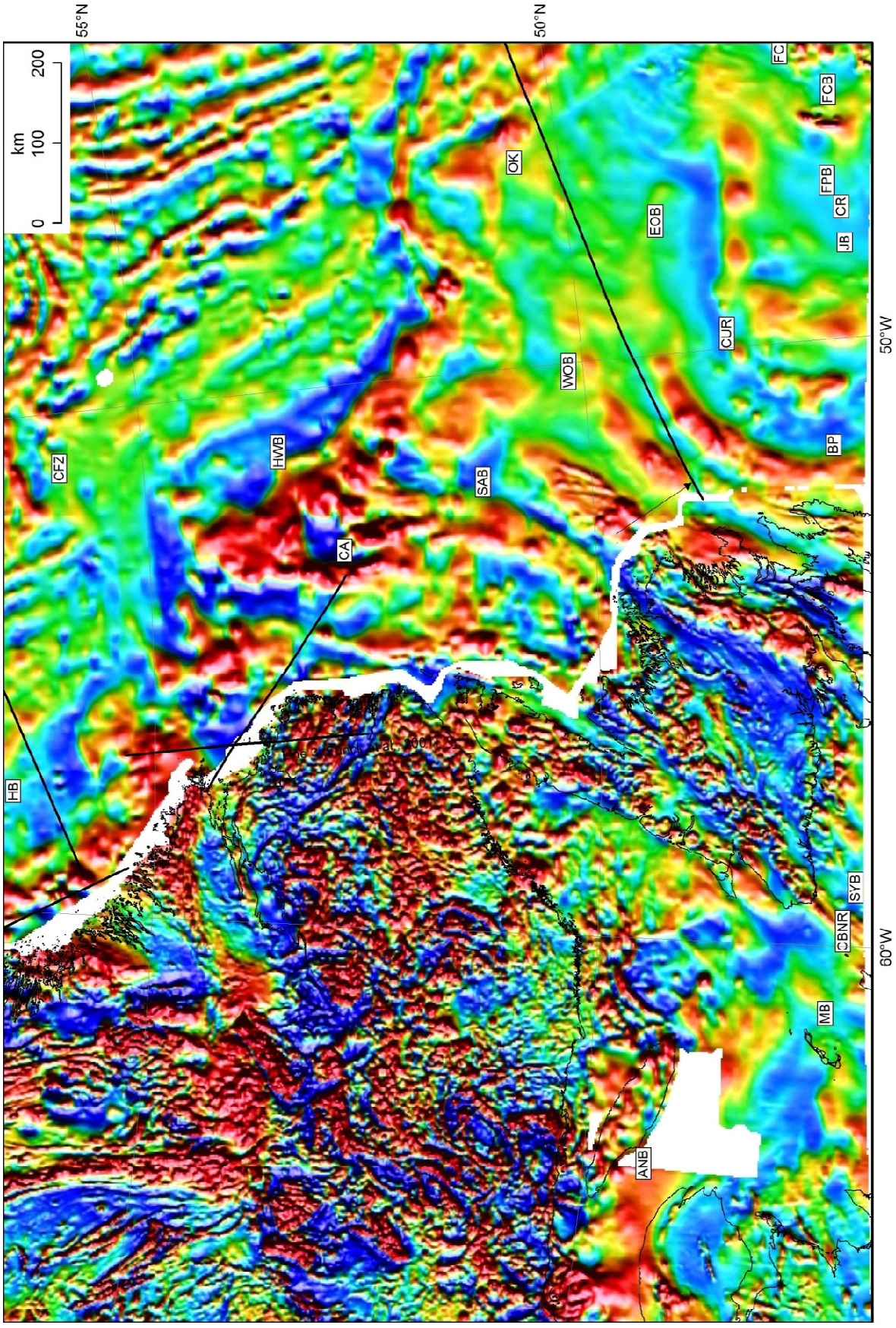

Figure 42 Total magnetic field over the area shown in Figure 41, based on a compilation by the Geological Survey of Canada. For key to abbreviations see Figure 41

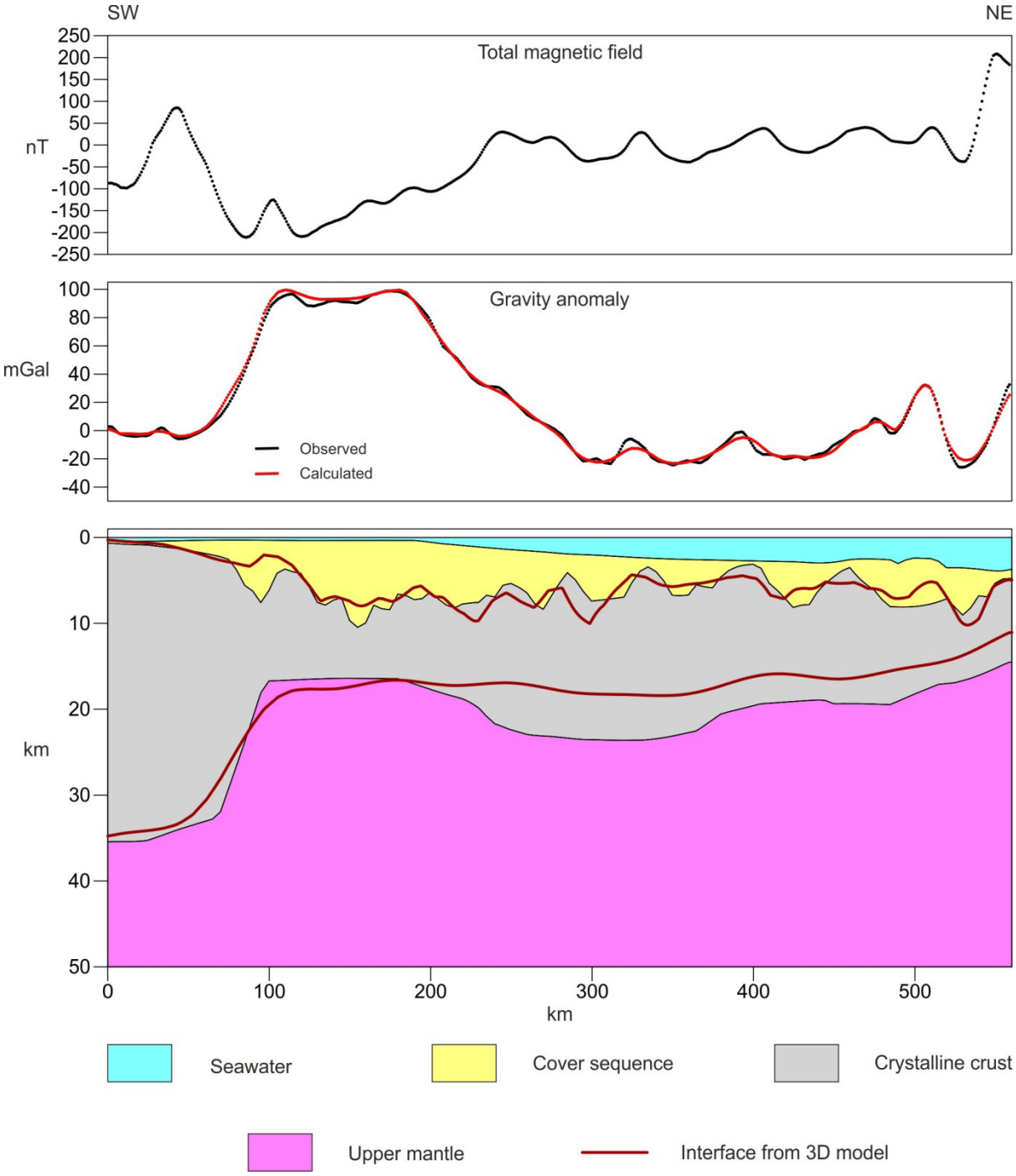

Figure 43 Top basement and Moho interfaces from the 3D model superimposed on a simplified version of the published interpretation of seismic reflection/refraction line 84-3/86-6/86-8 (Chian et al., 2001)

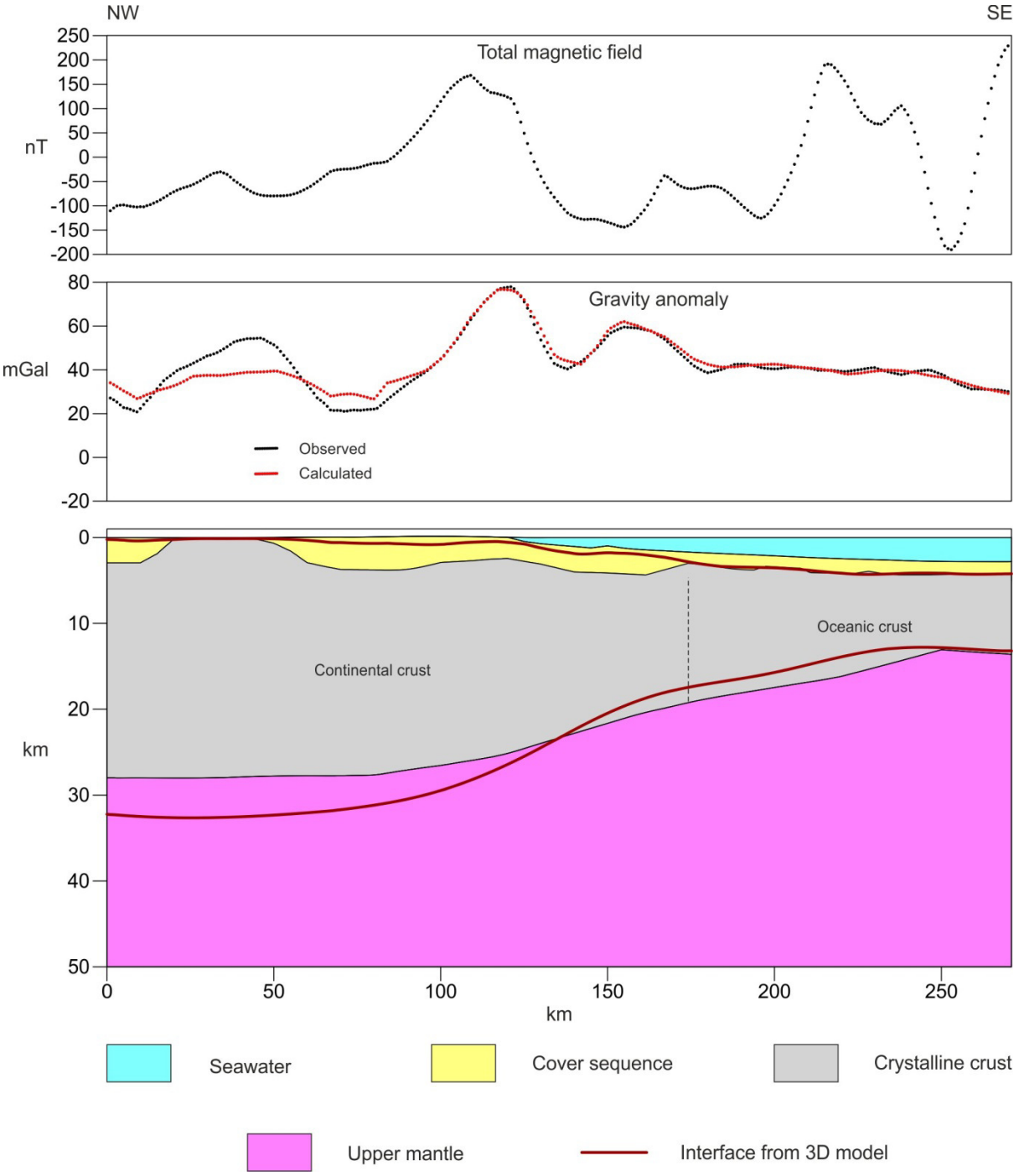

Figure 44 Top basement and Moho interfaces from the 3D model superimposed on a simplified version of the published interpretation of seismic refraction line SIGMA 4 (Holbrook et al., 2001)

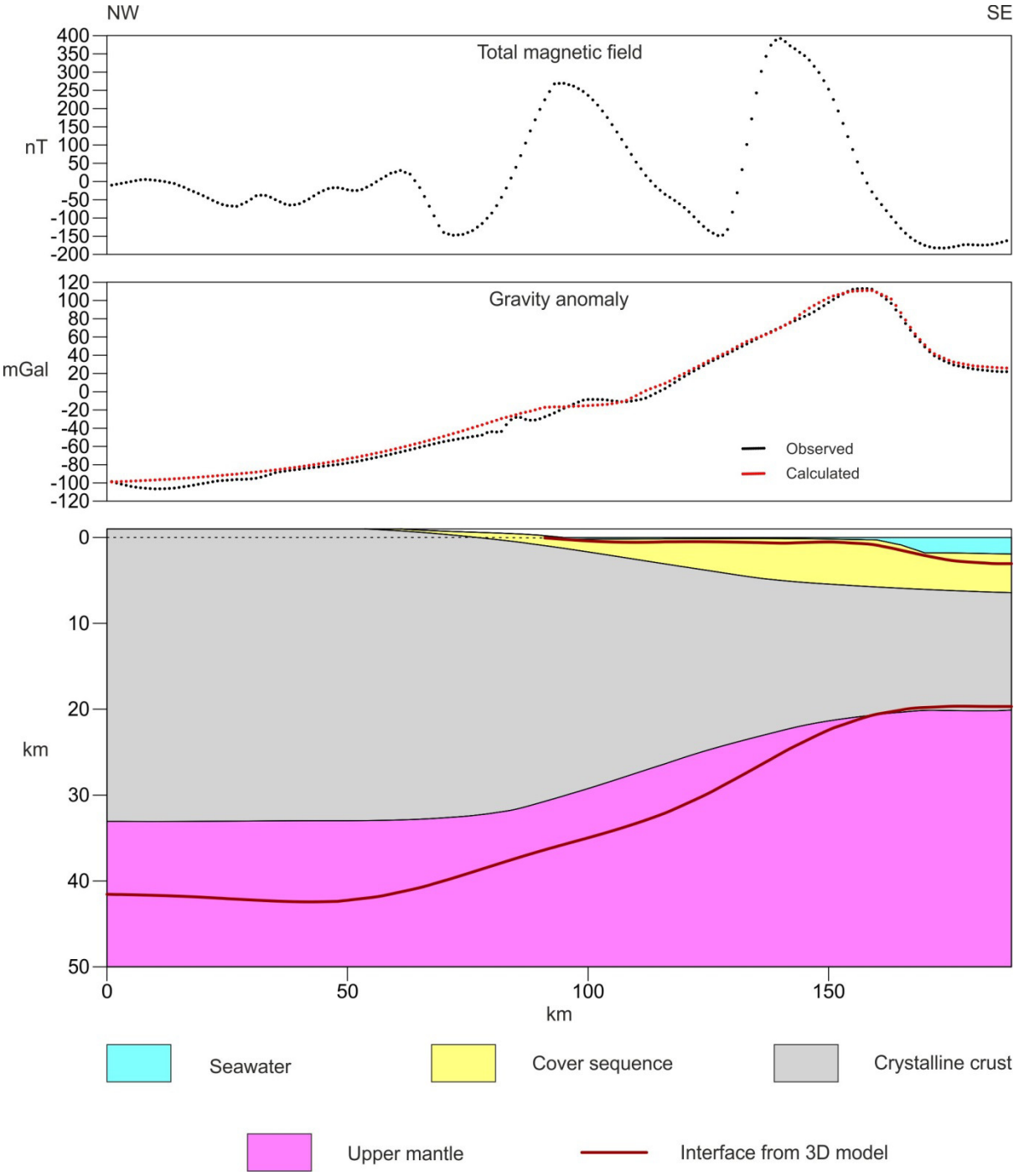

Figure 45 Top basement and Moho interfaces from the 3D model superimposed on a simplified version of the published interpretation of seismic refraction line SIGMA 3 (Holbrook et al., 2001)

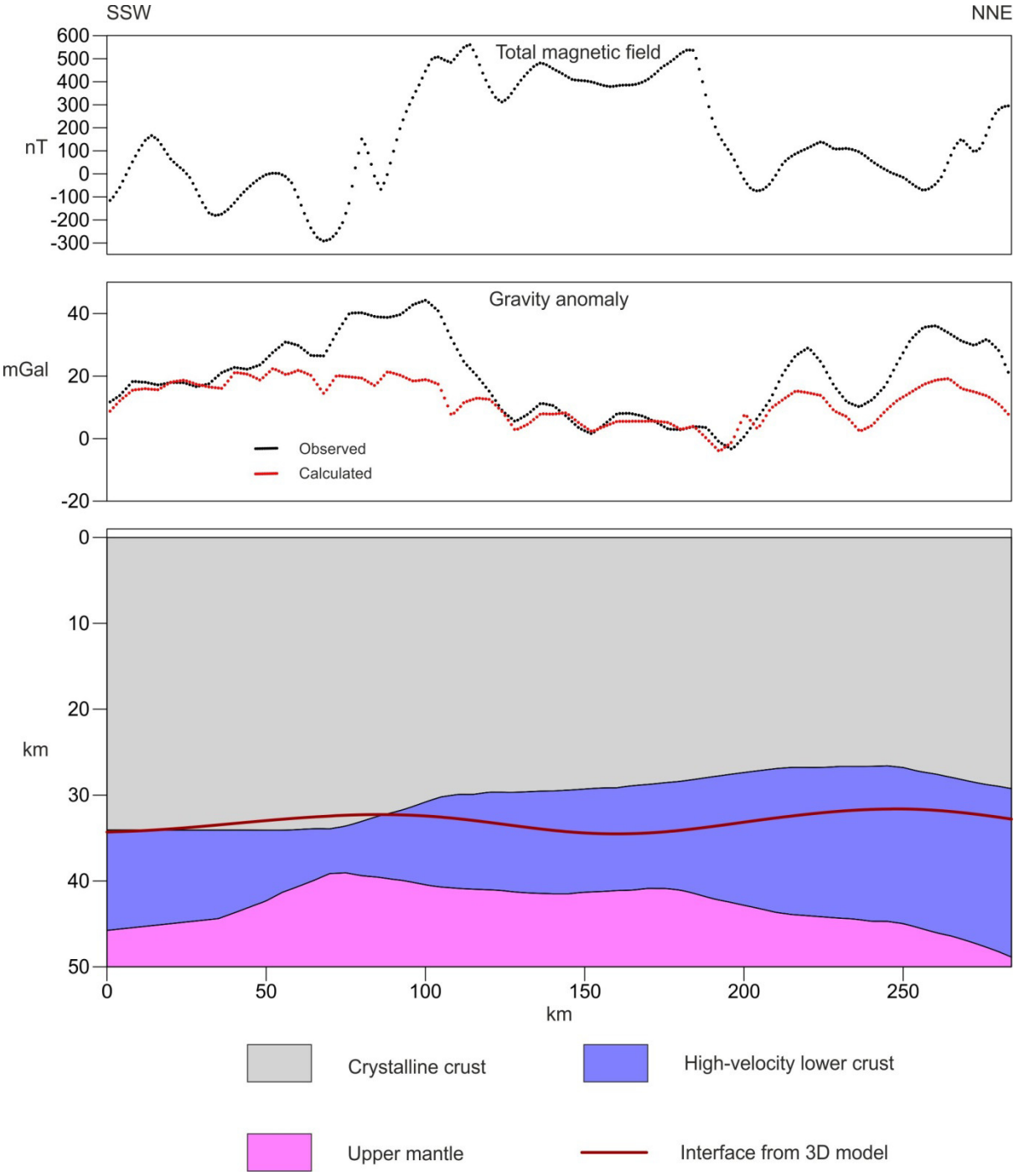

Figure 46 Moho interface from the 3D model superimposed on a simplified version of the published interpretation of seismic refraction line DLC94-5 (Dahl Jensen et al., 1998)